BIOPHYSICAL AND CELL BIOLOGICAL STUDIES CHARACTERIZING THE VERTEBRATE IRON EXPORTER FERROPORTIN

Thesis by

Adrian Edward Rice

In Partial Fulfillment of the Requirements for the

Degree of

Doctor of Philosophy

CALIFORNIA INSTITUTE OF TECHNOLOGY

Pasadena, California

2009

(Defended April 29, 2009)

ACKNOWLEDGEMENTS

Graduate school has been an incredible experience. I feel privileged to have been given so much support by so many remarkable people during my time here, and I will do my best to express my most sincere thanks here.

First, I'd like to thank my co-advisors, Pamela Björkman and Doug Rees. I came to Caltech specifically hoping to work with either one of you and instead found myself lucky enough to work with both of you! Thank you for giving me the opportunity to work on such a fascinating project, for helping me think through all of its various manifestations, and for providing such an excellent environment in which to practice science. I truly appreciate it.

I'd like to thank my thesis committee, Professors Harry Gray, David Chan, and Grant Jensen. Thank you for helping me think about the project in interesting new ways and for keeping me focused on goals within reach.

I have had a lot of technical help, which came in various forms, from a number of people, and I'll try to thank them for it here. Thanks to Mike Mendez for getting insect cell expression of Fpn off the ground. Thanks to Craig Hokanson (and Mike again) for teaching me how to keep insect cells happy in wave bags. Thanks to Damien Soghoian for helping with the project during the summers and for reminding me to "Make

well. Thanks to everyone else in the labs for general help and discussion, and for being such kind and helpful colleagues.

On a more personal level, I'd like to thank Devin Brent "Chess Master" Tesar, Alexander Hamilton "Burning Man" Farley, Tony "Adrian Hates Chocolate" Giannetti, and now Rachel "By the Scepter of Zeus!" Galimidi for being such stellar bay mates. You guys have been a lot of fun to pipette within arms-reach of. I'd also like to thank Devin for saving Sharla from the crickets, to thank Tony for not forcing me to go to yoga, and I'd like to apologize to Rich for the cotton-candy incident.

On an even more personal level, none of this would have been possible without the support of my family. I'd like to thank my wife Sharla for putting up with all of my shenanigans over the years, and to preemptively thank you for continuing to do so for the foreseeable future. Thanks to my brothers, Adam and Quintin, for moral support and for the video-game and skiing breaks over the holidays. Thanks to Sheila Miss for so much help in the past year and a half, and thanks to Wade for letting her! Thanks to Uncle Kit and Aunt Patti for lots of love and being our southern California family. I'd also like to thank Melissa Marnelle for being two-and-a-half feet tall.

Most of all, I'd like to thank my parents, Beverly and Dale Rice. You have always been there when I needed you and have given me nothing but love and support. I want you to

know that I appreciate everything you've done, and that it is to you that I dedicate this

work.

ABSTRACT

Mammalian iron homeostasis is maintained by an intricate network of diverse proteins that constantly survey systemic iron levels and carefully regulate the uptake of iron from the diet. Control of this uptake is critically important because once iron is absorbed, mammals have no regulated mechanism for its removal. The portal through which iron enters the body is ferroportin, a multipass membrane protein expressed on the basolateral membrane of epithelial cells in the duodenum. The iron export function of ferroportin is primarily regulated by the serum peptide hormone hepcidin, which is secreted from the liver when systemic iron levels are high. Hepcidin acts as a negative regulator of iron uptake by binding to ferroportin at the cell surface and inducing its internalization and degradation. Genetic defects in ferroportin, hepcidin, or the proteins involved with sensing systemic iron levels lead to iron overload diseases known as hereditary hemochromatosis. Using the tools of biophysics and cell biology, we sought to study ferroportin and its interaction with hepcidin in order to better understand this critical bottleneck in iron uptake and how genetic defects within ferroportin might lead to disease. We developed the first protocols for the overexpression, detergent-solubilization, and purification of recombinant ferroportin. We determined that detergent-solubilized ferroportin is a monomer capable of binding hepcidin *in vitro*. We characterized the expression and subcellular localization of ferroportin in mammalian tissue culture and determined that both the amino- and carboxy-termini of ferroportin are cytosolic. We developed cell-based assays for the hepcidin-induced internalization of ferroportin and used these to characterize the route of internalization from the plasma membrane through

early endosomes to degradative lysosomal compartments. Using live-cell imaging techniques, we showed that this internalization depended on intact microtubules. We expanded this cell-biological study to include sixteen disease-related ferroportin mutants and reported that each mutant was expressed on the plasma membrane like wild-type ferroportin, but that only a subset of the mutants were capable of being internalized by hepcidin. These studies form a foundation for future biophysical and cell-biological studies of ferroportin function.

TABLE OF CONTENTS

Chapter 1:

Introduction

INTRODUCTION

Iron's Biological Importance

Life, as we know it, depends on iron. Its relative abundance on Earth, coupled with its capacity to facilitate the rapid transfer of electrons and perform redox chemistry under physiological conditions has led to its incorporation in many important biological pathways. The roles that iron plays in the fixation of nitrogen, oxidative phosphorylation, and the transport of oxygen in higher organisms are briefly highlighted below.

All life relies on the fixation of nitrogen (N_2), the relatively inert atmospheric gas, to the more chemically reactive ammonia (NH_3).   This reduction is catalyzed by microorganisms harboring the enzyme nitrogenase (Rees and Howard 2000). Nitrogenase is a metalloenzyme complex that utilizes the precise redox properties of iron (contained within various iron-sulfur clusters) to coordinate the iterative passage of electrons from donors to the nitrogenase active site (Tezcan *et al.* 2005). Without these microorganisms and their iron-containing nitrogenase enzymes, the nitrogen cycle, upon which all life depends, would not be maintained. Furthermore, higher organisms depend on iron for the electron transport central to the redox chemistry of aerobic respiration. As was the case with nitrogenase, the transfer of electrons by proteins in the aerobic respiration chain of oxidative phophorylation is facilitated by iron. Each of the integral membrane protein complexes I through IV as well as the soluble enzyme cytochrome C

utilize iron in the form of iron-sulfur clusters and/or iron-containing heme groups to carry out this electron transfer (Hatefi, 1985). Other important iron proteins include those involved in the transportation of O_2 to the sites of respiration, such as hemoglobin and myoglobin. These proteins utilize iron coordinated by a porphyrin ring heme moiety. In the case of hemoglobin, this large iron-containing hydrophobic ring system is used to bind O_2 in the capillaries of the lungs and then release it in the deoxygenated capillaries of the extremities. The affinity switch that iron-bound heme exhibits for O_2, within the proteinaceous context of hemoglobin, makes it particularly useful for O_2 transport proteins in the many organisms employing aerobic respiration in tissues too deep for diffusion alone to meet the O_2 need.

In each of these examples, iron plays a critical role in the function of proteins necessary for life, however, in each of these examples iron is also sequestered in a heme or iron-sulfur cluster moiety. In addition, organisms have evolved complicated and diverse mechanisms to regulate the uptake, transport, and storage of iron. It is thought that purely ionic iron is rarely (if ever) observed in healthy organisms, and extreme care is taken to ensure that ionic iron is carefully chaperoned while in transit to more permanent cellular and enzymatic locales. These intricate mechanisms of sequestration, some of which will be described further below, are partially due to the low solubility of ferric iron, but also due to the high reactivity of ionic iron, particularly its ability to promote the creation of organic free-radicals through Fenton chemistry (Halliwell and

Gutteridge, 1990). Free radicals are highly reactive species and have been shown to damage lipid bilayers, DNA, and proteins (Halliwell and Gutteridge, 1990).

Iron Uptake

In humans, the regulation of iron homeostasis is tightly controlled at both systemic and cellular levels. Dietary iron uptake is tightly controlled at the brush border of the duodenum portion of the proximal small intestine (figure 1.1). Dietary iron can be absorbed in ionic form by the divalent metal transporter 1 (DMT1, also called NRAMP2 and DCT1) (Fleming *et al.* 1997; Gunshin *et al.* 1997), or by an unidentified heme importer. DMT1 is a proton symporter that utilizes the pH gradient between the slightly basic pH of the cytoplasm and the acidic pH of the duodenum to drive the transport of Fe^{2+} and other divalent metal ions (Gunshin *et al.* 1997). The vast majority of dietary ionic iron is in the ferric state (Fe^{3+}). Prior to import, these ions are reduced to the ferrous state (Fe^{2+}) by the integral membrane protein ferroreductase duodenal cytochrome b (Dcytb) (McKie *et al.* 2001) and perhaps STEAP3 (Ohgami *et al.* 2006). Once Fe^{2+} is transported across the gut-facing apical membrane of the enterocyte, it enters the so-called labile iron pool (figure 1.1). Little is known about the iron in this pool. Presumably, these highly reactive ions in this labile pool are chaperoned by soluble carriers to prevent dangerous Fenton chemistry. From this pool, ionic iron can be incorporated into ferritin for long-term storage or it can be exported into the circulation. Ferritin, the long-term iron storage protein, is a hetero-oligomeric protein complex

containing 24 copies of L- and/or H-ferritin monomers (Theil, 1987). Each fully assembled ferritin can store ~4500 iron atoms (Theil, 1987). In times of iron need, ferritin can be disassembled and its iron released into the labile pool. In these duodenal enterocytes, iron not destined for storage can be transported across the basal membrane into the bloodstream through ferroportin (Fpn; figure 1.1) (Abboud and Haile 2000; Donovan *et al.* 2000; McKie *et al.* 2000). Fpn is an integral membrane iron exporter, although little is known about the specifics of how it functions. Some details, such as whether the process is driven by active transport or passive diffusion, the identification of the pore-forming amino acids, the oligomeric state of the functional transporter, and the details of its ion selectivity, are unknown. It has been suggested by some experiments that this transport is dependent on the extracellular copper-containing iron-oxidase ceruloplasmin (Jeong and David 2003; McKie *et al.* 2000). Ceruloplasmin is an abundant serum protein and can also be expressed as a GPI-linked splice variant in some cell types, where it has been shown to interact functionally and physically with Fpn (Jeong and David 2003). Hephaestin, an integral membrane protein homologue of ceruloplasmin expressed on the basal membrane of duodenal enterocytes, has also been implicated as a copper-containing iron-oxidase that may also interact with ferroportin (Vulpe *et al.* 1999). After Fe^{2+} has traveled across the basal membrane through ferroportin and has been oxidized to Fe^{3+}, it is bound by the soluble serum protein transferrin (Tf) (Andrews 2008). Tf is a monomeric protein containing two iron-binding sites, each of which can accommodate a single Fe^{3+} ion. Iron-loaded Tf (Fe-Tf) is the primary source of iron for most cell types, and is taken up by cells in need of iron through

the well-characterized transferrin-transferrin receptor (TfR1) iron-uptake pathway (figure 1.1) (Andrews 2008).

Unlike iron uptake, which is highly regulated, there is no known regulatory mechanism for the excretion of iron in humans. This implies that the integrity of iron homeostasis for a given individual depends entirely on the proper regulation of iron uptake. Iron is primarily lost through the routine sloughing of epithelial cells in the gastrointestinal tract, blood loss, and menstruation in females. These losses are balanced by a dietary absorption of up to approximately one milligram of iron per day (Sayers *et al.* 1994), however this uptake can be greatly increased, with 20–40 milligrams of iron absorbed per day in some cases of induced anemia and pregnancy (Finch, 1994). As will be seen below, this absorption is tightly regulated at both the cellular level of the enterocyte and the systemic level of the individual. Defects in this regulatory network lead to iron disorders, primarily a class of iron overload diseases collectively known as hereditary hemochromatosis.

Regulation of Iron Uptake

Duodenal enterocytes have a short life span. A typical cell differentiates as an enterocyte in the villus crypt and matures as it migrates up to the tip of the villus, where it is eventually sloughed off into the lumen of the intestine within a few days (Roy and Enns 2000). Any iron acquired by an enterocyte through DMT1 or the heme importer must be

exported through Fpn into the serum before this apoptotic sloughing takes place, or that iron will not be a part of the long-term body iron store. This mechanism allows for the absorption of multiple iron sources into the brush border cells through various import proteins, but allows for the regulation of a single protein, Fpn, as the bottleneck for systemic iron uptake. There are at least two mechanisms for the regulation of Fpn expression, an iron responsive element (IRE)-based regulation of the mRNA transcript resulting in more or less Fpn translated by the ribosome, and a post-translational control where a 25-residue serum peptide known as hepcidin-25 (also known as LEAP-1) binds to surface-localized Fpn causing its internalization and degradation.

The significance of the IRE-based regulation of Fpn *in vivo* is poorly understood (figure 1.2). The identification of Fpn revealed an IRE in the 5′ untranslated region (UTR) of the Fpn transcript (Abboud and Haile 2000; McKie *et al.* 2000). It was shown that this sequence is capable of binding to the iron regulatory proteins IRP1 and IRP2 in gel shift assays (McKie *et al.* 2000), and that this sequence has an iron-dependent effect on the expression of a luciferase reporter *in vitro* (Abboud and Haile 2000). The functional role in translational regulation that this sequence plays *in vivo* has been the subject of some debate (Abboud and Haile 2000; Frazer *et al.* 2003; Lymboussaki *et al.* 2003; Rolfs *et al.* 2002), however the finding that autosomal dominant iron overload can occur due to a mutation in the 5′ UTR of Fpn suggests that it has an important function *in vivo* (Liu *et al.* 2005a). This argument was further bolstered with a recent report in a murine model lacking IRP expression in the intestine (Galy *et al.* 2008). Using a mouse line harboring

a cre/lox recombinase approach for the intestine-specific ablation of IRP1 and IRP2, Galy *et al.* reported that these pups showed severe growth defects and died before weaning (Galy *et al.* 2008). They also reported the duodenal enterocyte protein expression levels were extremely low for DMT1 and TfR1, but extremely high for Fpn and ferritin (Galy *et al.* 2008). Whereas the DMT1 protein expression was correlated with a concomitant decrease in DMT1 transcript levels, the elevated Fpn protein expression was in the presence of similar Fpn mRNA levels and elevated hepcidin levels, strongly suggesting that the cellular IRP/IRE expression control mechanism can overpower or override the hepcidin control mechanism for the expression of Fpn in enterocytes (Galy *et al.* 2008).

The regulation of Fpn cell-surface expression, and thus iron uptake, by the peptide hormone hepcidin is now well recognized as a central theme in iron homeostasis (Andrews 2008; Brissot *et al.* 2008; Darshan and Anderson 2009; Ganz 2008; Nemeth 2008). The hepcidin gene encodes an 84-residue pre-protein (Krause *et al.* 2000; Park *et al.* 2001). Once expressed, the pre-protein can be processed by intracellular proteases cleaving off the amino-terminal ~60-residue and resulting in stable 20-, 22-, or 25-residue peptides (Park *et al.* 2001). These peptides contain several positively charged residues and 8 cysteines (Krause *et al.* 2000; Park *et al.* 2001). The solution structure of synthetic hepcidin-20 and hepcidin-25 revealed that the final folded conformation has four intramolecular disulfide bonds and the overall fold is composed of a beta-ribbon hairpin (Hunter *et al.* 2002). It has been suggested that these disulfides are not all present in the mature hepcidin *in vivo*, and that some of these cysteines may be involved in chelating

cationic metal ions such as copper or iron (Farnaud *et al.* 2006; Farnaud *et al.* 2008). Hepcidin-25 is the only version capable of binding and causing the internalization and destruction of Fpn (Nemeth *et al.* 2004b). It is unclear if hepcidin-20 and hepcidin-22 have functional roles *in vivo*. The primary site of hepcidin production is the liver, however hepcidin expression has been observed in other tissues, including adipose tissue, heart, lungs, spinal cord, and stomach (Bekri *et al.* 2006; Krause *et al.* 2000; Park *et al.* 2001; Pigeon *et al.* 2001). Hepcidin is also present in the urine, but whether hepcidin levels in the urine are a good measure of serum hepcidin levels is currently unclear (De Domenico *et al.* 2008). Techniques have been developed for the determination of hepcidin concentration in both blood and urine (De Domenico *et al.* 2008; Kemna *et al.* 2005b).

The main site of systemic iron sensing is the liver. Hepatocytes involved in this process employ an intricate network of proteins to sense body iron stores and/or body iron need in order to respond appropriately. While many of the proteins involved in this network have been identified and some critical work in the field has recently been reported, the exact picture of how these cells respond to systemic iron levels is not fully understood. Generally, it is known that high iron levels and inflammation induce the expression and secretion of hepcidin into the blood, whereas low iron levels, erythropoiesis, and hypoxia act to repress hepcidin expression (Darshan and Anderson 2009). The molecular pathways that integrate these signals are poorly understood, but several recent reports have made significant progress elucidating the roles that some members of this network

play (figure 1.3). There are at least two signaling pathways that up-regulate the transcription of the hepcidin gene—the bone morphogenetic growth factor protein (BMP) receptor complex pathway and the IL-6 receptor pathway, and at least one pathway that acts to repress hepcidin expression—the hypoxia-inducible factor (HIF) pathway (figure 1.3). These will be discussed below.

Regulation of Hepcidin Expression

The BMP receptor pathway had been previously shown to play important roles in the differentiation and maintenance of certain stem cell lines (Wagner 2007), as well as in the post-natal development of bone growth (Chen *et al.* 2004), however the discovery of its involvement in the up-regulation of hepcidin came as a surprise (Babitt *et al.* 2006). The hepcidin transcript has several candidate BMP-responsive elements ~120–210 base pairs upstream of the hepcidin start codon, and it was shown that the cytokines BMPs 2, 4 and 9 can activate this pathway by binding to the BMP-receptor in complex with hemojuvelin (HJV) (Babitt *et al.* 2006). HJV is a glycophosphatidylinositol (GPI)-linked protein that was recently identified and shown to be involved in iron homeostasis by virtue of the fact that mutations in this gene lead to an autosomal recessive form of juvenile iron overload (Type 2 hereditary hemochromatosis) (Papanikolaou *et al.* 2004). HJV can be cleaved from the membrane by furin-like proteases or by matriptase-2, and this soluble form of HJV is capable of repressing the BMP-receptor pathway by competing for receptor binding with GPI-linked HJV, when exogenously added (Babitt *et al.* 2006; Lin *et al.*

2005; Silvestri *et al.* 2008). The role of soluble HJVs cleaved by either furins or matriptase-2 *in vivo* is unclear. The activation of this receptor complex initiates a signal transduction cascade by phosphorylating R-SMADs. Phosphorylated R-SMADs bind to SMAD4 and localize to the nucleus where the complex acts as a transcription factor to promote transcription of hepcidin pre-protein mRNA (Babitt *et al.* 2006). Mice deficient for this signaling pathway, using a cre/lox targeted-disruption of SMAD4 expression in the liver, displayed extremely reduced hepcidin expression, increased expression of the Fpn and DMT1 in the intestine, and tissue specific iron overload in liver, pancreas, and kidney (Wang *et al.* 2005). Wang *et al.* also showed that hepcidin expression was not induced by iron overload or by the addition of BMP or IL-6 in these mice (Wang *et al.* 2005). Reports of preliminary data suggesting that HFE and transferrin receptor 2 (TfR2) also contribute to the BMB/SMAD signaling pathway by binding to HJV have recently emerged (Ganz 2008; Nemeth 2008). These reports, in conjunction with recent data suggesting that HFE and TfR2 act as iron sensors (Goswami and Andrews 2006; Johnson and Enns 2004; Robb and Wessling-Resnick 2004), could explain how iron sensing ties into a signal transduction pathway regulating hepcidin expression in hepatocytes. Briefly, HFE is a ß$_2$-microglobulin-associated MHC class I homologue, which competes for the Tf binding site on TfR1 (Feder *et al.* 1996; Lebron *et al.* 1998). TfR2, like TfR1, is capable of binding and internalizing iron-loaded transferrin, however unlike TfR1 its expression is restricted to only a few tissue types, with the major site of expression being the liver (Kawabata *et al.* 1999). As will be described in further detail below, defects in HFE and TfR2 lead to hereditary hemochromatosis (HH) types I and III, respectively.

IL-6 is a serum cytokine secreted under conditions of inflammation and infection and binds to cells expressing the IL-6-receptor, thus activating the JAK/STAT signaling cascade (Murray 2007). There is a STAT-3-responsive element ~70 base pairs upstream of the hepcidin gene, and it has been shown that the intravenous administration of IL-6 will induce the expression of hepcidin and reduce serum iron levels within a few hours (Nemeth *et al.* 2004a; Wrighting and Andrews 2006). Similarly, lipopolysaccharide injection in humans shows a correlation between a rise in IL-6 concentration and a rise in urinary hepcidin along with a drop in serum iron (Kemna *et al.* 2005a). The up-regulation of hepcidin expression under inflammatory conditions has been shown to be similarly high as wild-type in mice with HFE and TfR2 knockouts, thus these genes are not required for the activation of this pathway (Frazer *et al.* 2004; Lee *et al.* 2004). The lack of IL-6-induced hepcidin expression in BMP-signaling-deficient mice with liver-specific SMAD4 ablation, suggests that the BMP/SMAD and IL-6/JAK/STAT pathways converge (Wang *et al.* 2005).

Hypoxia has been shown to down-regulate hepcidin expression *in vitro* in the HepG2 hepatic cell line and *in vivo* in hypoxic mice (Nicolas *et al.* 2002). Initial clues pointed to the hypoxia-inducible factor (HIF) transcriptional regulatory complex HIF-1 as the pathway responsible for this regulation of hepcidin by a study in mice with a liver-specific disruption of a gene for a member of the protein complex involved in inactivating HIF-1, the von Hippel-Lindau (VHL) gene (Peyssonnaux *et al.* 2007). The

authors showed that these mice, which constitutively expressed HIF-1 in liver, had a suppressed hepcidin expression phenotype and furthermore, went on to show that HIF-1 is capable of binding to the hepcidin promoter (Peyssonnaux *et al.* 2007). A recent study in HepG2 cells reports evidence that this suppression of hepcidin expression under hypoxia is independent of HIF-1, suggesting that more work will be required to fully elucidate this pathway (Choi *et al.* 2007).

Erythropoiesis, the production of red blood cells, requires a great deal of iron and leads to an increase in iron need, and thus a decrease in hepcidin production. Several studies have focused on determining the molecular basis for this regulation (Pak *et al.* 2006; Vokurka *et al.* 2006), but no pathway has been fully revealed. It was shown that serum from patients with ß-thalassemia, where erythropoiesis is up-regulated to account for a genetic deficiency in hemoglobin production, was able to suppress hepcidin expression in HepG2 cells suggesting an unidentified component of serum, up-regulated in ß-thalassemia, could induce this hepcidin repression despite the associated anemia (Kemna *et al.* 2008). An additional study on a patient group with thalassemia intermedia showed that before transfusion, patients have inappropriately low urinary hepcidin levels (Origa *et al.* 2007). A comparative analysis of the erythroblast transcriptome profiles between controls and patients with ß-thalassemia revealed an over-expression of growth differentiation factor 15 (GDF15) in the thalassemic group (Tanno *et al.* 2007). They found that adding GDF15 to serum would recapitulate hepcidin repression and that depletion of GDF15 would partially recover hepcidin expression in primary human hepatocytes (Tanno *et al.*

2007). Determining whether GDF15 is the sole erythropeoitic hepcidin regulator or not will require further investigation.

Genetic Diseases of Iron Homeostasis

Genetic defects in this network of proteins involved in the regulation of iron homeostasis leads to iron imbalance in the form of iron overload, known as hereditary hemochromatosis (HH), or insufficient iron, known as anemia (table 1.1). Both types of disorders have numerous causes. Anemias can be caused by an inadequate supply of dietary iron, extensive blood loss, as well as by a slew of genetic diseases. Some iron homeostatic disorders are caused by defects in hemoglobin synthesis and erythropoiesis, such as the thalessemias, sickle cell anemia, and diseases of bone marrow failure. Other forms of genetic iron imbalance lead to a so-called iron-loading anemia. Some of these include aceruloplasminemia, hypotransferrinemia (also known as atransferrinemia), anemia of chronic inflammation (also known as anemia of chronic disease), and iron-refractory iron-deficiency anemia. Aceruloplasminemia is caused by a deficiency of the serum iron reductase ceruloplasmin, and is characterized by a serum iron deficiency with iron loading in the liver and brain (Harris *et al.* 1995).

Table 1.1. Genetic diseases of iron homeostasis

Gene	Associated Disease	Inheritance	Disease Summary
Ceruloplasmin	aceruloplasminemia	autosomal recessive	ceruloplasmin deficiency leading to low blood iron levels and iron accumulation in liver and brain
Ferroportin	type IV hemochromatosis or ferroportin disease	autosomal dominant	presents as either anemia associated with iron-loading in macrophages or as iron overload in blood and liver
Hemoglobin	sickle cell anemia	autosomal recessive	hemoglobin defects cause formation of malformed red blood cells, which can lead to capillary obstruction, anemia, and other complications
Hemoglobin	thallassemias	autosomal recessive	low hemoglobin expression levels lead to anemia
Hemojuvelin	type II hemochromatosis or juvenile hemochromatosis	autosomal recessive	severe iron overload in blood and liver, presenting in the 2nd or 3rd decade
Hepcidin	type II hemochromatosis or juvenile hemochromatosis	autosomal recessive	severe iron overload in blood and liver, presenting in the 2nd or 3rd decade
HFE	type I hemochromatosis	autosomal recessive	accumulation of iron in blood and liver, presenting in 4th or 5th decade
Transferrin	hypotransferrinemia	autosomal recessive	transferrin deficiency leading to anemia and iron overload in liver and heart, presenting in 1st decade
Transferrin Receptor 2	type III hemochromatosis	autosomal recessive	accumulation of iron in blood and liver, presenting in 4th or 5th decade

Much like hereditary anemias, hereditary iron overload or hereditary hemochromatosis can have many causes. Defects in the expression and function of HFE, hemojuvelin, TfR2, hepcidin, and ferroportin all lead to various types of HH. All of these genes have been discovered within the last 15 years, and as each new gene was discovered and its corresponding disease characterized, our understanding of iron homeostasis broadened. Various schemes for the classification of known HHs have been proposed based on the chronology of identification (Bomford 2002; Camaschella *et al.* 2002), pathophysiology (Pietrangelo 2007), or groupings related to the regulation of hepcidin expression (Andrews 2008). While the latter two grouping schema are very informative and potentially helpful toward understanding themes in iron disease, the former will be used here below to explain the pathologies of HH.

The first HH characterized at the molecular level was HFE-related HH, or type I HH. Type I HH is an autosomal recessive disease where patients are homozygous for the mutant C282Y HFE allele (Feder *et al.* 1996). The HFE gene was identified in 1996 by an extensive sequencing and analysis of chromosomal regions proximal to the major histocompatibility complex (MHC) in patients with HH (Feder *et al.* 1996). They identified HFE (then called HLA-H) as an MHC class I homologue and identified the C282Y mutation in 83% of their 178 HH patient pool (Feder *et al.* 1996). Another mutation, H63D HFE, is also a clinically relevant HH mutant, however it rarely leads to HH unless paired with a C282Y allele to form a so-called C282Y/H63D compound heterozygote (Ayonrinde *et al.* 2008). Like classical MHC class I proteins, HFE folds as an obligate heterodimer with the soluble protein ß2-microglobulin (ß2M) as a light chain. Subsequent analysis showed that cysteine 282 is involved in a disulfide bridge in the α3 domain of the HFE heavy chain, thus the C282Y mutation disrupted HFE's ability to fold and complex with ß2M, preventing its presentation on the cell surface (Feder *et al.* 1997). Structural analysis of HFE revealed that the canonical binding cleft is present, but too narrow to accommodate a peptide, as observed in classical MHC class I structures, which play a critical role in the immune system by presenting peptide antigens to T cells (Lebron *et al.* 1998). To date, type I HH is the most prevalent form of HH worldwide, and in comparison to HH types 2–4, it has been the subject of the most extensive analyses. One such analysis studying HFE alleles in northern European populations showed that C282Y/C282Y, C282Y/wild-type, and C282Y/H63D were present in the population at frequencies of 0.3%–0.5%, 10%–40%, and 2%–4%, respectively (Adams *et*

al. 2005; Olynyk *et al.* 1999). The penetrance for type I HH in individuals homozygous for the C282Y HFE mutation can be as low as 28.4% for men and 1.2% for women (Allen *et al.* 2008). Affected patients show systemic iron loading leading to organ damage, morbidity and mortality. Iron overload in these patients is typically a slow process and often presents in the fourth or fifth decade of life, with initial iron overload in the liver parenchyma followed by iron loading in the heart, pancreas and/or the joints. Type I HH is a progressive disease, and if untreated, this overload can result in hepatic cancer, organ failure, and death. Even though HFE has been shown to interact with a number of proteins involved in iron homeostasis, the molecular basis for this disease has been difficult to fully characterize. For instance, HFE has been shown to bind TfR1 (Feder *et al.* 1998; Lebron *et al.* 1998), that the HFE binding site on TfR1 overlaps significantly but is not identical with the Tf binding site (Bennett *et al.* 2000; Giannetti *et al.* 2003), and that Tf and HFE directly compete for TfR1 binding at the cell surface (Giannetti and Björkman 2004). An interaction between HFE and the TfR1 homologue, TfR2, was initially hypothesized, however *in vitro* binding analyses between soluble ectodomains of HFE and TfR2 were shown to not interact (West *et al.* 2000). Further studies using transfected versions of full-length HFE and TfR2 expressed on the cell surface of several different cell types have shown that HFE does in fact interact with TfR2, and that this binding is in competition with TfR1 (Goswami and Andrews 2006). Recent findings suggest that HFE activates hepcidin expression and that its sequestration by binding to TfR1 can prevent this activation (Schmidt *et al.* 2008). It has been suggested that this dynamic interplay between HFE, TfR1, TfR2, and Fe-Tf may be the

main mechanism by which hepatocytes sense body iron stores (Darshan and Anderson 2009; Nemeth 2008). HFE's role as a member of the putative iron sensor will require further work to fully establish. Another report has shown that HFE inhibits iron uptake by down-regulation of Zip14, a proposed iron importer (Gao *et al.* 2008), though the importance of this regulation is unclear, as the role of Zip14 in iron homeostasis is not well established.

Another class of HH known as juvenile hemochromatosis or type II HH, has a strong iron-overload pathology consisting of cardiopathy, hypogonadism and often skin pigmentation presenting in the second or third decade of life (Camaschella *et al.* 2002; Papanikolaou *et al.* 2004). The pathology of type II HH is severe, and unless iron levels are reduced by phlebotomy, patients typically die from cardiomyopathy (Camaschella 1998). Type II HH is inherited in an autosomal recessive fashion by mutations in either the hepcidin (Roetto *et al.* 2003) or HJV genes (Papanikolaou *et al.* 2004), though the HJV variant appears to be more common (Rivard *et al.* 2003b). The mutations identified in hepcidin have been point mutations resulting in the introduction of a stop codon or a nonsense frame-shift mutation in the pro-hepcidin gene leading to the truncation or nonsense expression of the C-terminal sequence of pro-hepcidin (Roetto *et al.* 2003). Mutations in hemojuvelin have typically been missense point mutations resulting in full-length mutant expression of mutant proteins (Papanikolaou *et al.* 2004). Mutations of both sorts, in HJV or the hepcidin gene, result in no hepcidin expression, and thus no systemic control of iron uptake down-regulation.

Type III HH is caused by mutations in TfR2. Its presentation in affected patients is similar to that of HFE-caused type I HH, as is its method of treatment, namely phlebotomy. Type III HH patients have reduced hepcidin levels, despite high serum iron, suggesting that TfR2 is involved in regulating hepcidin expression (Nemeth *et al.* 2005). TfR2 is a homologue of TfR1, and while it has been shown to interact with iron-loaded Tf and is capable of facilitating its import, the uptake of iron appears to not be the primary purpose for TfR2 (Kawabata *et al.* 1999). As described above, TfR2 is now thought to interact with HFE at the cell surface (Goswami and Andrews 2006), and through the dynamics of the interactions between HFE, Tf, TfR1 and TfR2, it is thought to be involved in the sensing of systemic iron levels (Darshan and Anderson 2009; Nemeth 2008). In addition TfR2 has been shown to localize to lipid raft domains on the cell surface by virtue of its co-localization with caveolin-1 (Calzolari *et al.* 2006). This same study showed that TfR2 can also initiate signal transduction via the ERK1/ERK2 and p38 MAPK pathways by binding iron-loaded Tf at the cell surface (Calzolari *et al.* 2006).

Type IV HH is an autosomal dominant iron overload disease caused by point mutations in the ferroportin gene, and will be the in-depth subject of the following section.

Ferroportin Disease

Type IV HH, also known as ferroportin disease, has been difficult to characterize due to a

mixture of phenotypes and variations in how different individuals present their iron

loading. Some individuals present with similar symptoms to type I HH, elevated Tf

saturation and serum ferritin levels in conjunction with hepatocyte iron deposits

(Pietrangelo 2004). However, other individuals present symptoms more like those seen in

iron-loading anemia, including low Tf saturation and serum ferritin levels, but also with

significant iron loading in macrophages of the liver and spleen (Pietrangelo 2004). These

phenotypic differences are easiest identified early in the disease progression as patients

with advanced ferroportin disease tend to show iron overload in all repositories (Njajou *et

al.* 2002; Pietrangelo *et al.* 1999).   Both forms of the disease are inherited in an

autosomal dominant manner, unlike the other main forms of HH. The reported defects in

the Fpn gene are almost exclusively missense point mutations within the coding region,

with one example of a truncation after residue 330 (Lee *et al.* 2007) and one example of a

mutation within the 5' untranslated region (UTR) of the Fpn mRNA (Liu *et al.* 2005a).

More than 15 distinct mutations in the Fpn gene have been reported, however a lack of

pedigree analysis and liver biopsies for many of the reported mutants have made it

difficult to fully characterize this disease. Reports including patient data for the known

Fpn mutants include (in order of occurrence within the gene): adenine 117 to guanine in

the 5' UTR of the Fpn transcript (Liu *et al.* 2005a); Y64N (Jouanolle *et al.* 2003; Rivard

et al. 2003a); A77D (Corradini *et al.* 2005; De Domenico *et al.* 2006; Montosi *et al.*

2001); G80S (Corradini *et al.* 2005; De Domenico *et al.* 2006); N144D (Wallace *et al.* 2004); N144H (Njajou *et al.* 2002; Njajou *et al.* 2001); N144T (Arden *et al.* 2003); I152F (Girelli *et al.* 2008); D157G (Hetet *et al.* 2003); ΔV160 (Cazzola *et al.* 2002; Devalia *et al.* 2002; Roetto *et al.* 2002; Wallace *et al.* 2002); N174I (Corradini *et al.* 2005; De Domenico *et al.* 2006); Q182H (Hetet *et al.* 2003); L233P (Girelli *et al.* 2008); Q248H (Beutler *et al.* 2003; Gordeuk *et al.* 2003); D270V (Robson *et al.* 2004); G323V (Hetet *et al.* 2003); C326S (Sham *et al.* 2005); C326Y (Robson *et al.* 2004); truncation after G330 (Lee *et al.* 2007); and G490D (Jouanolle *et al.* 2003). Some of the disease-related data for the patients described in these reports are summarized in table 1.2.

In an effort to determine the disease-causing defects associated with some Fpn mutations, *in vitro* analyses of these Fpn mutants have been reported (De Domenico *et al.* 2006; De Domenico *et al.* 2005; Drakesmith *et al.* 2005; Girelli *et al.* 2008; Liu *et al.* 2005b; McGregor *et al.* 2005; Rice *et al.* 2009; Schimanski *et al.* 2005), however linking these defects to the disease phenotypes for each case *in vivo* has been difficult.

The Fpn gene encodes a protein of 562, 570, or 571 amino acids in zebrafish, mouse, or human, respectively. Fpn has been identified in all vertebrate genomes sequenced, and thus far it the only protein identified as an ionic iron exporter. Three groups independently reported the discovery of Fpn in the year 2000 (Abboud and Haile 2000; Donovan *et al.* 2000; McKie *et al.* 2000). Through a positional cloning effort in zebrafish, Donovan *et al.* showed that mutations in the Fpn gene lead to the

Table 1.2. Summary of *in vivo* and *in vitro* studies on disease-related ferroportin mutants

| | Prior Literature | | | | | | | | Rice *et al.* 2009 | | | |
| | HH patients, *in vivo* | | | | *in vitro* | | | | *in vitro* | | | |
Mutation	transferrin saturation	serum ferritin (µg/L)	hepatocyte iron loading?	Kupffer/macrophage iron loading?	Fpn localization	iron export?	hepcidin binding?	hepcidin-induced internalization?	Fpn localization	hepcidin binding?	hepcidin-induced internalization?	Mutation
wild type	20%-50% (4); 15%-45% (9)	12-300 (4); 20-250 (9)	NO	NO	PM (1); PM (3); PM (4); PM (14); PM (21); PM (23)	YES (1); YES (2); YES (14); YES (25)	YES (1)	YES (1)	PM	YES	YES	wild type
5' UTR	92%* (22)	9660* (22)	NO	YES (22)				-	-	-	-	5' UTR
Y64N	47%-98% (10)	176-2800 (10)	YES (10)	YES (10)	PM (14)	YES (2)	-	NO (14)	PM	-	NO	Y64N
A77D	20%-89% (18); 20%-35% (19)	650-5800 (18); 950-2100 (19)	YES/SOME (18)	YES (4); YES (18); YES (19)	INTRA (4)	LOW (2); LOW (25)	NO (4)	NO (4)	PM	-	YES	A77D
G80S	23%-60% (4, 19)	1100-4500 (4, 19)	-	YES (4); YES (19)	PM (4)	YES (4)	YES (4)	YES (4)	PM	-	NO	G80S
N144D	99%* (20)	7500-10500 (20)	YES (20)	YES/SOME (20)	PM (14)	YES (2)	YES (14)	PARTIAL (14)	PM	-	YES	N144D
N144H	13%-86% (8)	31-2200 (8)	YES (8)	YES (8)	PM (1); PM (14)	YES (1); YES (2); LOW (25)	YES (1); YES (14)	NO (1); PARTIAL (14)	PM	-	YES	N144H
N144T	80%* (12)	2937* (12)	YES* (12)	YES** (12)					PM	-	YES	N144T
I152F	23%* (23)	900-1770 (23)	NO* (23)	YES** (23)	PM (23)	LOW (23)		YES (23)	-	-	-	I152F
D157G	44%* (11)	4069* (11)	-	-	PM (1); PM (3)	LOW (1)	NO (1)	NO (1)	PM	-	YES	D157G
ΔV160	30%-40% (5); 20%-80% (6); 20%-35% (7); 17%-30% (9)	1150-4850 (5); 1100-12000 (6); 1000-5400 (7); 400-7500 (9)	YES/SOME (5); YES/SOME (6); YES/SOME (7)	YES (5); YES (6); YES (7)	PM/INTRA (1); PM/INTRA (3)	LOW (1); LOW (2); LOW (25)	NO (1)	NO (1)	PM	-	YES	ΔV160
N174I	39%-48% (4, 19)	3000-5800 (4, 19)	-	YES (4); YES (19)	PM/INTRA (4)	NO (4)	PARTIAL (4)	NO (4)	PM	-	YES	N174I
Q182H	16%* (11)	3018* (11)	-	-	PM (1); PM (3)	YES (1)	YES (1)	YES (1)	PM	-	YES	Q182H
L233P	75%* (23)	9000* (23)	YES* (23)	YES** (23)	PM/INTRA (23)	NO (23)	-	YES (23)	-	-	-	L233P
Q248H	24%-62%** (15); 21%-28%** (16)	46-2700 (15); 63-1000** (16)	-	-	PM(14)	LOW (25)	YES (14)	YES (14)	PM	-	YES	Q248H
D270V	-	-	-	-	PM/INTRA (1); PM/INTRA (3)	-	-	-	PM	-	YES	D270V
G323V	"normal"* (11)	1700-2000* (11)	-	-	PM (1); PM (3)	LOW (1)	NO (1)	NO (1)	PM	-	YES	G323V
C326S	84%-97% (17)	151-300 (17)	YES (17)	-			-		PM	-	NO	C326S
C326Y	-	-	-	-	PM (14)	YES (2)	-	NO (14)	PM	-	NO	C326Y
Δ331-571	25%* (24)	1364* (24)	YES* (24)	YES** (24)					-	-	-	Δ331-571
G490D	19%-53% (13)	1300-9000 (13)	YES (13)	YES (13)	PM/INTRA (1)	LOW (1); NO (2)	NO (1)	NO (1)	PM	-	NO	G490D

* Data is from a single patient; ** Data is a range of averages, not a range of values. References: (1) De Domenico *et al.* 2005; (2) Schimanski *et al.* 2005; (3) Goncalves *et al.* 2006; (4) De Domenico *et al.* 2006; (5) Devalia *et al.* 2002; (6) Wallace *et al.* 2002; (7) Roetto *et al.* 2002; (8) Njajou *et al.* 2002; (9) Cazzola *et al.* 2002; (10) Rivard *et al.* 2003; (11) Hetet *et al.* 2003; (12) Arden *et al.* 2003; (13) Jouanolle *et al.* 2003; (14) Drakesmith *et al.* 2005; (15) Gordeuk *et al.* 2003; (16) Beutler *et al.* 2003; (17) Sham *et al.* 2005; (18) Pietrangelo *et al.* 1999; (19) Corradini *et al.* 2005; (20) Wallace *et al.* 2004; (21) Nemeth *et al.* 2004; (22) Liu *et al.* 2005; (23) Girelli *et al.* 2008; (24) Lee *et al.* 2007; (25) McGregor *et al.* 2005

hypochromatic *weh* phenotype caused by a lack of iron import (Donovan *et al.* 2000). They further showed that this mutant phenotype can be rescued by iron-dextran injections or by Fpn-GFP transfection (Donovan *et al.* 2000). Using a subtractive cloning strategy involving cDNA libraries from wild-type and the hypotransferrinemic *hpx* mouse, McKie *et al.* identified Fpn and similarly characterized it as an iron exporter in an iron efflux assay with *Xenopus* oocytes (McKie *et al.* 2000). A third study using an mRNA library of sequences enriched for IRP1 binding was used to search for novel transcripts involved in iron uptake in the murine duodenum (Abboud and Haile 2000). These studies each showed that Fpn is expressed at the site of dietary iron absorption in mammals—the basal membrane of the proximal duodenum, as well as other important sites of iron export, namely the liver, spleen, and placenta (Abboud and Haile 2000; Donovan *et al.* 2000; McKie *et al.* 2000). They also reported that Fpn is the likely iron exporter, either directly through radioactive iron efflux analyses in microinjected *Xenopus* oocytes (Donovan *et al.* 2000; McKie *et al.* 2000) or indirectly by observing reduced intracellular ferritin levels in transfected HEK293T cells (Abboud and Haile 2000). Fpn is highly conserved between species, with human Fpn sharing 91.2% identity with mouse Fpn and 76% identity with zebrafish Fpn, using the ClustalW algorithm (Larkin *et al.* 2007).

The transmembrane domain (TM) topology of Fpn protein has been predicted in numerous reports ranging from 9 to 12 TMs (Devalia *et al.* 2002; Donovan *et al.* 2000; Goncalves *et al.* 2006; Liu *et al.* 2005b; McKie *et al.* 2000; Rice *et al.* 2009), however a consensus has emerged where the 12 TM model proposed by Liu *et al.* based on

insertional mutagenesis has now been widely accepted (De Domenico *et al.* 2008; Liu *et al.* 2005b; Rice *et al.* 2009).

The oligomeric state of Fpn has also been the subject of significant debate. Reports have conflicted, with some reporting Fpn as a monomer (Goncalves *et al.* 2006; Pignatti *et al.* 2006; Schimanski *et al.* 2008) and others reporting it as a dimer/multimer (De Domenico *et al.* 2007b; De Domenico *et al.* 2005). Reports from the Kaplan lab have provided evidence that differentially tagged Fpns (wild-type-wild-type or wild-type-ΔV160) interact by co-immunoprecipitation in co-transfected HEK293T cells (De Domenico *et al.* 2007b; De Domenico *et al.* 2005), however similar experiments in another laboratory did not reproduce their results (Goncalves *et al.* 2006). Furthermore, a report from Schimanski *et al.* cited a lack of evidence for an interaction between differentially tagged wild-type Fpns in a FRET assay, as well as a lack of interaction between differentially tagged wild-type and ΔV160 Fpn in a degradation assay, both performed in co-transfected HEK293T cells (Schimanski *et al.* 2008). Proponents of the dimer/multimer Fpn model further cite genetic data in murine systems. For instance, it has been shown that mice heterozygous for an Fpn knockout do not show signs of Type IV HH (Donovan *et al.* 2005), which would be expected in heterozygotes if Fpn haploinsufficiency were the cause of disease. They argue that if Fpn were a dimer, and heterodimers between mutant and wild-type Fpn molecules were inactive, then only 25% of dimers would be functional and would more convincingly describe the severe phenotype observed in this autosomal dominant disease. The only report of Fpn overexpression and purification has

shown that detergent-solubilized Fpn, capable of binding hepcidin-25, is a monomer (Rice *et al.* 2009). In summary, the oligomeric status of Fpn *in vivo* is unresolved. It remains possible that Fpn exists in two distinct oligomeric states at different stages of its function and that the discrepancies in the literature reflect a biologically relevant oligomeric equilibrium.

The regulation of Fpn at the cell surface has been more carefully characterized with respect to its interaction with hepcidin-25. As mentioned above, hepcidin is a 25-residue peptide expressed in the liver when systemic iron levels are high and secreted into the serum where it can bind Fpn causing its internalization and degradation (Nemeth et al. 2004b). The binding of hepcidin-25 to Fpn appears to be facilitated by a 19-residue stretch, termed the hepcidin binding domain (HBD), of Fpn's 4th extracellular loop between TMs 7 and 8 (De Domenico *et al.* 2008). A 19-residue HBD peptide from this region was shown to recapitulate the Fpn-hepcidin interaction in an *in vitro* bead assay and that this binding was temperature dependent (De Domenico *et al.* 2008), as had been previously described (Nemeth *et al.* 2004b). Interestingly, the HBD contains only one position known to cause Type IV HH upon mutation—cysteine 326. After hepcidin-25 binds to Fpn, tyrosine 302 or tyrosine 303 are phosphorylated at the cell surface and internalized (De Domenico *et al.* 2007a). Upon internalization, Fpn is dephosphorylated and ubiquitinated leading to its degradation in lysosomes (De Domenico *et al.* 2007a). The internalization of Fpn has been shown to progress through early endosomal antigen 1-positive (EEA1-positive) endosomes on its way to lysosome-associated membrane

proteins 1 and 2 (LAMP1 and LAMP2) positive compartments in Fpn-GFP-transfected HeLa cells (Rice *et al.* 2009). Furthermore, the transport of hepcidin-induced Fpn internalization was dependent on intact microtubules (Rice *et al.* 2009).

Fpn's role as a critical bottleneck in iron uptake and in type IV HH make it an important molecule to study. Further understanding of its function and regulation are needed to understand iron uptake and homeostasis, and those insights could lead to advances in the treatment of disorders involving the dysregulation of iron intake.
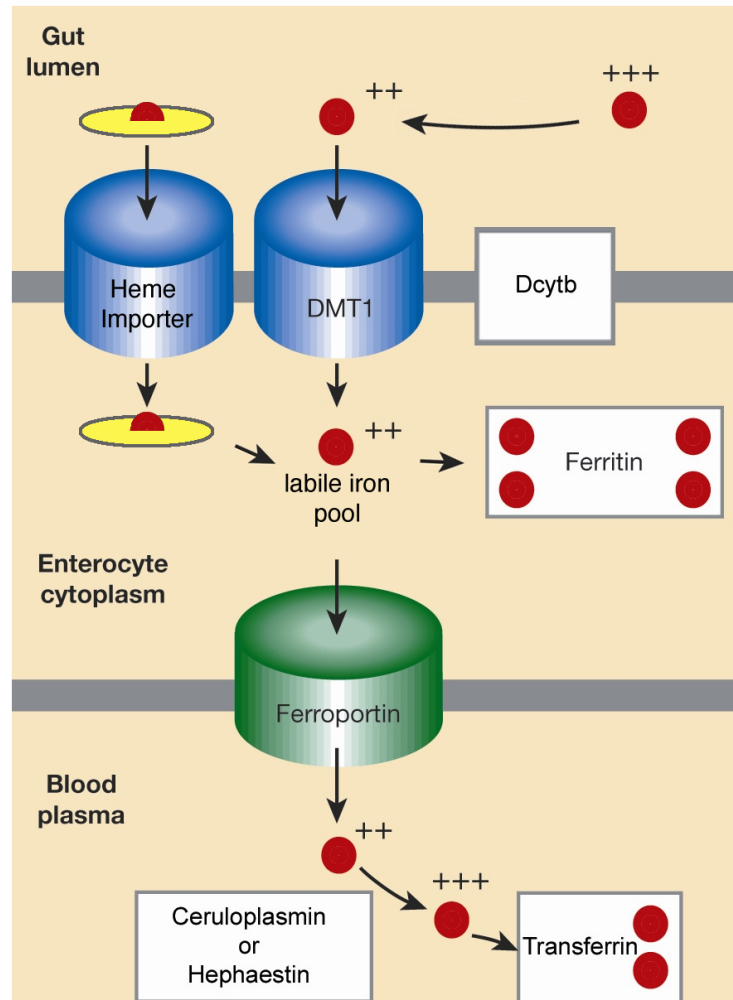
Figure 1.1. Iron uptake in the proximal duodenum. Adapted from Kaplan and Kushner 2000.
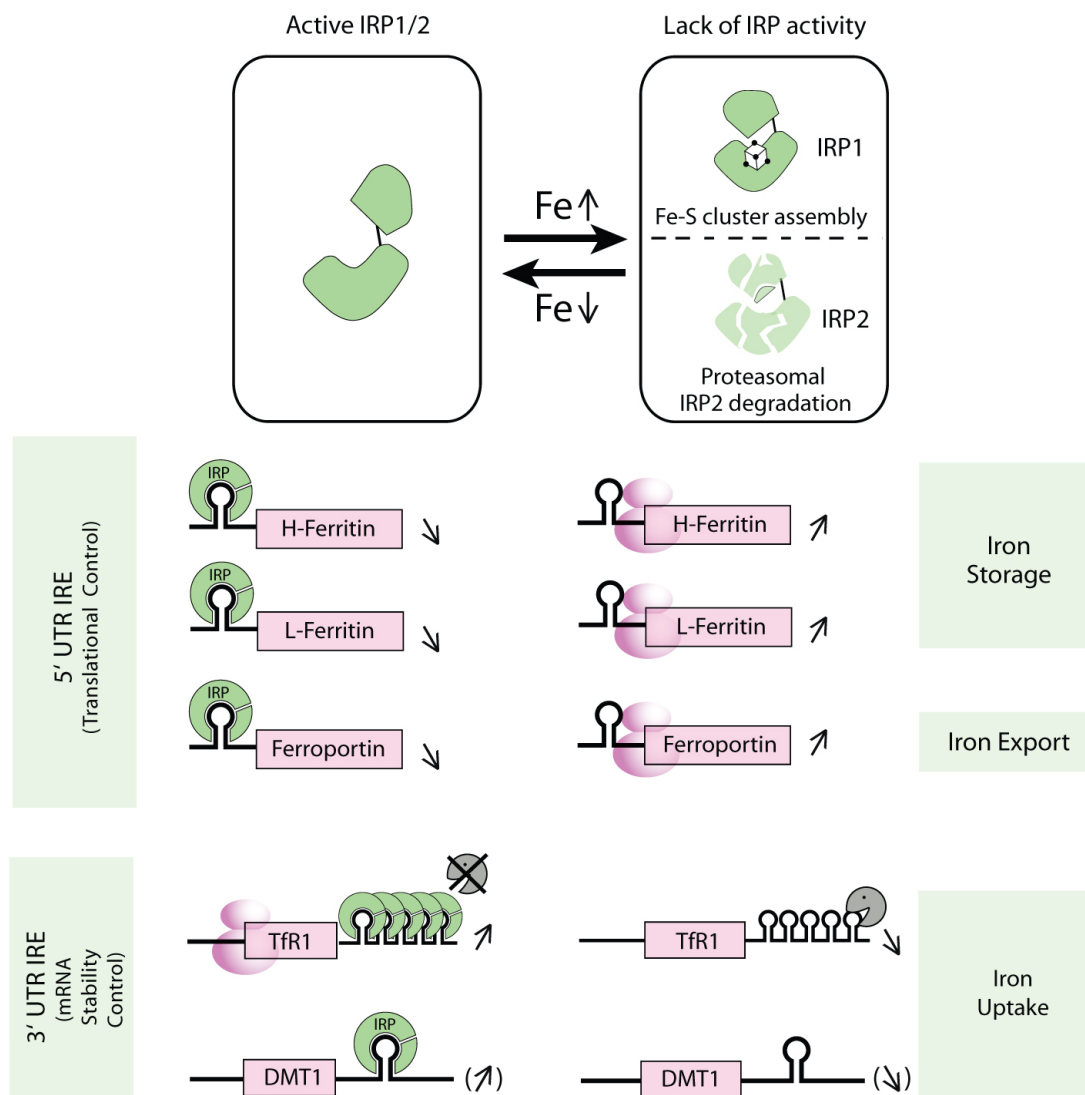
Figure 1.2. IRE/IRP translational control of proteins in iron homeostasis. Iron responsive proteins 1 and 2 (IRP1 and IRP2) bind to iron responsive element (IRE) hairpin loops in the untranslated region (UTR) of transcripts when iron levels are low. The binding of IRP to a 5′ IRE prevents translation, whereas IRP binding to a 3′ IRE stabilizes the transcript and boosts expression. The effects of the IRE/IRP system are shown for ferritin, Fpn, TfR, and DMT1. Adapted from Muckenthaler *et al.* 2008.
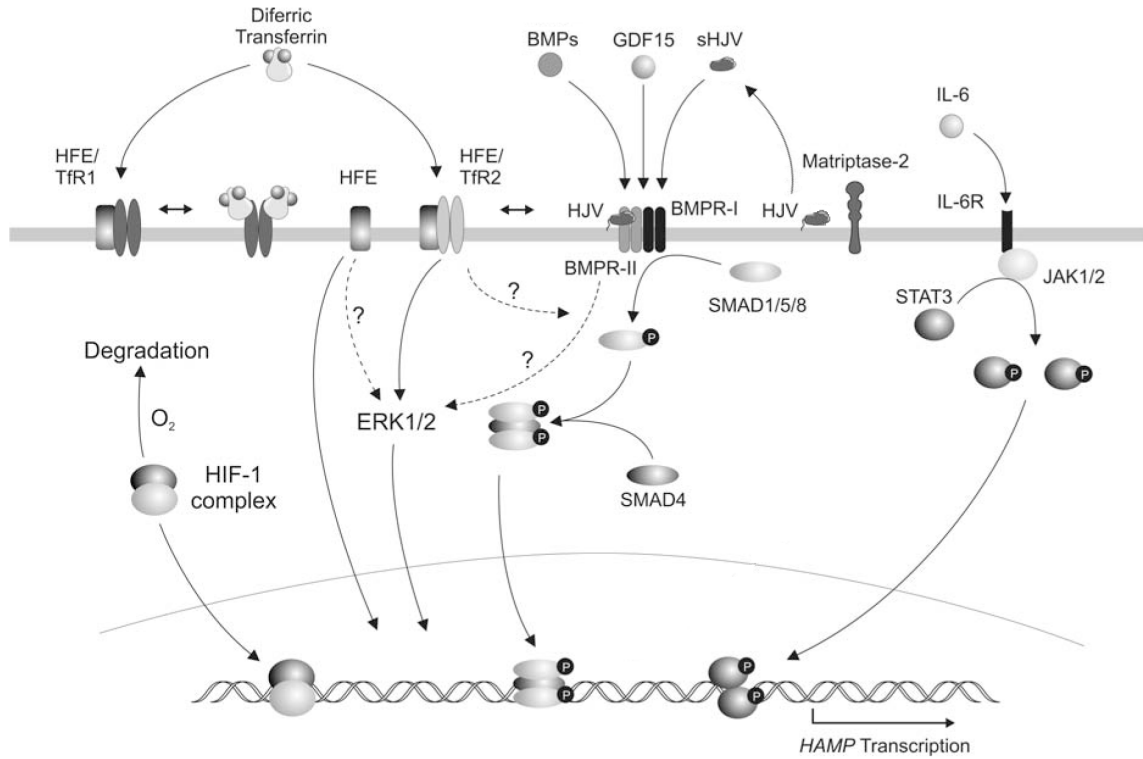
Figure 1.3. The regulatory network of hepcidin transcription. Adapted from Darshan and Anderson 2009.

References

Abboud, S., and Haile, D. J. (2000). A novel mammalian iron-regulated protein involved in intracellular iron metabolism. *J Biol Chem* **275**, 19906–19912.

Adams, P. C., Reboussin, D. M., Barton, J. C., McLaren, C. E., Eckfeldt, J. H., McLaren, G. D., Dawkins, F. W., Acton, R. T., Harris, E. L., Gordeuk, V. R*., et al.* (2005). Hemochromatosis and iron-overload screening in a racially diverse population. *N Engl J Med* **352**, 1769–1778.

Allen, K. J., Gurrin, L. C., Constantine, C. C., Osborne, N. J., Delatycki, M. B., Nicoll, A. J., McLaren, C. E., Bahlo, M., Nisselle, A. E., Vulpe, C. D*., et al.* (2008). Iron-overload-related disease in HFE hereditary hemochromatosis. *N Engl J Med* **358**, 221–230.

Andrews, N. C. (2008). Forging a field: The golden age of iron biology. *Blood* **112**, 219–230.

Arden, K. E., Wallace, D. F., Dixon, J. L., Summerville, L., Searle, J. W., Anderson, G. J., Ramm, G. A., Powell, L. W., and Subramaniam, V. N. (2003). A novel mutation in ferroportin1 is associated with haemochromatosis in a Solomon Islands patient. *Gut* **52**, 1215–1217.

Ayonrinde, O. T., Milward, E. A., Chua, A. C., Trinder, D., and Olynyk, J. K. (2008). Clinical perspectives on hereditary hemochromatosis. *Crit Rev Clin Lab Sci* **45**, 451–484.

Babitt, J. L., Huang, F. W., Wrighting, D. M., Xia, Y., Sidis, Y., Samad, T. A., Campagna, J. A., Chung, R. T., Schneyer, A. L., Woolf, C. J*., et al.* (2006). Bone morphogenetic protein signaling by hemojuvelin regulates hepcidin expression. *Nat Genet* **38**, 531–539.

Bekri, S., Gual, P., Anty, R., Luciani, N., Dahman, M., Ramesh, B., Iannelli, A., Staccini-Myx, A., Casanova, D., Ben Amor, I*., et al.* (2006). Increased adipose tissue expression of hepcidin in severe obesity is independent from diabetes and NASH. *Gastroenterology* **131**, 788–796.

Bennett, M. J., Lebron, J. A., and Björkman, P. J. (2000). Crystal structure of the hereditary haemochromatosis protein HFE complexed with transferrin receptor. *Nature* **403**, 46–53.

Beutler, E., Barton, J. C., Felitti, V. J., Gelbart, T., West, C., Lee, P. L., Waalen, J., and Vulpe, C. (2003). Ferroportin 1 (SCL40A1) variant associated with iron overload in African-Americans. *Blood Cells Mol Dis* **31**, 305–309.

Bomford, A. (2002). Genetics of haemochromatosis. *Lancet* **360**, 1673–1681.

Brissot, P., Troadec, M. B., Bardou-Jacquet, E., Le Lan, C., Jouanolle, A. M., Deugnier, Y., and Loreal, O. (2008). Current approach to hemochromatosis. *Blood Reviews* **22**, 195–210.

Calzolari, A., Raggi, C., Deaglio, S., Sposi, N. M., Stafsnes, M., Fecchi, K., Parolini, I., Malavasi, F., Peschle, C., Sargiacomo, M*., et al.* (2006). TfR2 localizes in lipid raft domains and is released in exosomes to activate signal transduction along the MAPK pathway. *J Cell Sci* **119**, 4486–4498.

Camaschella, C. (1998). Juvenile haemochromatosis. *Baillieres Clin Gastroenterol* **12**, 227–235.

Camaschella, C., Roetto, A., and De Gobbi, M. (2002). Genetic haemochromatosis: genes and mutations associated with iron loading. *Best Pract Res Clin Haematol* **15**, 261–276.

Cazzola, M., Cremonesi, L., Papaioannou, M., Soriani, N., Kioumi, A., Charalambidou, A., Paroni, R., Romtsou, K., Levi, S., Ferrari, M*., et al.* (2002). Genetic hyperferritinaemia and reticuloendothelial iron overload associated with a three base pair deletion in the coding region of the ferroportin gene (SLC11A3). *Br J Haematol* **119**, 539–546.

Chen, D., Zhao, M., and Mundy, G. R. (2004). Bone morphogenetic proteins. *Growth Factors (Chur, Switzerland)* **22**, 233–241.

Choi, S. O., Cho, Y. S., Kim, H. L., and Park, J. W. (2007). ROS mediate the hypoxic repression of the hepcidin gene by inhibiting C/EBPalpha and STAT-3. *Biochem Biophys Res Commun* **356**, 312–317.

Corradini, E., Montosi, G., Ferrara, F., Caleffi, A., Pignatti, E., Barelli, S., Garuti, C., and Pietrangelo, A. (2005). Lack of enterocyte iron accumulation in the ferroportin disease. *Blood Cells Mol Dis* **35**, 315–318.

Darshan, D., and Anderson, G. J. (2009). Interacting signals in the control of hepcidin expression. *Biometals* **22**, 77–87.

De Domenico, I., McVey Ward, D., Nemeth, E., Ganz, T., Corradini, E., Ferrara, F., Musci, G., Pietrangelo, A., and Kaplan, J. (2006). Molecular and clinical correlates in iron overload associated with mutations in ferroportin. *Haematologica* **91**, 1092–1095.

De Domenico, I., Nemeth, E., Nelson, J. M., Phillips, J. D., Ajioka, R. S., Kay, M. S., Kushner, J. P., Ganz, T., Ward, D. M., and Kaplan, J. (2008). The hepcidin-binding site on ferroportin is evolutionarily conserved. *Cell Metabolism* **8**, 146–156.

De Domenico, I., Ward, D. M., Langelier, C., Vaughn, M. B., Nemeth, E., Sundquist, W. I., Ganz, T., Musci, G., and Kaplan, J. (2007a). The molecular mechanism of hepcidin-mediated ferroportin down-regulation. *Mol Biol Cell* **18**, 2569–2578.

De Domenico, I., Ward, D. M., Musci, G., and Kaplan, J. (2007b). Evidence for the multimeric structure of ferroportin. *Blood* **109**, 2205–2209.

De Domenico, I., Ward, D. M., Nemeth, E., Vaughn, M. B., Musci, G., Ganz, T., and Kaplan, J. (2005). The molecular basis of ferroportin-linked hemochromatosis. *Proc Natl Acad Sci USA* **102**, 8955–8960.

Devalia, V., Carter, K., Walker, A. P., Perkins, S. J., Worwood, M., May, A., and Dooley, J.S. (2002). Autosomal dominant reticuloendothelial iron overload associated with a 3-base pair deletion in the ferroportin 1 gene (SLC11A3). *Blood* **100**, 695–697.

Donovan, A., Brownlie, A., Zhou, Y., Shepard, J., Pratt, S.J., Moynihan, J., Paw, B. H., Drejer, A., Barut, B., Zapata, A*., et al.* (2000). Positional cloning of zebrafish ferroportin1 identifies a conserved vertebrate iron exporter. *Nature* **403**, 776–781.

Donovan, A., Lima, C. A., Pinkus, J. L., Pinkus, G. S., Zon, L. I., Robine, S., and Andrews, N. C. (2005). The iron exporter ferroportin/Slc40a1 is essential for iron homeostasis. *Cell Metabolism* **1**, 191–200.

Drakesmith, H., Schimanski, L. M., Ormerod, E., Merryweather-Clarke, A. T., Viprakasit, V., Edwards, J. P., Sweetland, E., Bastin, J. M., Cowley, D., Chinthammitr, Y*., et al.* (2005). Resistance to hepcidin is conferred by hemochromatosis-associated mutations of ferroportin. *Blood* **106**, 1092–1097.

Farnaud, S., Patel, A., and Evans, R. W. (2006). Modelling of a metal-containing hepcidin. *Biometals* **19**, 527–533.

Farnaud, S., Rapisarda, C., Bui, T., Drake, A., Cammack, R., and Evans, R. W. (2008). Identification of an iron-hepcidin complex. *Biochem J* **413**, 553–557.

Feder, J. N., Gnirke, A., Thomas, W., Tsuchihashi, Z., Ruddy, D.A., Basava, A., Dormishian, F., Domingo, R., Jr., Ellis, M. C., Fullan, A.*, et al.* (1996). A novel MHC class I-like gene is mutated in patients with hereditary haemochromatosis. *Nat Genet* **13**, 399–408.

Feder, J. N., Penny, D. M., Irrinki, A., Lee, V. K., Lebron, J. A., Watson, N., Tsuchihashi, Z., Sigal, E., Björkman, P. J., and Schatzman, R. C. (1998). The hemochromatosis gene product complexes with the transferrin receptor and lowers its affinity for ligand binding. *Proc Natl Acad Sci USA* **95**, 1472–1477.

Feder, J. N., Tsuchihashi, Z., Irrinki, A., Lee, V. K., Mapa, F. A., Morikang, E., Prass, C. E., Starnes, S. M., Wolff, R. K., Parkkila, S.*, et al.* (1997). The hemochromatosis founder mutation in HLA-H disrupts ß2-microglobulin interaction and cell surface expression. *J Biol Chem* **272**, 14025–14028.

Finch, C. (1994). Regulators of iron balance in humans. *Blood* **84**, 1697–1702.

Fleming, M. D., Trenor, C. C., Su, M. A., Foernzler, D., Beier, D. R., Dietrich, W. F., and Andrews, N. C. (1997). Microcytic anaemia mice have a mutation in Nramp2, a candidate iron transporter gene. *Nature Genetics* **16**, 383–386.

Frazer, D. M., Wilkins, S. J., Becker, E. M., Murphy, T. L., Vulpe, C. D., McKie, A. T., and Anderson, G. J. (2003). A rapid decrease in the expression of DMT1 and Dcytb but not Ireg1 or hephaestin explains the mucosal block phenomenon of iron absorption. *Gut* **52**, 340–346.

Frazer, D. M., Wilkins, S. J., Millard, K. N., McKie, A. T., Vulpe, C. D., and Anderson, G. J. (2004). Increased hepcidin expression and hypoferraemia associated with an acute phase response are not affected by inactivation of HFE. *Br J Haematol* **126**, 434–436.

Galy, B., Ferring-Appel, D., Kaden, S., Grone, H. J., and Hentze, M. W. (2008). Iron regulatory proteins are essential for intestinal function and control key iron absorption molecules in the duodenum. *Cell Metabolism* **7**, 79–85.

Ganz, T. (2008). Iron homeostasis: fitting the puzzle pieces together. *Cell Metabolism* **7**, 288–290.

Gao, J., Zhao, N., Knutson, M. D., and Enns, C. A. (2008). The hereditary hemochromatosis protein, HFE, inhibits iron uptake via down-regulation of Zip14 in HepG2 cells. *J Biol Chem* **283**, 21462–21468.

Giannetti, A. M., and Björkman, P. J. (2004). HFE and transferrin directly compete for transferrin receptor in solution and at the cell surface. *J Biol Chem* **279**, 25866–25875.

Giannetti, A. M., Snow, P. M., Zak, O., and Björkman, P. J. (2003). Mechanism for multiple ligand recognition by the human transferrin receptor. *PLoS Biol* **1**, 341–350.

Girelli, D., De Domenico, I., Bozzini, C., Campostrini, N., Busti, F., Castagna, A., Soriani, N., Cremonesi, L., Ferrari, M., Colombari, R*., et al.* (2008). Clinical, pathological, and molecular correlates in ferroportin disease: a study of two novel mutations. *J Hepatol* **49**, 664–671.

Goncalves, A. S., Muzeau, F., Blaybel, R., Hetet, G., Driss, F., Delaby, C., Canonne-Hergaux, F., and Beaumont, C. (2006). Wild-type and mutant ferroportins do not form oligomers in transfected cells. *Biochem J* **396**, 265–275.

Gordeuk, V. R., Caleffi, A., Corradini, E., Ferrara, F., Jones, R. A., Castro, O., Onyekwere, O., Kittles, R., Pignatti, E., Montosi, G*., et al.* (2003). Iron overload in Africans and African-Americans and a common mutation in the SCL40A1 (ferroportin 1) gene. *Blood Cells Mol Dis* **31**, 299–304.

Goswami, T., and Andrews, N. C. (2006). Hereditary hemochromatosis protein, HFE, interaction with transferrin receptor 2 suggests a molecular mechanism for mammalian iron sensing. *J Biol Chem* **281**, 28494–28498.

Gunshin, H., Mackenzie, B., Berger, U. V., Gunshin, Y., Romero, M. F., Boron, W. F., Nussberger, S., Gollan, J. L., and Hediger, M. A. (1997). Cloning and characterization of a mammalian proton-coupled metal ion transporter. *Nature* **388**, 482–488.

Halliwell, B., and Gutteridge, J. M. (1990). The antioxidants of human extracellular fluids. *Arch Biochem Biophys* **280**, 1–8.

Harris, Z. L., Takahashi, Y., Miyajima, H., Serizawa, M., MacGillivray, R. T., and Gitlin, J. D. (1995). Aceruloplasminemia: molecular characterization of this disorder of iron metabolism. *Proc Natl Acad Sci USA* **92**, 2539–2543.

Hatefi, Y. (1985). The mitochondrial electron transport and oxidative phosphorylation system. *Annu Rev Biochem* **54**, 1015–1069.

Hetet, G., Devaux, I., Soufir, N., Grandchamp, B., and Beaumont, C. (2003). Molecular analyses of patients with hyperferritinemia and normal serum iron values reveal both L ferritin IRE and 3 new ferroportin (slc11A3) mutations. *Blood* **102**, 1904–1910.

Hunter, H. N., Fulton, D. B., Ganz, T., and Vogel, H. J. (2002). The solution structure of human hepcidin, a peptide hormone with antimicrobial activity that is involved in iron uptake and hereditary hemochromatosis. *J Biol Chem* **277**, 37597–37603.

Jeong, S. Y., and David, S. (2003). Glycosylphosphatidylinositol-anchored ceruloplasmin is required for iron efflux from cells in the central nervous system. *J Biol Chem* **278**, 27144–27148.

Johnson, M. B., and Enns, C. A. (2004). Diferric transferrin regulates transferrin receptor 2 protein stability. *Blood* **104**, 4287–4293.

Jouanolle, A. M., Douabin-Gicquel, V., Halimi, C., Loreal, O., Fergelot, P., Delacour, T., de Lajarte-Thirouard, A. S., Turlin, B., Le Gall, J. Y., Cadet, E*., et al.* (2003). Novel mutation in ferroportin 1 gene is associated with autosomal dominant iron overload. *J Hepatol* **39**, 286–289.

Kaplan, J., and Kushner, J. P. (2000). Mining the genome for iron. *Nature* **403**, 711–713.

Kawabata, H., Yang, R., Hirama, T., Vuong, P. T., Kawano, S., Gombart, A. F., and Koeffler, H. P. (1999). Molecular cloning of transferrin receptor 2. A new member of the transferrin receptor-like family. *J Biol Chem* **274**, 20826–20832.

Kemna, E., Pickkers, P., Nemeth, E., van der Hoeven, H., and Swinkels, D. (2005a). Time-course analysis of hepcidin, serum iron, and plasma cytokine levels in humans injected with LPS. *Blood* **106**, 1864–1866.

Kemna, E., Tjalsma, H., Laarakkers, C., Nemeth, E., Willems, H., and Swinkels, D. (2005b). Novel urine hepcidin assay by mass spectrometry. *Blood* **106**, 3268–3270.

Kemna, E., Kartikasari, A. E., van Tits, L. J., Pickkers, P., Tjalsma, H., and Swinkels, D. W. (2008). Regulation of hepcidin: insights from biochemical analyses on human serum samples. *Blood Cells Mol Dis* **40**, 339–346.

Krause, A., Neitz, S., Magert, H. J., Schulz, A., Forssmann, W. G., Schulz-Knappe, P., and Adermann, K. (2000). LEAP-1, a novel highly disulfide-bonded human peptide, exhibits antimicrobial activity. *FEBS Lett* **480**, 147–150.

Larkin, M. A., Blackshields, G., Brown, N. P., Chenna, R., McGettigan, P. A., McWilliam, H., Valentin, F., Wallace, I. M., Wilm, A., Lopez, R.*, et al.* (2007). Clustal W and Clustal X version 2.0. *Bioinformatics* **23**, 2947–2948.

Lebron, J. A., Bennett, M. J., Vaughn, D. E., Chirino, A. J., Snow, P. M., Mintier, G. A., Feder, J. N., and Björkman, P. J. (1998). Crystal structure of the hemochromatosis protein HFE and characterization of its interaction with transferrin receptor. *Cell* **93**, 111–123.

Lee, P., Peng, H., Gelbart, T., and Beutler, E. (2004). The IL-6- and lipopolysaccharide-induced transcription of hepcidin in HFE-, transferrin receptor 2-, and beta 2-microglobulin-deficient hepatocytes. *Proc Natl Acad Sci USA* **101**, 9263–9265.

Lee, P. L., Gelbart, T., West, C., and Barton, J. C. (2007). SLC40A1 c.1402G→A results in aberrant splicing, ferroportin truncation after glycine 330, and an autosomal dominant hemochromatosis phenotype. *Acta Haematol* **118**, 237–241.

Lin, L., Goldberg, Y. P., and Ganz, T. (2005). Competitive regulation of hepcidin mRNA by soluble and cell-associated hemojuvelin. *Blood* **106**, 2884–2889.

Liu, W., Shimomura, S., Imanishi, H., Iwamoto, Y., Ikeda, N., Saito, M., Ohno, M., Hara, N., Yamamoto, T., Nakamura, H*., et al.* (2005a). Hemochromatosis with mutation of the ferroportin 1 (IREG1) gene. *Intern Med* **44**, 285–289.

Liu, X. B., Yang, F., and Haile, D. J. (2005b). Functional consequences of ferroportin 1 mutations. *Blood Cells Mol Dis* **35**, 33–46.

Lymboussaki, A., Pignatti, E., Montosi, G., Garuti, C., Haile, D. J., and Pietrangelo, A. (2003). The role of the iron responsive element in the control of ferroportin1/IREG1/ MTP1 gene expression. *J Hepatol* **39**, 710–715.

McGregor, J. A., Shayeghi, M., Vulpe, C. D., Anderson, G. J., Pietrangelo, A., Simpson, R. J., and Mckie, A. T. (2005). Impaired iron transport activity of ferroportin 1 in hereditary iron overload. *Journal of Membrane Biology* **206**, 3–7.

McKie, A. T., Barrow, D., Latunde-Dada, G. O., Rolfs, A., Sager, G., Mudaly, E., Mudaly, M., Richardson, C., Barlow, D., Bomford, A*., et al.* (2001). An iron-regulated ferric reductase associated with the absorption of dietary iron. *Science* **291**, 1755–1759.

McKie, A. T., Marciani, P., Rolfs, A., Brennan, K., Wehr, K., Barrow, D., Miret, S., Bomford, A., Peters, T. J., Farzaneh, F*., et al.* (2000). A Novel Duodenal Iron-Regulated Transporter, IREG1, Implicated in the Basolateral Transfer of Iron to the Circulation. *Molecular Cell* **5**, 299–309.

Montosi, G., Donovan, A., Totaro, A., Garuti, C., Pignatti, E., Cassanelli, S., Trenor, C. C., Gasparini, P., Andrews, N. C., and Pietrangelo, A. (2001). Autosomal-dominant hemochromatosis is associated with a mutation in the ferroportin (SLC11A3) gene. *J Clin Invest* **108**, 619–623.

Muckenthaler, M. U. (2008). Fine tuning of hepcidin expression by positive and negative regulators. *Cell Metabolism* **8**, 1–3.

Murray, P. J. (2007). The JAK-STAT signaling pathway: input and output integration. *J Immunol* **178**, 2623–2629.

Nemeth, E. (2008). Iron regulation and erythropoiesis. *Curr Opin Hematol* **15**, 169–175.

Nemeth, E., Rivera, S., Gabayan, V., Keller, C., Taudorf, S., Pedersen, B. K., and Ganz, T. (2004a). IL-6 mediates hypoferremia of inflammation by inducing the synthesis of the iron regulatory hormone hepcidin. *J Clin Invest* **113**, 1271–1276.

Nemeth, E., Roetto, A., Garozzo, G., Ganz, T., and Camaschella, C. (2005). Hepcidin is decreased in TFR2 hemochromatosis. *Blood* **105**, 1803–1806.

Nemeth, E., Tuttle, M. S., Powelson, J., Vaughn, M. B., Donovan, A., Ward, D. M., Ganz, T., and Kaplan, J. (2004b). Hepcidin regulates cellular iron efflux by binding to ferroportin and inducing its internalization. *Science* **306**, 2090–2093.

Nicolas, G., Chauvet, C., Viatte, L., Danan, J. L., Bigard, X., Devaux, I., Beaumont, C., Kahn, A., and Vaulont, S. (2002). The gene encoding the iron regulatory peptide hepcidin is regulated by anemia, hypoxia, and inflammation. *J Clin Invest* **110**, 1037–1044.

Njajou, O. T., de Jong, G., Berghuis, B., Vaessen, N., Snijders, P., Goossens, J. P., Wilson, J. H. P., Breuning, M. H., Oostra, B. A., Heutink, P*., et al.* (2002). Dominant hemochromatosis due to N144H mutation of SLC11A3: Clinical and biological characteristics. *Blood Cells Mol Dis* **29**, 439–443.

Njajou, O. T., Vaessen, N., Joosse, M., Berghuis, B., van Dongen, J. W., Breuning, M. H., Snijders, P. J., Rutten, W. P., Sandkuijl, L. A., Oostra, B. A*., et al.* (2001). A mutation in

SLC11A3 is associated with autosomal dominant hemochromatosis. *Nat Genet* **28**, 213–214.

Ohgami, R. S., Campagna, D. R., McDonald, A., and Fleming, M. D. (2006). The Steap proteins are metalloreductases. *Blood* **108**, 1388–1394.

Olynyk, J. K., Cullen, D. J., Aquilia, S., Rossi, E., Summerville, L., and Powell, L. W. (1999). A population-based study of the clinical expression of the hemochromatosis gene. *N Engl J Med* **341**, 718–724.

Origa, R., Galanello, R., Ganz, T., Giagu, N., Maccioni, L., Faa, G., and Nemeth, E. (2007). Liver iron concentrations and urinary hepcidin in beta-thalassemia. *Haematologica* **92**, 583–588.

Pak, M., Lopez, M. A., Gabayan, V., Ganz, T., and Rivera, S. (2006). Suppression of hepcidin during anemia requires erythropoietic activity. *Blood* **108**, 3730–3735.

Papanikolaou, G., Samuels, M. E., Ludwig, E. H., MacDonald, M. L., Franchini, P. L., Dube, M. P., Andres, L., MacFarlane, J., Sakellaropoulos, N., Politou, M.*, et al.* (2004). Mutations in HFE2 cause iron overload in chromosome 1q-linked juvenile hemochromatosis. *Nat Genet* **36**, 77–82.

Park, C. H., Valore, E. V., Waring, A. J., and Ganz, T. (2001). Hepcidin, a urinary antimicrobial peptide synthesized in the liver. *J Biol Chem* **276**, 7806–7810.

Peyssonnaux, C., Zinkernagel, A. S., Schuepbach, R. A., Rankin, E., Vaulont, S., Haase, V. H., Nizet, V., and Johnson, R. S. (2007). Regulation of iron homeostasis by the hypoxia-inducible transcription factors (HIFs). *J Clin Invest* **117**, 1926–1932.

Pietrangelo, A. (2004). The ferroportin disease. *Blood Cells Mol Dis* **32**, 131–138.

Pietrangelo, A. (2007). Hemochromatosis: an endocrine liver disease. *Hepatology* **46**, 1291–1301.

Pietrangelo, A., Montosi, G., Totaro, A., Garuti, C., Conte, D., Cassanelli, S., Fraquelli, M., Sardini, C., Vasta, F., and Gasparini, P. (1999). Hereditary hemochromatosis in adults without pathogenic mutations in the hemochromatosis gene. *N Engl J Med* **341**, 725–732.

Pigeon, C., Ilyin, G., Courselaud, B., Leroyer, P., Turlin, B., Brissot, P., and Loreal, O. (2001). A new mouse liver-specific gene, encoding a protein homologous to human antimicrobial peptide hepcidin, is overexpressed during iron overload. *J Biol Chem* **276**, 7811–7819.

Pignatti, E., Mascheroni, L., Sabelli, M., Barelli, S., Biffo, S., and Pietrangelo, A. (2006). Ferroportin is a monomer in vivo in mice. *Blood Cells Mol Dis* **36**, 26–32.

Rees, D. C., and Howard, J. B. (2000). Nitrogenase: standing at the crossroads. *Curr Opin Chem Biol* **4**, 559–566.

Rice, A. E., Mendez, M. J., Hokanson, C. A., Rees, D. C., and Björkman, P. J. (2009). Investigation of the biophysical and cell biological properties of ferroportin, a multipass integral membrane protein iron exporter. *J Mol Biol* **386**, 717–732.

Rivard, S. R., Lanzara, C., Grimard, D., Carella, M., Simard, H., Ficarella, R., Simard, R., D'Adamo, A. P., De Braekeleer, M., and Gasparini, P. (2003a). Autosomal dominant reticuloendothelial iron overload (HFE type 4) due to a new missense mutation in the FERROPORTIN 1 gene (SLC11A3) in a large French-Canadian family. *Haematologica* **88**, 824–826.

Rivard, S. R., Lanzara, C., Grimard, D., Carella, M., Simard, H., Ficarella, R., Simard, R., D'Adamo, A. P., Ferec, C., Camaschella, C.*, et al.* (2003b). Juvenile hemochromatosis locus maps to chromosome 1q in a French Canadian population. *Eur J Hum Genet* **11**, 585–589.

Robb, A., and Wessling-Resnick, M. (2004). Regulation of transferrin receptor 2 protein levels by transferrin. *Blood* **104**, 4294–4299.

Robson, K. J. H., Merryweather-Clarke, A. T., Cadet, E., Viprakasit, V., Zaahl, M. G., Pointon, J. J., Weatherall, D. J., and Rochette, J. (2004). Recent advances in

understanding haemochromatosis: a transition state. *Journal of Medical Genetics* **41**, 721–730.

Roetto, A., Merryweather-Clarke, A. T., Daraio, F., Livesey, K., Pointon, J. J., Barbabietola, G., Piga, A., Mackie, P. H., Robson, K. J., and Camaschella, C. (2002). A valine deletion of ferroportin 1: a common mutation in hemochromastosis type 4. *Blood* **100**, 733–734.

Roetto, A., Papanikolaou, G., Politou, M., Alberti, F., Girelli, D., Christakis, J., Loukopoulos, D., and Camaschella, C. (2003). Mutant antimicrobial peptide hepcidin is associated with severe juvenile hemochromatosis. *Nature Genetics* **33**, 21–22.

Rolfs, A., Bonkovsky, H. L., Kohlroser, J. G., McNeal, K., Sharma, A., Berger, U. V., and Hediger, M. A. (2002). Intestinal expression of genes involved in iron absorption in humans. *Am J Physiol Gastrointest Liver Physiol* **282**, G598–607.

Roy, C. N., and Enns, C. A. (2000). Iron homeostasis: new tales from the crypt. *Blood* **96**, 4020–4027.

Sayers, M. H., English, G., and Finch, C. (1994). Capacity of the store-regulator in maintaining iron balance. *Am J Hematol* **47**, 194–197.

Schimanski, L. M., Drakesmith, H., Merryweather-Clarke, A. T., Viprakasit, V., Edwards, J. P., Sweetland, E., Bastin, J. M., Cowley, D., Chinthammitr, Y., Robson, K. J*., et al.* (2005). In vitro functional analysis of human ferroportin (FPN) and hemochromatosis-associated FPN mutations. *Blood* **105**, 4096–4102.

Schimanski, L. M., Drakesmith, H., Talbott, C., Horne, K., James, J. R., Davis, S. J., Sweetland, E., Bastin, J., Cowley, D., and Townsend, A. R. (2008). Ferroportin: Lack of evidence for multimers. *Blood Cells Mol Dis* **40**, 360–369.

Schmidt, P. J., Toran, P. T., Giannetti, A. M., Björkman, P. J., and Andrews, N. C. (2008). The transferrin receptor modulates Hfe-dependent regulation of hepcidin expression. *Cell Metabolism* **7**, 205–214.

Sham, R. L., Phatak, P. D., West, C., Lee, P., Andrews, C., and Beutler, E. (2005). Autosomal dominant hereditary hemochromatosis associated with a novel ferroportin mutation and unique clinical features. *Blood Cells Mol Dis* **34**, 157–161.

Silvestri, L., Pagani, A., Nai, A., De Domenico, I., Kaplan, J., and Camaschella, C. (2008). The serine protease matriptase-2 (TMPRSS6) inhibits hepcidin activation by cleaving membrane hemojuvelin. *Cell Metabolism* **8**, 502–511.

Tanno, T., Bhanu, N. V., Oneal, P. A., Goh, S. H., Staker, P., Lee, Y. T., Moroney, J. W., Reed, C. H., Luban, N. L., Wang, R. H*., et al.* (2007). High levels of GDF15 in

thalassemia suppress expression of the iron regulatory protein hepcidin. *Nat Med* **13**, 1096–1101.

Tezcan, F. A., Kaiser, J. T., Mustafi, D., Walton, M. Y., Howard, J. B., and Rees, D. C. (2005). Nitrogenase complexes: multiple docking sites for a nucleotide switch protein. *Science* **309**, 1377–1380.

Theil, E. C. (1987). Ferritin: structure, gene regulation, and cellular function in animals, plants, and microorganisms. *Annu Rev Biochem* **56**, 289–315.

Vokurka, M., Krijt, J., Sulc, K., and Necas, E. (2006). Hepcidin mRNA levels in mouse liver respond to inhibition of erythropoiesis. *Physiol Res* **55**, 667–674.

Vulpe, C. D., Kuo, Y. M., Murphy, T. L., Cowley, L., Askwith, C., Libina, N., Gitschier, J., and Anderson, G. J. (1999). Hephaestin, a ceruloplasmin homologue implicated in intestinal iron transport, is defective in the sla mouse. *Nat Genet* **21**, 195–199.

Wagner, T. U. (2007). Bone morphogenetic protein signaling in stem cells—one signal, many consequences. *The FEBS journal* **274**, 2968–2976.

Wallace, D. F., Clark, R. M., Harley, H. A., and Subramaniam, V. N. (2004). Autosomal dominant iron overload due to a novel mutation of ferroportin1 associated with parenchymal iron loading and cirrhosis. *J Hepatol* **40**, 710–713.

Wallace, D. F., Pedersen, P., Dixon, J. L., Stephenson, P., Searle, J. W., Powell, L. W., and Subramaniam, V. N. (2002). Novel mutation in ferroportin1 is associated with autosomal dominant hemochromatosis. *Blood* **100**, 692–694.

Wang, R. H., Li, C., Xu, X., Zheng, Y., Xiao, C., Zerfas, P., Cooperman, S., Eckhaus, M., Rouault, T., Mishra, L*., et al.* (2005). A role of SMAD4 in iron metabolism through the positive regulation of hepcidin expression. *Cell Metabolism* **2**, 399–409.

West, A. P., Bennett, M. J., Sellers, V. M., Andrews, N. C., Enns, C. A., and Björkman, P. J. (2000). Comparisons of the interactions of transferrin receptor and transferrin receptor 2 with transferrin and the hereditary hemochromatosis protein HFE. *J Biol Chem* **275**, 38135–38138.

Wrighting, D. M., and Andrews, N. C. (2006). Interleukin-6 induces hepcidin expression through STAT3. *Blood* **108**, 3204–3209.

Chapter 2:

Investigation of the Biophysical and Cell Biological Properties of Ferroportin, a Multipass Integral Membrane Protein Iron Exporter

In this paper we report the over-expression, purification, biophysical, and cell biological characterization of recombinant human ferroportin. Michael Mendez and Craig Hokanson brought with them expertise in the expression of membrane proteins using baculovirus-infected insect cells and helped get this system started for ferroportin expression.

JMB

Available online at www.sciencedirect.com

ScienceDirect

ELSEVIER

Investigation of the Biophysical and Cell Biological Properties of Ferroportin, a Multipass Integral Membrane Protein Iron Exporter

Adrian E. Rice[1], Michael J. Mendez[2,3], Craig A. Hokanson[2], Douglas C. Rees[3,4] and Pamela J. Björkman[2,4]*

[1]*Graduate Option in Biochemistry and Molecular Biophysics, California Institute of Technology, Pasadena, CA 91125, USA*

[2]*Division of Biology, California Institute of Technology, Pasadena, CA 91125, USA*

[3]*Division of Chemistry and Chemical Engineering, California Institute of Technology, Pasadena, CA 91125, USA*

[4]*Howard Hughes Medical Institute, California Institute of Technology, Pasadena, CA 91125, USA*

Ferroportin is a multipass membrane protein that serves as an iron exporter in many vertebrate cell types. Ferroportin-mediated iron export is controlled by the hormone hepcidin, which binds ferroportin, causing its internalization and degradation. Mutations in ferroportin cause a form of the iron overload hereditary disease hemochromatosis. Relatively little is known about ferroportin's properties or the mechanism by which mutations cause disease. In this study, we expressed and purified human ferroportin to characterize its biochemical/biophysical properties in solution and conducted cell biological studies in mammalian cells. We found that purified detergent-solubilized ferroportin is a well-folded monomer that binds hepcidin. In cell membranes, the N- and C-termini were both cytosolic, implying an even number of transmembrane regions, and ferroportin was mainly localized to the plasma membrane. Hepcidin addition resulted in a redistribution of ferroportin to intracellular compartments that labeled with early endosomal and lysosomal, but not Golgi, markers and that trafficked along microtubules. An analysis of 16 disease-related ferroportin mutants revealed that all were expressed and trafficked to the plasma membrane but that some were resistant to hepcidin-induced internalization. The characterizations reported here form a basis upon which models for ferroportin's role in regulating iron homeostasis in health and disease can be interpreted.

Introduction

Hereditary hemochromatosis is an iron overload disease caused by defects in the regulation of cellular and systemic iron levels.[1,2] One type of hemochromatosis, known as type IV hereditary hemochroma-

tosis or ferroportin disease, is caused by missense mutations in the gene encoding the iron export protein ferroportin (Fpn, also known as IREG1 or MTP1; accession number Q9NP59).[3] Fpn is a multipass integral membrane protein found in vertebrates.[4–6] All cell types that export ionic iron express Fpn, including duodenal enterocytes, white blood cells involved in erythrophagocytosis, Kupffer cells, brain astrocytes, and placental cells.[4–7] Although Fpn has been implicated as the iron exporter in these cells, whether this export process is active or passive is unknown. Fpn expression levels are regulated posttranslationally by interaction with hepcidin-25, a peptide hormone[8] produced in the liver[9] and secreted into the blood when iron levels are high.[10] Hepcidin binds to Fpn at the cell surface and is internalized with Fpn.[8] In HEK293T

*Corresponding author. E-mail address:
bjorkman@caltech.edu.

Abbreviations used: DM, *n*-decyl-β-ᴅ-maltoside; DDM, *n*-dodecyl-β-ᴅ-maltoside; SEC, size-exclusion chromatography; LS, light scattering; RI, refractive index; GFP, green fluorescent protein; MDCK, Madin–Darby canine kidney; TM, transmembrane; FSEC, fluorescent SEC; 3D, three-dimensional; PBS, phosphate-buffered saline.

cells, and presumably *in vivo*, the binding of hepcidin to Fpn results in the phosphorylation, ubiquitination, and internalization of Fpn,[11] ultimately leading to its degradation in lysosomes.[8]

Ferroportin disease usually presents as one of two phenotypes—one in which patients display macrophage iron loading, low transferrin iron saturation, and high serum ferritin levels and another in which patients display hepatocyte iron loading and high transferrin saturation. A number of point mutations in the Fpn gene have been identified.[3,12–25] Recent *in vitro* studies focused on characterizing subsets of these mutants in an effort to reveal the nature of the defects caused by the disease-causing Fpn mutations.[26–31]

Here, we report recombinant expression of Fpn in insect cells and a biophysical characterization of purified detergent-solubilized Fpn, including a determination of its oligomeric state and its binding interactions with different forms of hepcidin. We also compared the expression and subcellular localization of wild-type and mutant Fpn's in the presence and in the absence of hepcidin and studied wild-type Fpn-trafficking using live-cell imaging.

Results

Expression and characterization of Fpn expressed in insect cells

Human, mouse, and zebrafish Fpn's were expressed in baculovirus-infected insect cells. Expression constructs were created encoding tagged versions of full-length human, mouse, and zebrafish Fpn's. Addition of an N-terminal Rho tag, the first 20 aa of bovine rhodopsin, which boosts expression levels for some eukaryotic membrane proteins,[32] was required for detectable expression in insect cells. C-terminal FLAG and/or His tags were added to aid in affinity purification, resulting in Rho-Fpn-His-FLAG and Rho-Fpn-His constructs. Insect cell membranes were analyzed by fractionation analysis using a discontinuous sucrose gradient,[33] and Fpn was found in the plasma membranes of infected cells (data not shown). Several detergents could be used to solubilize Fpn from isolated plasma membranes, including [3-[(3-cholamidopropyl)-dimethylammonio]-1-propane-sulfonate (Chaps), 6-cyclohexyl-1-hexyl-β-D-malto-side (CYMAL-6), lauryldimethylamine-*N*-oxide (LDAO) and polyoxyethylene(8)dodecyl ether ($C_{12}E_8$), *n*-decyl-β-D-maltoside (DM), and *n*-dode-cyl-β-D-maltoside (DDM)]. Human Rho-Fpn-His and Rho-Fpn-His-FLAG were purified in DM or DDM using affinity chromatography with yields of ~50–100 μg of Fpn per liter of insect cell culture. Similar results were obtained for mouse and zebrafish Fpn's, but the analyses reported in the remainder of this study were conducted using human Fpn. More highly purified Fpn was obtained from the Rho-Fpn-His-FLAG construct

using a two-step His/FLAG affinity purification protocol. SDS-PAGE analysis of purified Rho-Fpn-His and Rho-Fpn-His-FLAG revealed a single predominant band migrating with an apparent molecular mass of ~60 kDa (Fig. 1a). Western analysis showed this band to be positive for both the N- and C-terminal tags, thus demonstrating expression of full-length Fpn (data not shown).

To verify biological activity, we evaluated the ability of purified detergent-solubilized human Fpn to bind hepcidin. Rho-Fpn-His was purified from insect cell membranes in DM or DDM on a cobalt affinity resin and then captured on a CM5 biosensor surface with an immobilized anti-Rho antibody. Hepcidin-25 or a non-Fpn-binding version lacking the five N-terminal amino acids (hepcidin-20)[8] was injected at 10 μM. In three independent experiments, we found that ~10-fold more hepcidin-25 than hepcidin-20 bound to the Fpn surface (Fig. 1b). In an attempt to obtain an equilibrium dissociation constant (K_d) for the interaction between Fpn and hepcidin-25, we performed surface plasmon resonance binding experiments between coupled Fpn and a dilution series of hepcidin-25 (0.625–10 μM) (Fig. 1b). While the data did not fit well to a 1:1 binding model, presumably due to complex binding events related to aggregation of the injected hepcidin (see Materials and Methods), the results suggested a low micromolar K_d.

Detergent-solubilized Fpn is monomeric

In order to determine the molecular mass and hence the oligomeric state of purified Fpn, we performed size-exclusion chromatography (SEC) in conjunction with multiangle light scattering (LS), differential refractive index (RI), and ultraviolet absorption (UV) spectroscopy analysis.[34] SEC-LS/UV/RI can be used to determine the absolute molecular mass of a protein in complex with non-UV-absorbing modifiers, such as carbohydrates, lipids, and detergents.[34,35] Purified human Fpn (Rho-Fpn-His-FLAG) solubilized in DDM was used for these experiments. The UV chromatogram for Fpn was observed as a single peak at ~13.5 mL, whereas the LS and RI traces were both doublets, with one peak at ~13.5 mL and another at ~15.5 mL (Fig. 1c). The first peak in the doublets overlaid with the UV peak and corresponded to the Fpn–detergent micelle complex, while the second peak corresponded to free detergent micelles. The free-micelle peak of DDM detergent gave a calculated molecular mass of 75.8±6.8 kDa, consistent with the DDM micelle size measured by the vendor†. Although the Fpn–detergent peak was not fully resolved from the DDM free-micelle peak, large regions of each peak were sufficiently separated and could be selected for analysis (Fig. 1c). The molecular mass of the Fpn–detergent complex determined using this method was 201±18 kDa, with 69.1±6.2 kDa of this
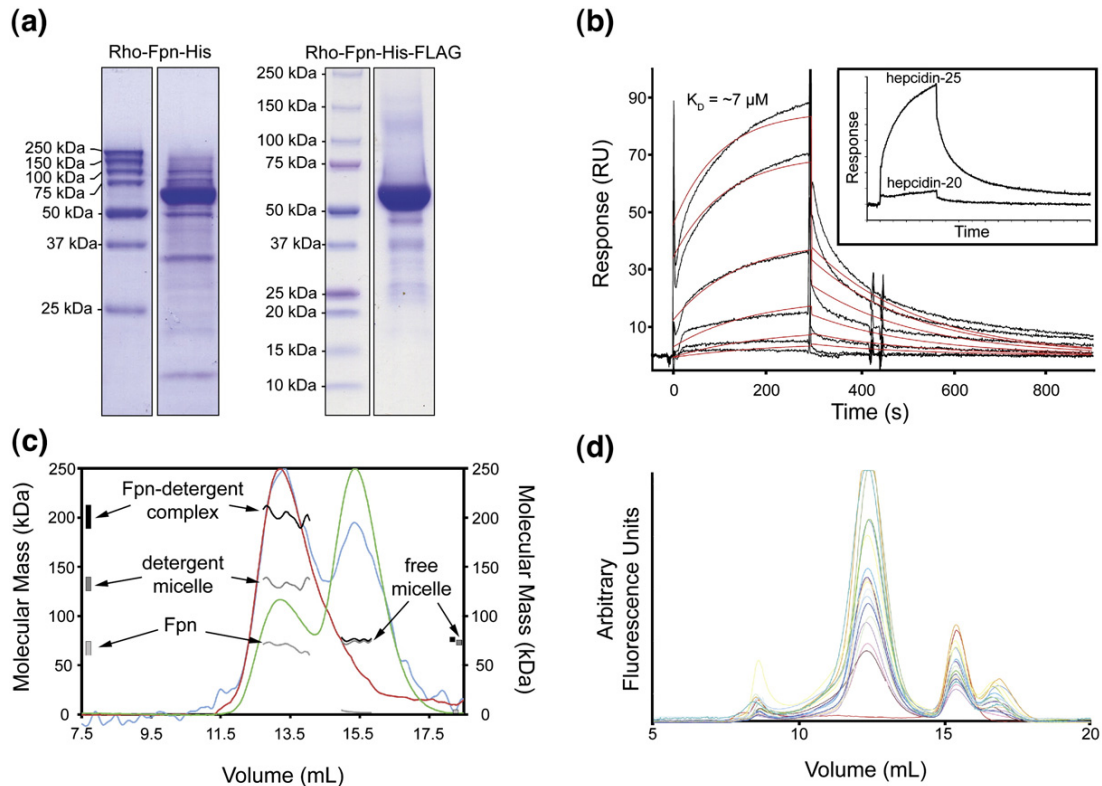
---

† http://www.anatrace.com

Fig. 1. Biophysical characterization of purified Fpn. (a) SDS-PAGE analysis of purified Rho-Fpn-His (estimated to be ~70% pure) and Rho-Fpn-His-FLAG (estimated to be ~90% pure) proteins. Samples were run under reducing conditions in SDS loading buffer without boiling on 15% (Rho-Fpn-His) or 4%–20% (Rho-Fpn-His-FLAG) polyacrylamide gels. (b) Biosensor analysis of the Fpn–hepcidin interaction. Hepcidin-25 was injected over immobilized Fpn as a series of dilutions (0.625, 1.25, 2.5, 5.0, 8.0, and 10 μM). Sensorgrams (black lines) are overlaid on the simulated response (red lines) derived using a 1:1 binding model. The fit of the binding model to the data is poor, perhaps resulting from the presence of hepcidin-25 aggregates. The inset shows results from injections of 10 μM hepcidin-25 and hepcidin-20. (c) SEC-LS/UV/RI analysis of DDM-solubilized Fpn. Normalized traces for UV absorbance at 280 nm (red), 90° LS signal (blue), and differential RI (green) signals are shown. Molecular mass values calculated for the protein–detergent complex (black), detergent micelle (dark gray), and protein (light gray) are displayed as overlays on the peaks at ~13.5 and ~15.5 mL, and the range of calculated molecular masses is projected onto the left and right axes. (d) Comparison of mobility by FSEC for wild-type Fpn *versus* disease-related Fpn mutants. Wild-type Fpn and 16 Fpn mutants were transiently expressed as GFP fusion proteins in HEK293T cells. Whole cell lysates were passed over a gel filtration column, and the migration of each protein was monitored by fluorescence. Wild-type Fpn-GFP and all the Fpn-GFP mutants exhibited a peak at ~12 mL, which was not found in lysates from untransfected HEK293T cells (red curve). The peak at ~16 mL was found in samples prepared from both transfected and untransfected cells.

attributed to protein and 132±12 kDa attributed to bound detergent plus lipids and/or carbohydrate. The molecular mass derived for the protein component of the Fpn–detergent complex is in agreement with the predicted molecular mass of 69,015 g/mol for Rho-Fpn-His-FLAG, thus suggesting that detergent-solubilized Fpn is a monomer.

Topology of Fpn in the plasma membrane

The locations of the N- and C-termini of Fpn have been the subject of debate, with some studies finding one or both termini to be extracellular[27,28,36] and others finding one or both termini to be intracellular.[26,37,38] In order to resolve this issue, we expressed N- and C-terminally tagged Fpn [Rho-Fpn-GFP (green fluorescent protein)] in three mam-

malian cell lines and used confocal immunofluorescence microscopy to compare the accessibility of the tags in permeabilized *versus* nonpermeabilized cells. Although the Rho tag was required for expression in insect cells, we found that Fpn could be expressed in mammalian cells without this tag, so we evaluated the location of the C-terminus in independent experiments. If the N- or C-terminus is extracellular, we would expect to find no difference in permeabilized *versus* nonpermeabilized cells when probing with an antibody against the relevant tag. If a terminus was intracellular, we would expect to see antibody staining in permeabilized, but not nonpermeabilized, cells.

Fpn-GFP or Rho-Fpn-GFP constructs were transiently expressed in HEK293T, HeLa, and Madin–Darby canine kidney (MDCK) cells. Both constructs
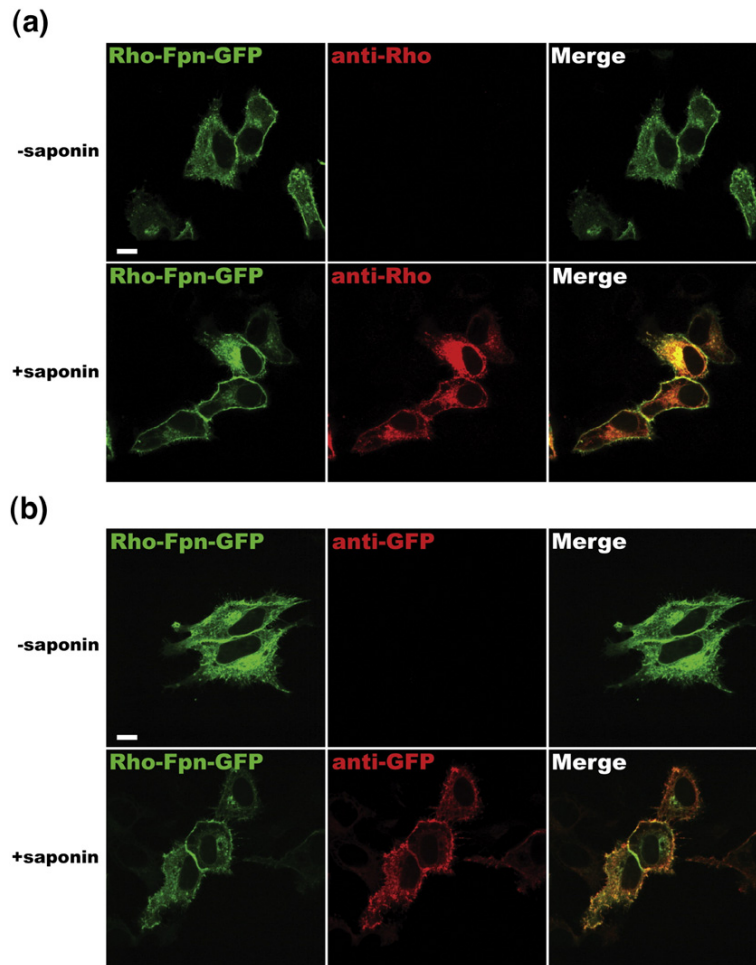
(a)

(b)

Fig. 2. Analysis of Fpn membrane topology. Bar represents 10 μm. Rho-Fpn-GFP was transiently expressed in HeLa cells. Fixed cells were probed against a labeled antibody against the N-terminal Rho tag (a) or against the C-terminal GFP tag (b) under permeabilizing (+saponin) and nonpermeabilizing (−saponin) conditions. Similar results were found for Rho-Fpn-GFP expressed in HEK293T and MDCK cells and for Fpn-GFP expressed in HeLa, HEK293T (Fig. 3), and MDCK cells (data not shown).

were used to determine the location of the C-terminus using a labeled anti-GFP antibody, and the Rho-Fpn-GFP construct was used to determine the location of the N-terminus using a labeled anti-Rho antibody. Full confocal stacks were recorded for each condition, with representative slices displayed in Figs. 2 and 3. GFP fluorescence from the C-terminal tag was visible at the plasma membrane under permeabilizing and nonpermeabilizing conditions, and it served as a marker for successfully transfected cells. Antibody staining of the N-terminal Rho or the C-terminal GFP tag was only observed under permeabilizing conditions or when the plasma membrane was compromised by a visible tear. This result was consistent for both Rho-Fpn-GFP and Fpn-GFP in three cell lines (Figs. 2 and 3). We conclude that the N- and C-termini of Fpn are cytosolic in HeLa, HEK293T, and MDCK cells, implying that Fpn contains an even number of transmembrane (TM) domains.

Disease-related Fpn mutants behave like the wild type in detergent and are expressed at the plasma membrane

To determine if disease-related mutations in Fpn altered its detergent solubility and oligomeric state,

we expressed 16 Fpn-GFP mutants transiently in HEK293T cells and compared them with wild-type Fpn-GFP. Rather than purify each of the mutants and conduct SEC-LS/UV/RI experiments, we used fluorescent SEC (FSEC), a method to obtain a SEC profile of a GFP-tagged protein in a complex mixture of proteins.[39] We found that the FSEC traces for Fpn-GFP and the suite of disease-causing mutant proteins were similar (Fig. 1d). Given that SEC-LS/UV/RI analysis demonstrated that wild-type Fpn is well folded (i.e., it migrates in SEC as a defined peak outside the void volume) and a monomer (Fig. 1c), the finding of similar SEC profiles for wild-type and mutant Fpn's indicates that the mutants were also well-folded monomers that could be solubilized in detergent.

We next determined the subcellular localizations of wild-type and mutant Fpn-GFP proteins expressed transiently in different cell lines. Expression of wild-type Fpn-GFP in polarized cells (filter-grown MDCK cells) revealed that Fpn-GFP was expressed primarily on the cell surface (Fig. 4). Expression was observed along the entire basolateral membrane below the tight junctions, but not at the apical surface, as determined by anti-ZO1 staining of the tight junctions (data not shown). In a nonpolarized cell line (HeLa), fluorescence for wild-type Fpn-
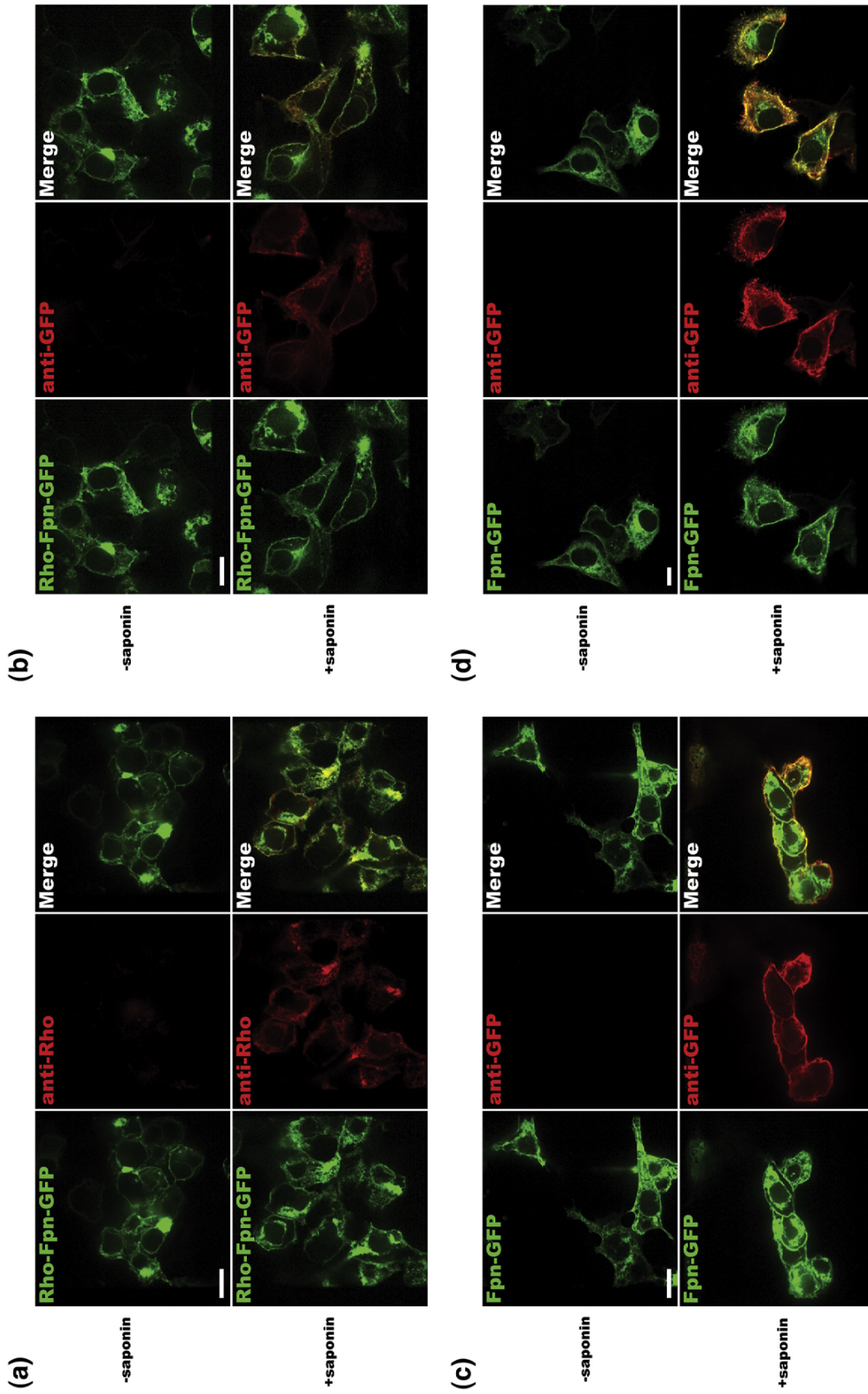
Fig. 3. Analysis of Fpn membrane topology. Bar represents 10 μm. (a and b) Rho-Fpn-GFP was transiently expressed in HEK293T cells. Fixed cells were probed against a labeled antibody against the N-terminal Rho tag (a) or against the C-terminal GFP tag (b) under permeabilizing (+saponin) and nonpermeabilizing (−saponin) conditions. (c and d) Fpn-GFP was transiently expressed in HEK293T (c) or HeLa (d) cells. Fixed cells were probed against a labeled antibody against the C-terminal GFP tag under permeabilizing (+saponin) and nonpermeabilizing (−saponin) conditions.
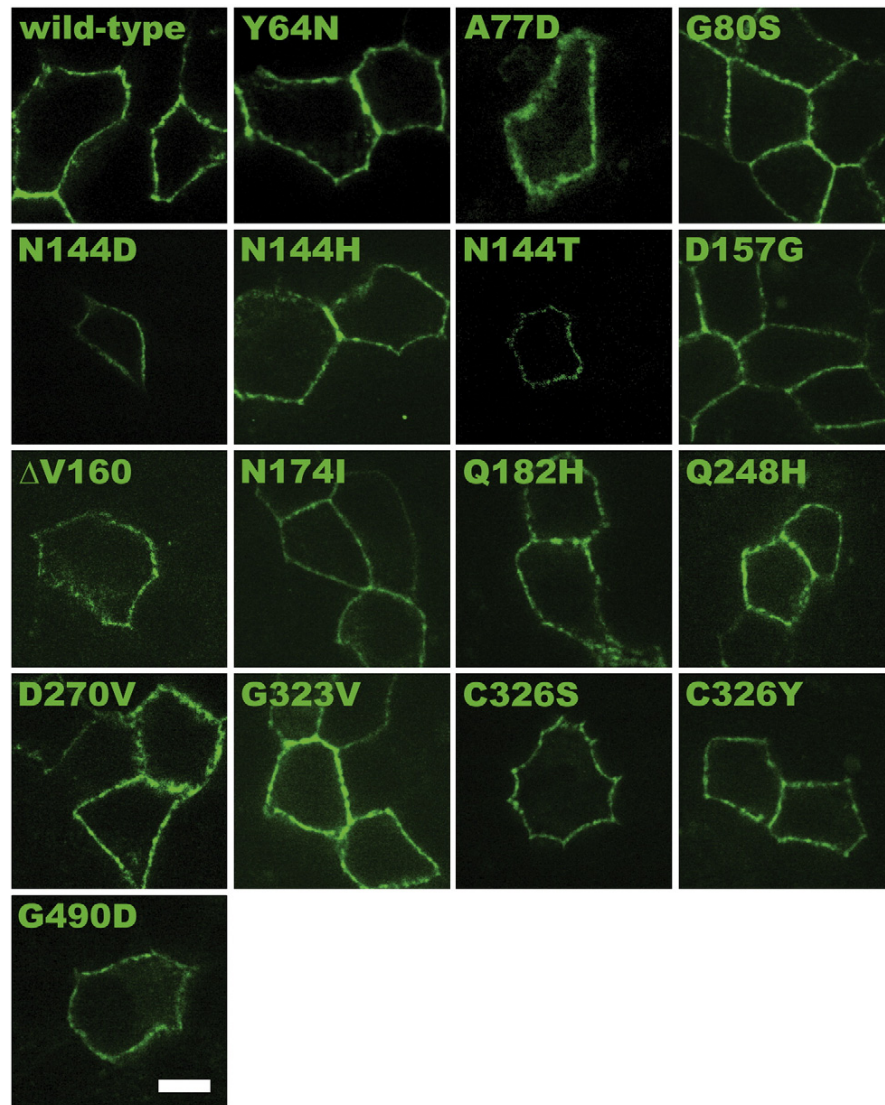
Fig. 4. Fpn-GFP subcellular localization in MDCK cells. Bar represents 10 μm. Fpn-GFP and disease-related Fpn-mutants were transiently expressed in filter-grown polarized MDCK cells.

GFP was found around the entire cell surface as well as in intracellular compartments (Fig. 2), as previously described for expression in HeLa and HEK293T cells.[8] Upon treatment with the protein synthesis inhibitor cycloheximide, a larger proportion of Fpn-GFP localized to the plasma membrane and the intracellular Fpn-GFP signal that remained was faint and diffuse compared with the fluorescence at the plasma membrane (Fig. 5), suggesting that much of the intracellular Fpn-GFP signal observed in untreated cells represented newly synthesized protein on its way to the cell surface.

The localization of each of the disease-related Fpn mutants was examined in cycloheximide-treated HeLa cells (Fig. 5) and in untreated filter-grown polarized MDCK cells (Fig. 4). Each of the mutants localized similarly to wild-type Fpn-GFP (i.e., with little internal fluorescence and a strong cell surface signal). Evidence for the primarily surface localization of Fpn-GFP proteins can be difficult to convey in two-dimensional images of flat HeLa cells, so we present side views of cells for all the Fpn mutants (Fig. 5) and movies of three-dimensional (3D) reconstructions for selected mutants (Movies S1–S5). These data suggested that all the disease-related Fpn mutants examined here trafficked normally to the plasma membrane.

Effects of hepcidin on disease-related Fpn mutants

Previous studies demonstrated that wild-type Fpn is internalized into lysosomes upon treatment with hepcidin-25.[8] To compare the effects of hepcidin on
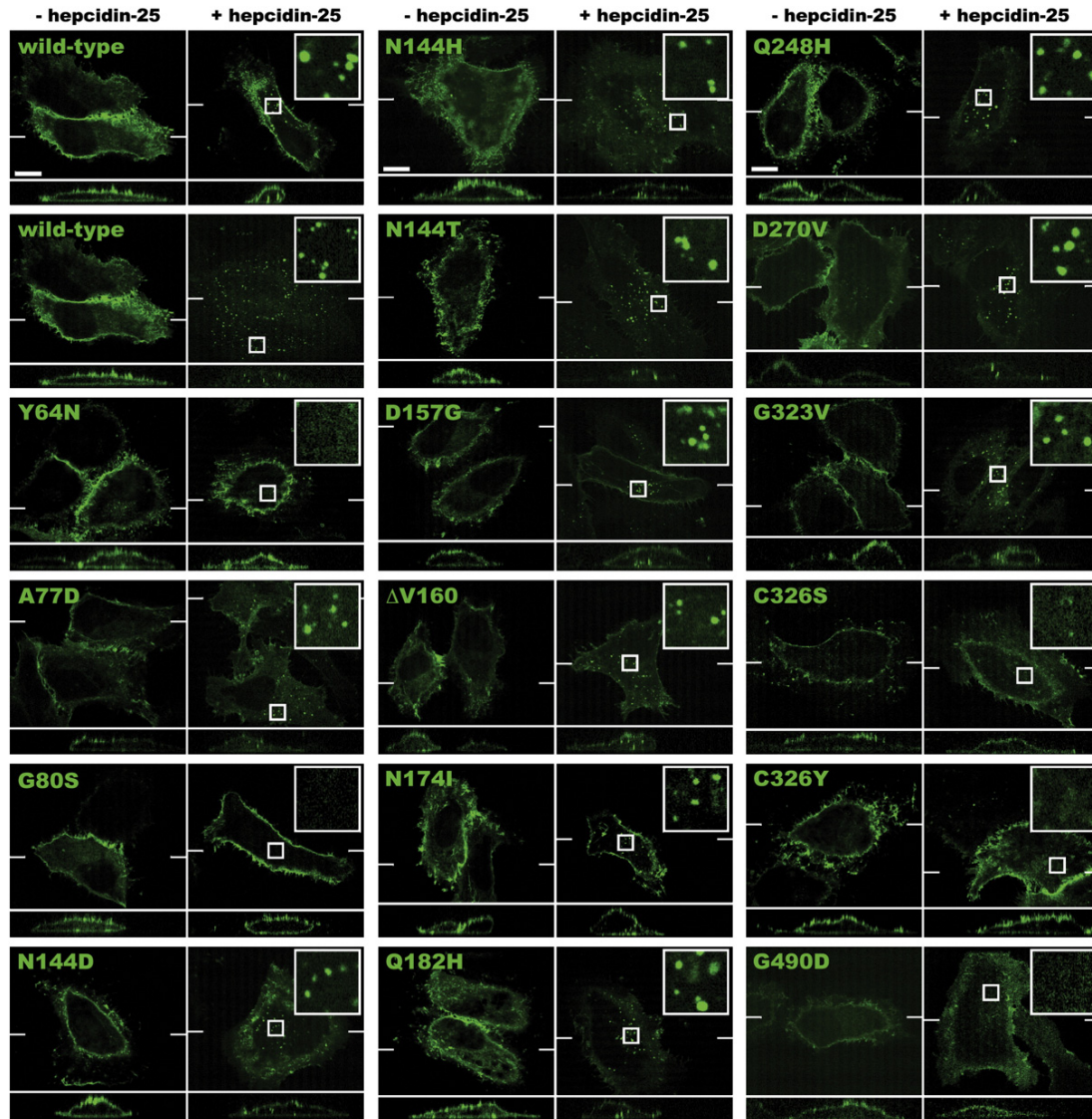
Fig. 5. Fpn-GFP localization and sensitivity to hepcidin-25. Bar represents 10 μm; the inset is shown at a magnification of 5×. Fpn-GFP and disease-related Fpn-GFP mutants were transiently expressed in HeLa cells, which were pretreated with cycloheximide and then incubated for 4 h with or without 2 μM hepcidin-25. Each panel is a representative slice from a confocal stack. Below each panel is a reconstructed side view for the region in a plane denoted by the thin white line in the main panel. The side views were elongated by a factor of 2 in the z-direction to facilitate visualization of fluorescence in these thin cells.

wild-type and mutant Fpn's, we expressed Fpn-GFP proteins transiently in HeLa cells, pretreated the cells with cycloheximide to reduce intracellular fluorescence, and then incubated them in the presence or absence of 2 μM hepcidin-25. After 4 h, the cells were fixed and examined by confocal fluorescence imaging. Wild-type Fpn-GFP was internalized in all cells imaged, but the level of internalization at any tested time point varied from cell to cell. At the 4-h time point used for this study, the GFP signal in some cells was observed as fully internalized puncta, whereas other cells displayed a portion of their GFP signal at the plasma membrane (see the two wild-type Fpn-GFP panels in Fig. 5). The surface signal tended to decrease over time as

the hepcidin-25 incubation progressed (data not shown). We expect that these differences were due to varying levels of Fpn-GFP expression from cell to cell in the transient transfection.

Most of the disease-related Fpn mutants were internalized upon treatment with hepcidin-25 (Fig. 5), with internalization observed as bright puncta throughout the cytoplasm. Hepcidin-sensitive Fpn-GFP constructs included wild-type Fpn and the A77D, N144D, N144H, N144T, D157G, ΔV160, N174I, Q182H, Q248H, D270V, and G323V Fpn mutants. Like wild-type Fpn-GFP, the hepcidin-sensitive Fpn-GFP mutants displayed a distribution of internalization completeness, with some cells within a sample showing residual surface signals.
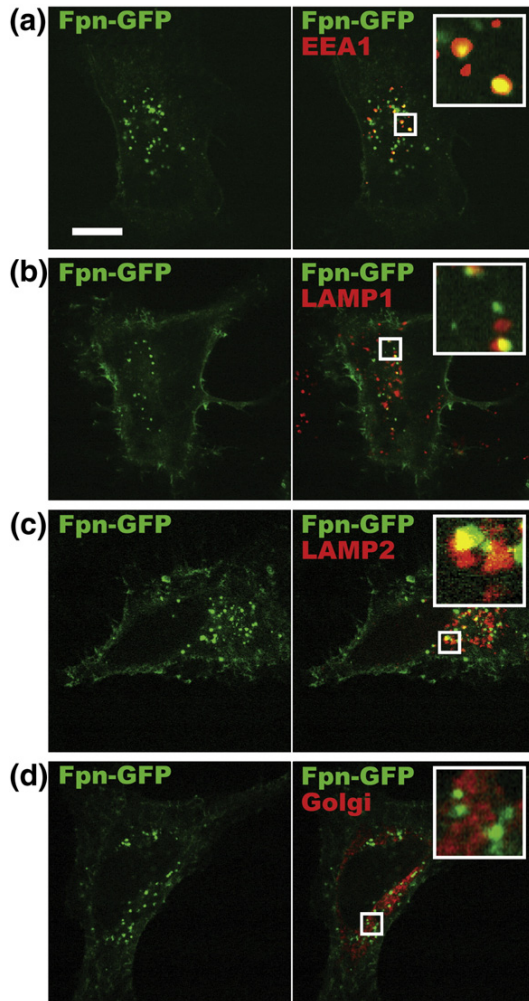
Fig. 6. Mapping of the intracellular locations of hepcidin-internalized Fpn-GFP. Bar represents 10 μm; the inset is at a magnification of 5×. (a–d) Fpn-GFP was transiently expressed in HeLa cells, which were pretreated with cycloheximide and incubated with 2 μM hepcidin-25. Fixed cells were probed with antibodies against markers for early endosomes (EEA1; a), lysosomes (LAMP1 and LAMP2; b and c), and the Golgi (58-kDa Golgi protein; d). LAMP1 staining adjacent to the Fpn-GFP-positive cell in (b) represents endogenous LAMP1 from a neighboring cell that did not express Fpn-GFP.

Representative cells from these experiments can be found in Fig. 5. The Y64N, G80S, C326S, C326Y, and G490D Fpn mutants showed no internalized punctum and were therefore classified as resistant to hepcidin-induced internalization (Fig. 5).

Characterization of hepcidin-induced Fpn internalization in HeLa cells

To further study the pathway by which Fpn is internalized upon treatment with hepcidin, we identified Fpn-positive compartments using antibodies against endosomal and lysosomal markers. For these experiments, wild-type Fpn-GFP was transiently expressed in HeLa cells, pretreated with cycloheximide, and then incubated with hepcidin-25 for 4 h, as described above. Cells were fixed and probed with fluorescent antibodies against the early endosomal marker EEA1, the lysosomal marker LAMP1 or LAMP2, or a 58-kDa Golgi-resident protein. Internalized Fpn-GFP puncta were found to partially co-localize with EEA1, LAMP1, and LAMP2, but not with the 58-kDa Golgi marker (Fig. 6).

Hepcidin-induced internalization of Fpn-GFP was also investigated in live HeLa cells using spinning-disk confocal microscopy, which enables rapid image acquisition to monitor dynamic biological processes.[40] Fpn-expressing HeLa cells were grown in glass-bottomed dishes, and imaging was performed at 37 °C in a temperature-controlled enclosure. Fpn-GFP-positive intracellular compartments, which were observed within 15 min of hepcidin addition, were seen to travel throughout much of the cytoplasm in a relatively random fashion (data not shown). Over the course of hours, accumulation of bright puncta in regions proximal to the nucleus was observed, as seen in the fixed cell images, which were acquired 4 h after hepcidin addition (Fig. 5).

When trafficking was monitored for a shorter time (0.5–5 min), Fpn-GFP compartments traveled in many directions with no apparent net directionality. Interestingly, some of the Fpn-GFP-positive compartments moved back and forth along what
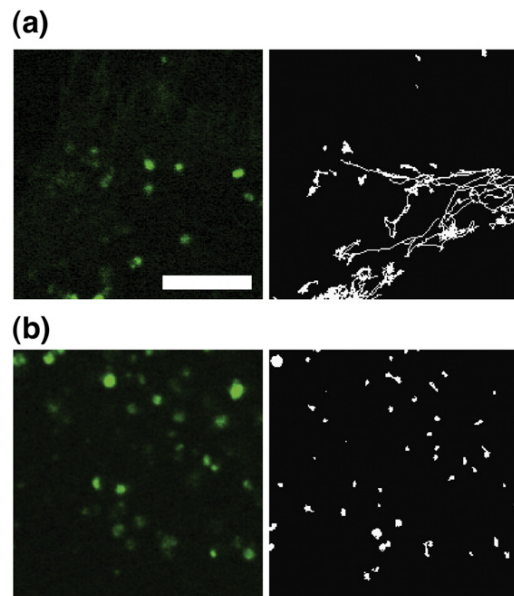
Fig. 7. Effects of nocodazole on internalized Fpn. Bar represents 5 μm. Fpn-GFP was transiently expressed in HeLa cells, which were pretreated with cycloheximide, incubated with 2 μM hepcidin-25, and then imaged live in the presence or absence of 10 μg/mL of nocodazole. GFP-positive compartments were tracked as described in Materials and Methods. Tracks throughout a 90-s time course were overlaid on representative images of an untreated cell (a) or a nocodazole-treated cell (b).

(a)

(b)
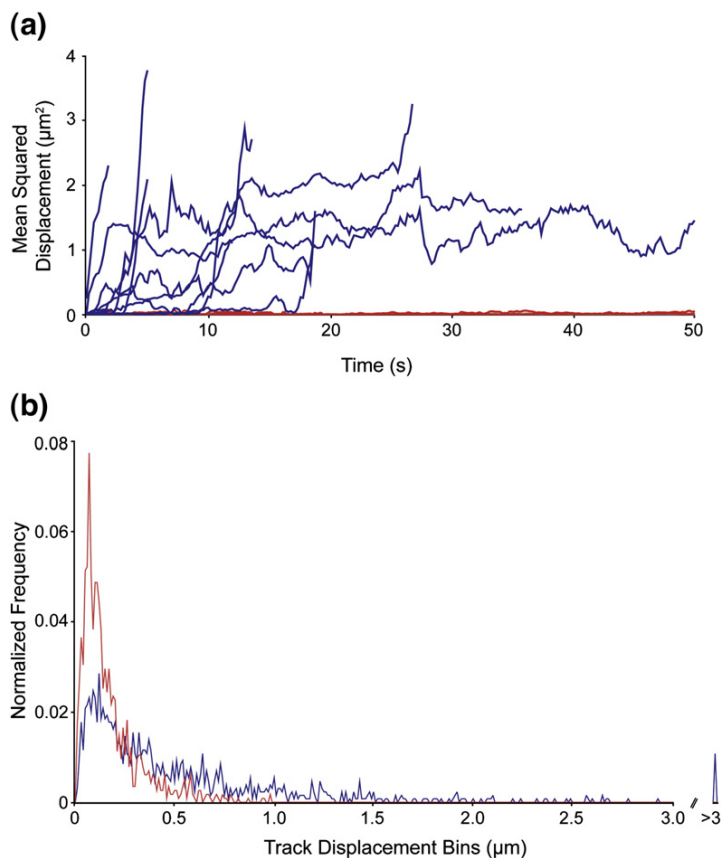
Fig. 8. Tracking Fpn-GFP-positive compartments in HeLa cells in the presence and in the absence of nocodazole. Cells were treated and imaged as described in Fig. 7. (a) The mean-square displacement of representative tracks in untreated (blue) *versus* nocodazole-treated (red) cells showed that nocodazole treatment produced a marked reduction in Fpn-GFP trafficking. (b) Track displacements for the set of tracked vesicles in untreated (blue) and nocodazole-treated (red) cells presented as a histogram.

appeared to be a track. To determine if the tracks represented microtubules, we imaged the cells in the presence and in the absence of the microtubule depolymerizing agent nocodazole. In the presence of nocodazole, trafficking of Fpn-GFP-positive compartments was almost entirely halted (Fig. 7; Movies S6 and S7). Tracking analyses were performed on >1100 Fpn-positive compartments per condition, and the disruption of overall trafficking by nocodazole was evident in terms of a reduction of mean-square displacement for individual compartments (Fig. 8a) and in a reduction of overall track displacement length for the full set of tracks (Fig. 8b). In the presence of nocodazole, no compartment was found more than 0.98 μm from their starting points, whereas in untreated cells, 178 compartments (15.9%) were located at a distance of 1 μm or farther from their starting points.

Discussion

Although Fpn plays a key role in the maintenance and regulation of systemic iron homeostasis, many of its basic features remain controversial. We sought

to characterize some of the biophysical and cell biological properties of Fpn using purified detergent-solubilized protein and Fpn expressed in eukaryotic cells. Here, we report an insect cell expression system that can be used to produce recombinant human Fpn for structural and biophysical studies.

The oligomeric state of Fpn has been debated for several years—the protein has been reported to be a monomer[36,38,41] as well as a dimer/multimer.[30,37] Using SEC-LS/UV/RI, a shape- and model-independent method to obtain a molecular mass,[34] we determined that purified detergent-solubilized Fpn is monomeric (Fig. 1c). This result does not explicitly address the oligomeric state of Fpn in its native environment of the lipid bilayer. However, in previous studies of other membrane proteins, including LacY and GlyT1, the oligomeric state determined for the purified protein in detergent correlated with the oligomeric state in the membrane bilayer.[42,43] Thus, although this result cannot rule out a transient dimerization/multimerization event, it suggests that homophilic interactions that might exist in the context of a bilayer are sufficiently weak so as to be disrupted by a nonionic detergent. A recent report

Extracellular

Fig. 9. Prediction of membrane topology of Fpn. Sequences for full-length human, mouse, and zebrafish Fpn's were submitted to the TMHMM v2.0 prediction server.[46] Each sequence was predicted to contain 12 regions that were 21–23 aa in length with a significant (>60%) probability of being a TM region (see Materials and Methods). TMHMM predicted that the N- and C-termini of Fpn are cytosolic, consistent with our data (Figs. 2 and 3). Highlighted amino acids indicate positions where disease-related mutations have been identified. Red positions indicate hepcidin resistance, whereas blue positions indicate hepcidin sensitivity. Only the C326Y and C326S mutations fall in the hepcidin-binding domain (residues 324–343).[44]

showed that a 19-aa peptide derived from an extracellular loop of Fpn (the hepcidin-binding domain; residues 324–343) is capable of binding hepcidin-25 but not hepcidin-20.[44] In support of the contention that purified Fpn monomers are functional, we showed that purified Fpn exhibits physiologically relevant binding to hepcidin-25 but not hepcidin-20 (Fig. 1b), suggesting that detergent-solubilized Fpn effectively presents the hepcidin-binding domain. Although we were unable to obtain an accurate K_d for the Fpn–hepcidin-25 interaction, the data suggested a low micromolar affinity, consistent with the ~ 0.7 μM IC_{50} value obtained in *in vitro*[8] and *in vivo* experiments in which a serum concentration of 1.4 μM hepcidin-25 induced a prolonged reduction in serum ferritin levels.[45]

The membrane topology of Fpn and the related issue of how many TM domains it contains have also been the subject of debate. In particular, different

results have been obtained for the location of the Fpn C-terminus. Fluorescent antibodies against a C-terminal tag on Fpn have been used to label live cells in flow cytometry experiments,[27,28,36] implying an extracellular location. Immunofluorescence microscopy has been used to suggest both an extracellular[36] and an intracellular[26,37,38] localization for the Fpn C-terminus. Our results using two ferroportin constructs in three mammalian cell lines strongly support an intracellular location for the N- and C-termini of Fpn. A recent report may explain the discrepancy in the studies regarding the accessibility of the Fpn termini: the C-terminus of Fpn was found to be normally cytosolic but accessible to labeled antibodies in nonpermeabilized cells when the cells were undergoing apoptosis due to reduced intracellular iron levels.[38] Thus, previous reports of the detection of C- and N-terminal tags in nonpermeabilized cells may have resulted from inclusion of apoptotic cells in the analyses.

Cytoplasm

Assuming that the N- and C-termini of Fpn are cytosolic, as suggested by our data and some previous studies,[26,37,38] Fpn must have an even number of TM spanning domains. Using the prediction software TMHMM[46] and an alignment of human, mouse, and zebrafish Fpn sequences, we predicted that Fpn contains 12 TM domains (Fig. 9), differing from prior predictions of 9 or 10 membrane spanning regions[4,5,13] but similar to a recent prediction published in conjunction with insertion mutagenesis analyses.[26] Our model places the tyrosines that become phosphorylated upon hepcidin-25 binding, Y302 and Y303,[11] in the middle of TM region 6 (TM6) and thus not accessible to cytosolic kinases. The model may be inaccurate in the region of TM6, or, alternatively, the binding of hepcidin-25 to the extracellular loop located between TM6 and TM7 could cause a conformational shift that adjusts the location of TM6 such that Y302 and Y303 become accessible to the cytosol where they can be phosphorylated.

Although Fpn has been reported to be predominantly localized to the plasma membrane in the absence of the peptide hormone hepcidin, previous studies showed visible internal staining when Fpn was stably or transiently expressed in HEK293T cells.[8,27–30,36] Here, we showed that much of the internal Fpn-GFP signal was eliminated by treatment with the protein synthesis inhibitor cycloheximide when Fpn-GFP was transiently expressed in HeLa cells (Fig. 5). Having worked out conditions such that the majority of wild-type Fpn was localized to the plasma membrane in the absence of hepcidin, we were able to rapidly screen the localization of disease-related Fpn mutants in the presence and in the absence of hepcidin.

We found that wild-type Fpn-GFP and 16 of 16 disease-related Fpn-GFP mutants tested in this assay localized primarily to the plasma membrane of HeLa cells (Fig. 5) upon treatment with cycloheximide in the absence of hepcidin. These results conflict with those of some studies conducted in the absence of cycloheximide, with, for example, one report suggesting that the A77D Fpn mutant is intracellular[29] and others suggesting that the A77D,[26] D157G,[26] ΔV160,[26,30,36] N174I,[29] G323V,[30,36] and G490D[30] Fpn mutants exhibited partial internalization. The discrepancies may reflect cell type-specific differences in folding rates; thus, slowly folding mutants might appear to be intracellular in cells that were not treated with cycloheximide. This is clearly not the case for all cells, however, as we observed primarily plasma membrane localization for wild-type Fpn-GFP and the 16 disease-related mutants in polarized MDCK cells, in which case the use of cycloheximide to eliminate intracellular signals was not necessary (Fig. 4).

Using the cycloheximide treatment procedure for reproducibly expressing Fpn-GFP on the surface of HeLa cells, we next investigated the responses of Fpn mutants to hepcidin treatment. As previously described,[8] we found that wild-type Fpn-GFP was internalized by the addition of hepcidin-25 to HeLa cells (Fig. 5). In our experiments, we saw internalization of the Fpn-GFP signal within 1 h of incubation with 2.0 μM hepcidin-25, and by 4 h of incubation, the Fpn-GFP signal in many cells was entirely intracellular. Our experiments showed that the internalized Fpn-GFP passes through EEA1- and LAMP-positive compartments but does not accumulate in the Golgi (Fig. 6) and that this trafficking is dependent on intact microtubules (Fig. 7).

There was some variability in the degree of wild-type Fpn-GFP internalization in hepcidin-treated cells, presumably due to different expression levels in the transiently transfected cells; thus, we did not attempt to quantify relative levels of Fpn internalization for each of the mutants. Instead, we considered an Fpn mutant to be hepcidin sensitive if we observed distinct internal Fpn-GFP puncta after 4 h of incubation with 2 μM hepcidin-25 (a concentration chosen to ensure saturation) and to be hepcidin resistant if no distinct punctum was observed. Using these definitions, we report that the Fpn-GFP mutants A77D, N144D, N144H, N144T, D157G, ΔV160, N174I, Q182H, Q248H, D270V, and G323V were hepcidin sensitive and that the Fpn-GFP mutants Y64N, G80S, C326S, C326Y, and G490D were hepcidin resistant (Fig. 5). The N144T, D270V, and C326S Fpn mutants had not been tested for hepcidin internalization prior to this report. Some of the results for the other mutants conflict with those of prior studies, whereas others are in agreement. For example, one study reported N144H, D157G, ΔV160, and G323V as hepcidin resistant yet agreed with our results that G490D was resistant and that Q182H was sensitive.[30] Another study's results differed from our results by reporting that the A77D and N174I mutants were hepcidin resistant and that the G80S mutant was hepcidin sensitive.[29] A third study reported A77D, N144H, D157G, ΔV160, Q182H, and G323V all as hepcidin resistant.[26] These discrepancies may have arisen from different experimental conditions—the analyses described in these studies were performed without cycloheximide pretreatment and using a lower hepcidin-25 concentration of 0.36 or 0.7 μM. However, an additional study that used cycloheximide pretreatment and 0.5 μM hepcidin-25 agreed with our results that Y64N and C326Y were hepcidin resistant and that N144D, N144H, and Q248H were at least partially internalized upon hepcidin treatment.[28] It should be noted that our analysis does not distinguish between Fpn mutations within the hepcidin-binding site that cause a reduced affinity for hepcidin and mutations that prevent the Fpn–hepcidin complex from interacting properly with internalization machinery.

Linking the phenotypic manifestations of iron overload in patients affected by ferroportin disease caused by specific mutations with *in vitro* analyses on those same Fpn mutants has been difficult. This is due to the heterogeneity of patient phenotypes even between family members sharing the same Fpn mutation, the lack of data

for patients affected by certain mutations, and the difficulty of working with Fpn *in vitro* (as demonstrated by the conflicting experimental results reported to date). However, by combining our results with available clinical data, the data presented in our study support a model in which Fpn mutations resulting in hepcidin resistance *in vitro* manifest themselves as a disease with high transferrin saturation (observed in Y64N and C326S),[16,25] low to moderately high serum ferritin levels (observed in Y64N and C326S),[16,25] and hepatocyte iron loading (observed in Y64N, C326S, and G490D),[16,20,25] whereas Fpn mutations resulting in hepcidin sensitivity *in vitro* would produce disease with low transferrin saturation (observed in A77D, D157G, ΔV160, N174I, Q182H, Q248H, and G323V),[13–15,17,21,22,47–49] high serum ferritin (observed in A77D, N144D, N144H, N144T, D157G, ΔV160, N174I, Q182H, Q248H, and G323V),[13–15,17–19,21,22,47–50] and mostly macrophage/Kupffer cell iron loading with additional hepatocyte iron loading in extreme cases (observed in A77D, N144D, N144H, N144T, ΔV160, and N174I).[13,14,18,19,47–50]

Materials and Methods

Insect cell expression of Fpn

Genes encoding human and mouse Fpn's were gifts of Alain Townsend (Oxford), and the zebrafish Fpn gene was the gift of Nancy Andrews (Duke University School of Medicine). Human, mouse, and zebrafish Fpn's were expressed in a lytic baculovirus/insect cell expression system. A Rho tag was added to each construct using PCR by replacing the Fpn start codon with the first 20 aa of bovine rhodopsin and a linker (nucleic acid sequence, ATGAACGGGACCGAGGGCCCAAACTTCTACGTGCC-TTTCTCCAACAAGACGGGCGTGGTAGGCCGGCC GC-GGCCGCGA). The C-termini of the insect cell constructs were tagged with 10×-Histidine (Rho-Fpn-His) or tandem 10×-Histidine and FLAG (Rho-Fpn-His-FLAG) tags and a linker (nucleic acid sequence, AGCGGCCGC-GAAAACTTGTACTTTCAAGGCCATCACCATCACCAT-CACCATCACCATCACGACTACAAGGACGACGACGA-CAAGGGCGCGCCT). Constructs were subcloned into pBacPAK8 (Clontech), and viruses were constructed using ProGreen Baculovirus DNA (AB Vector). GFP expression was used to titrate the virus required to attain >95% infection. For protein expression, 5 L of High Five insect cells in ESF 921 medium (Expression Systems) was grown using a 20/50EH Wave Bioreactor (GE Healthcare) (settings: rocking speed, 9; angle, 20°; temperature, 27 °C; and ambient air pumped in at 0.3 L/min). Cells were infected at a density of $2.5–3.5 \times 10^6$ viable cells/mL and were harvested 48 h after infection.

Solubilization of Fpn from membranes

All steps were performed on ice or at 4 °C. Cell paste (110–140 g) was resuspended in 900 mL of resuspension buffer [50 mM Tris, pH 7.5, 150 mM NaCl, and 18 ethylenediaminetetraacetic acid (EDTA)-free complete protease inhibitor tablets (Roche)]. Cells were disrupted by sonication in 50-mL fractions on ice and placed in an ice bath between sonication rounds. Cell debris and membranes were pelleted at 125,000*g*.

Membrane pellets were resuspended using a Dounce homogenizer in 300 mL of detergent-free solubilization buffer [50 mM Tris, pH 7.5, 500 mM NaCl, 10 mM imidazole, pH 7.5, and six EDTA-free complete protease inhibitor tablets (Roche)]. Dry DM (Anatrace) or DDM (Anatrace) was added to 1% (w/v) to resuspended membranes and incubated with gentle stirring at 4 °C for 2.5 h. After pelleting at 125,000*g*, membrane suspensions were filtered at 0.45 μm.

Affinity purification of Fpn

Detergent-solubilized Fpn was purified by single (Rho-Fpn-His) or double (Rho-Fpn-His-FLAG) affinity steps. For His-tag purifications, TALON SuperFlow columns were preequilibrated with solubilization buffer containing 0.02% (w/v) DDM. Supernatants were passed over the column and washed to baseline. Nonspecific binders were washed off with equilibration buffer containing 30 mM imidazole, and Fpn was eluted with buffer containing 120 mM imidazole.

Rho-Fpn-His-FLAG was further purified using an anti-FLAG M2 affinity column (Sigma) equilibrated in TALON elution buffer. TALON eluates were passed over the affinity column twice, which was washed with M2 buffer [50 mM Tris, pH 7.5, 150 mM NaCl, and 0.02% (w/v) DDM] and eluted with M2 buffer containing 0.2 mg/mL of FLAG peptide (Sigma). Boiling of samples in SDS sample buffer resulted in aberrant migration near the top of an SDS-PAGE gel, so gel samples were not boiled prior to loading.

Molecular mass and oligomeric state determination by SEC-LS/UV/RI

SEC was conducted with in-line multiangle static LS to determine the molecular mass of purified Fpn. The FLAG column eluate was concentrated to 0.5 mL using a 50-kDa cutoff Amicon Ultra concentrator (Millipore) and passed over a Superdex 200 10/300 SEC column (GE Healthcare) preequilibrated in buffer containing 50 mM Tris–HCl, pH 7.5, 150 mM NaCl, and 0.02% (w/v) DDM at 0.5 mL/min. The SEC column was plumbed in-line with a multiangle static LS monitor at 658 nm (DAWN Helios, Wyatt), a differential RI monitor (Optilab rEX, Wyatt), and a UV absorbance monitor (AKTA Explorer, GE Healthcare). All calculations of molecular mass were performed using the protein conjugate template in the ASTRA 5.3.2 software package (Wyatt). The specific RI increment (dn/dc) values used were 0.185 for protein (Wyatt) and 0.133 for DDM.[51] The predicted molecular mass and extinction coefficient for UV absorbance at 280 nm for Rho-Fpn-His-FLAG were calculated from the amino acid sequence as 69,015 g/mol and 83,319 M^{-1} cm^{-1}, respectively.[52] Bovine serum albumin (GE Healthcare) was used as a calibration standard.

Fpn–hepcidin binding

Experiments evaluating the interaction between human Fpn and human hepcidin were performed at 25 °C using a Biacore 2000 Instrument (GE Healthcare). Interactions between immobilized Fpn on a sensor chip and hepcidin

injected over the sensor surface were monitored in real time as resonance units (RUs). An anti-Rho monoclonal antibody (see below) was immobilized at densities ranging from 1000 to 3000 RUs to the surface of a CM5 biosensor chip using primary amine chemistry as described in the Biacore manual. Purified Rho-Fpn-His in 50 mM Tris, pH 7.5, 150 mM NaCl, and 0.2% (w/v) DM was injected over the anti-Rho surface, capturing 1000–1500 RUs of Fpn. Flow cells containing immobilized anti-Rho antibody without captured Rho-Fpn-His were used as reference-subtracted negative controls. The sensor surface was monitored for >12 h in the same buffer until a stable baseline was reached. Hepcidin-25 (Bachem) or hepcidin-20 (gift of Prof. T. Ganz, UCLA) diluted in this buffer was injected over the Fpn surface at various concentrations. The surface was observed to return to baseline after 1 h, so no regeneration condition was required. Experiments directly comparing the binding of hepcidin-20 and that of hepcidin-25 to immobilized Fpn were performed using 10 μM hepcidin injections. For experiments to derive kinetic constants for the hepcidin-25–Fpn interaction, a dilution series (0.625, 1.25, 2.5, 5.0, 8.0, and 10 μM) of hepcidin-25 were injected, and the dissociation and association phases of all curves were simultaneously fit to derive kinetic constants using BIAevaluation 4.1 (GE Healthcare). The data did not fit well to a 1:1 binding model, which can result if the injected analyte is not homogeneous (e.g., the analyte contains a population of aggregates).[53] An approximate equilibrium dissociation constant (K_d) was calculated from the ratio of dissociation and association rate constants.

Construction and mutagenesis of mammalian expression constructs

Fpn-GFP and Rho-Fpn-GFP mammalian expression vectors were constructed in the pLox+CMV expression vector, containing the CMV promoter and SV40 polyA tail. PCR inserts containing the Fpn-GFP or Rho-Fpn-GFP were produced by bridging PCR using the Fpn gene and the GFP gene derived from pCGFP-EU.[39] Fpn-GFP mutants were produced using site-directed mutagenesis. All constructs were verified by sequencing.

Mammalian cell culture and transfections

HEK293T, HeLa, and MDCK cells were grown in Dulbecco's modified Eagle's medium containing 4.5 g/L of D-glucose, 4 mM L-glutamine, 110 mg/L of sodium pyruvate (Gibco) with 1× penicillin/streptomycin (Gibco), and 10% (v/v) fetal bovine serum (Atlanta Biologicals). All transfections were performed using Lipofectamine 2000 (Invitrogen) as per the manufacturer's instruction. MDCK cells grown on transwell filters were initially seeded into six-well plates and transfected at ~75% confluency. Twenty-four hours later, cells were treated with trypsin-EDTA and 5×10^5 cells were transferred to 12-mm polyester transwell permeable supports (Costar) with 0.5 mL of growth medium above and 1.0 mL of growth medium below the support. Transfected cells were grown for 4 days postconfluency before imaging to ensure full polarization and tight junction formation.

FSEC analysis

Wild-type and mutant human Fpn-GFP constructs were transiently expressed in HEK293T cells in a six-well format.

Cells were collected by pipetting 36–40 h post-transfection and then pelleted and resuspended in 500 μL of solubilization buffer [50 mM Tris, pH 7.5, 150 mM NaCl, and 1% (w/v) DDM]. Resuspended cells were lysed by sonication, and solubilization was performed with gentle agitation for 2.5 h at 4 °C. Unsolubilized material was pelleted at 125,000g. The supernatant was removed and filtered through a 0.22-μm Ultrafree-MC spin filter (Millipore). Filtered supernatant was loaded onto a Superdex 200 10/300 SEC column (GE Healthcare) and Fpn-GFP fluorescence was monitored using an online RF-10AXL fluorescence detector (488-nm excitation, 507-nm emission; Shimadzu). SEC was performed at 0.5 mL/min in 50 mM Tris, pH 7.5, 150 mM NaCl, and 0.2% (w/v) DDM.

Hepcidin-induced Fpn internalization

HeLa cells were seeded onto polylysine-coated glass coverslips at 10^6 cells/well in a six-well format, and Fpn-GFP constructs were transfected at ~80% confluency. After 20 h, cells were incubated in medium containing 75 μg/mL of cycloheximide (Sigma) for 2 h. This medium was then exchanged for medium containing 2.0 μM hepcidin-25 (Bachem) and 75 μg/mL of cycloheximide. Each internalization time point included a negative control in which cells were treated only with cycloheximide. Internalization was stopped by fixing cells at room temperature (~22 °C) for 15 min with 4% (v/v) paraformaldehyde in phosphate-buffered saline (PBS) containing 1 mM CaCl$_2$, 0.5 mM MgCl$_2$, and 0.25 mM MgSO$_4$. Fixed samples were washed twice and directly mounted on glass slides in ProLong GOLD Anti-Fade mounting medium containing DAPI (4′,6-diamidino-2-phenylindole) nuclear stain (Invitrogen) or quenched in PBS containing 75 mM NH$_4$Cl and 20 mM glycine for 10 min prior to blocking and further antibody treatments. After quenching, samples were incubated in blocking solution [PBS containing 8% (v/v) goat serum (Gibco) and 0.025% (w/v) saponin (Sigma)] for 30 min at room temperature. Primary antibody incubations were performed in blocking solution overnight at 4 °C. After primary incubation, cells were washed three times in PBS and then incubated in blocking solution containing secondary antibodies for 1 h at room temperature, fixed in PBS containing 4% (v/v) paraformaldehyde for 30 min, washed twice in PBS, and then mounted on glass slides as described above.

Antibodies

A mouse monoclonal anti-Rho tag antibody (hybridoma B630N) was purified from ascites fluid using a protein G affinity column followed by SEC. Other antibodies were purchased or received as gifts as indicated. Primary antibodies and the dilutions used for cell staining were the monoclonal mouse anti-Rho at 1 μg/mL, Alexa-647-conjugated rabbit polyclonal anti-GFP (Invitrogen, cat. no. A31852) at 1:500, AC17 mouse monoclonal anti-LAMP2 from E. Rodriguez-Boulan (Cornell University) at 1:1000, rabbit polyclonal anti-LAMP1 (Abcam, cat. no. ab24170) at 1:500, rabbit polyclonal anti-EEA1 (Santa Cruz Biotech, cat. no. SC-33585) at 1:100, and mouse monoclonal anti-Golgi 58-kDa protein (Abcam, cat. no. ab6284) at 1:100. Secondary antibodies and their dilutions were Alexa-647-conjugated goat anti-mouse immunoglobulin G (Invitrogen,

cat. no. A21235) at 1:500 and Alexa-647-conjugated F(ab')2 fragment of goat anti-rabbit immunoglobulin G (Invitrogen, cat. no. A21246) at 1:500.

Confocal imaging and image processing

Confocal images were recorded on an UltraVIEW ERS Rapid Confocal Imager (Perkin-Elmer) using 63×(Plan-APOCHROMAT 1.4 Oil DIC, Zeiss) or 100×(αPlan-APOCHROMAT 1.46 Oil DIC, Zeiss) objectives. GFP and Alexa-647 fluorophores were excited at 488 and 647 nm, respectively, using a 488/548/647 multiline argon/krypton laser (Melles Griot). All fixed cells that were imaged had intact nuclei, as determined by DAPI staining (data not shown). Confocal images shown from fixed samples are representative images from full 3D confocal stacks sampled at 0.25-μm spacing in *z*. Stacks of imaged HeLa, HEK293T, and MDCK cells were assembled, and thresholds were set in Imaris 6.0.1 (Bitplane) before single representative slices were exported and assembled into figures using Photoshop CS3 (Adobe).

Live imaging and tracking

HeLa cells were grown and transfected in 35-mm polylysine-coated glass-bottomed microwell dishes (Matek). Two dishes were seeded at a density of 10^6 cells/dish and transfected at ∼80% confluency on the following day with Fpn-GFP. After 20 h, the medium was exchanged for medium containing 75 μg/mL of cycloheximide lacking phenol red. After 2 h, the medium was exchanged for phenol red-free medium containing 2 μM hepcidin-25 and 75 μg/mL of cycloheximide. After another 2 h, dishes were chilled on ice and their medium was exchanged for phenol red-free medium containing 10 μg/mL of nocodazole, 2 μM hepcidin-25, and 75 μg/mL of cycloheximide or the same chilled medium lacking nocodazole. Samples were incubated for 30 min on ice and then moved to an UltraVIEW ERS Rapid Confocal Imager (Perkin-Elmer) with a temperature-controlled housing (Solent Scientific) where they were warmed to 37 °C for imaging. Fluorescent micrographs were collected at 100×(αPlan-APOCHROMAT 1.46 Oil DIC, Zeiss) in a single focal plane 1 μm above the glass support and imaged at 4.5 frames per second for 90 s per cell. Three cells from each condition were imaged. Fpn-GFP-containing compartments were tracked using the tracking module in Imaris 6.0.1 (Bitplane). Spots and tracks were automatically selected using Imaris parameters, estimated diameter=0.35 μm, threshold=8, Brownian motion tracking algorithm, maximum distance=0.66 μm, and gap size=3, with minimal manual removal required. Tracks shorter than 10 frames (2.2 s) were filtered out of the data set. The final data set includes 1295 tracks for the untreated sample and 1149 tracks for the nocodazole-treated sample.

Transmembrane topology prediction

DNA sequences for full-length human, mouse, and zebrafish Fpn's were submitted to TransMembrane Prediction using the Hidden Markov Model (TMHMM v2.0) prediction server.[46] Each sequence was predicted to contain 12 regions that were 21–23 aa in length with a significant (>60%) probability of being a TM region. TMHMM marked 10 of these regions as TMs in human and mouse Fpn's, and 8 in zebrafish Fpn, which upon alignment summed to a total of 11 TMs. A final region with much of its sequence at or above 60% probability of being a TM was not annotated as a TM in any of the three Fpn sequences, but we included it in our model for a final prediction of 12 TMs (Fig. 9). The approximate starting and ending points for the predicted TMs (using the residue numbering for human Fpn) are as follows: 12–34, 58–80, 93–115, 125–147, 175–195, 199–221, 293–315, 335–357, 373–395, 450–472, 492–514, and 519–541.

Supplementary Data

Supplementary data associated with this article can be found, in the online version, at doi:10.1016/j.jmb.2008.12.063

References

1. Pietrangelo, A. (2007). Hemochromatosis: an endocrine liver disease. *Hepatology*, **46**, 1291–1301.
2. Andrews, N. C. & Schmidt, P. J. (2007). Iron homeostasis. *Annu. Rev. Physiol.* **69**, 69–85.
3. Montosi, G., Donovan, A., Totaro, A., Garuti, C., Pignatti, E., Cassanelli, S. *et al.* (2001). Autosomal-dominant hemochromatosis is associated with a mutation in the ferroportin (SLC11A3) gene. *J. Clin. Invest.* **108**, 619–623.
4. McKie, A. T., Marciani, P., Rolfs, A., Brennan, K., Wehr, K., Barrow, D. *et al.* (2000). A novel duodenal iron-regulated transporter, IREG1, implicated in the basolateral transfer of iron to the circulation. *Mol. Cell*, **5**, 299–309.
5. Donovan, A., Brownlie, A., Zhou, Y., Shepard, J., Pratt, S. J., Moynihan, J. *et al.* (2000). Positional cloning of zebrafish ferroportin 1 identifies a conserved vertebrate iron exporter. *Nature*, **403**, 776–781.
6. Abboud, S. & Haile, D. J. (2000). A novel mammalian iron-regulated protein involved in intracellular iron metabolism. *J. Biol. Chem.* **275**, 19906–19912.
7. Jeong, S. Y. & David, S. (2003). Glycosylphosphatidylinositol-anchored ceruloplasmin is required for iron efflux from cells in the central nervous system. *J. Biol. Chem.* **278**, 27144–27148.
8. Nemeth, E., Tuttle, M. S., Powelson, J., Vaughn, M. B., Donovan, A., Ward, D. M. *et al.* (2004). Hepcidin regulates cellular iron efflux by binding to ferroportin and inducing its internalization. *Science*, **306**, 2090–2093.
9. Park, C. H., Valore, E. V., Waring, A. J. & Ganz, T. (2001). Hepcidin, a urinary antimicrobial peptide synthesized in the liver. *J. Biol. Chem.* **276**, 7806–7810.

10. Pigeon, C., Ilyin, G., Courselaud, B., Leroyer, P., Turlin, B., Brissot, P. & Loreal, O. (2001). A new mouse liver-specific gene, encoding a protein homologous to human antimicrobial peptide hepcidin, is overexpressed during iron overload. *J. Biol. Chem.* **276**, 7811–7819.

11. De Domenico, I., Ward, D. M., Langelier, C., Vaughn, M. B., Nemeth, E., Sundquist, W. I. *et al.* (2007). The molecular mechanism of hepcidin-mediated ferroportin down-regulation. *Mol. Biol. Cell*, **18**, 2569–2578.

12. Njajou, O. T., Vaessen, N., Joosse, M., Berghuis, B., van Dongen, J. W. F., Breuning, M. H. *et al.* (2001). A mutation in SLC11A3 is associated with autosomal dominant hemochromatosis. *Nat. Genet.* **28**, 213–214.

13. Devalia, V., Carter, K., Walker, A. P., Perkins, S. J., Worwood, M., May, A. & Dooley, J. S. (2002). Autosomal dominant reticuloendothelial iron overload associated with a 3-base pair deletion in the ferroportin 1 gene (SLC11A3). *Blood*, **100**, 695–697.

14. Wallace, D. F., Pedersen, P., Dixon, J. L., Stephenson, P., Searle, J. W., Powell, L. W. & Subramaniam, V. N. (2002). Novel mutation in ferroportin 1 is associated with autosomal dominant hemochromatosis. *Blood*, **100**, 692–694.

15. Cazzola, M., Cremonesi, L., Papaioannou, M., Soriani, N., Kioumi, A., Charalambidou, A. *et al.* (2002). Genetic hyperferritinaemia and reticuloendothelial iron overload associated with a three base pair deletion in the coding region of the ferroportin gene (SLC11A3). *Br. J. Haematol.* **119**, 539–546.

16. Rivard, S. R., Lanzara, C., Grimard, D., Carella, M., Simard, H., Ficarella, R. *et al.* (2003). Autosomal dominant reticuloendothelial iron overload (HFE type 4) due to a new missense mutation in the FERROPORTIN 1 gene (SLC11A3) in a large French-Canadian family. *Haematologica*, **88**, 824–826.

17. Hetet, G., Devaux, I., Soufir, N., Grandchamp, B. & Beaumont, C. (2003). Molecular analyses of patients with hyperferritinemia and normal serum iron values reveal both L ferritin IRE and 3 new ferroportin (slc11a3) mutations. *Blood*, **102**, 1904–1910.

18. Arden, K. E., Wallace, D. F., Dixon, J. L., Summerville, L., Searle, J. W., Anderson, G. J. *et al.* (2003). A novel mutation in ferroportin 1 is associated with haemochromatosis in a Solomon Islands patient. *Gut*, **52**, 1215–1217.

19. Wallace, D. F., Clark, R. M., Harley, H. A. & Subramaniam, V. N. (2004). Autosomal dominant iron overload due to a novel mutation of ferroportin 1 associated with parenchymal iron loading and cirrhosis. *J. Hepatol.* **40**, 710–713.

20. Jouanolle, A. M., Douabin-Gicquel, V., Halimi, C., Loreal, O., Fergelot, P., Delacour, T. *et al.* (2003). Novel mutation in ferroportin 1 gene is associated with autosomal dominant iron overload. *J. Hepatol.* **39**, 286–289.

21. Gordeuk, V. R., Caleffi, A., Corradini, E., Ferrara, F., Jones, R. A., Castro, O. *et al.* (2003). Iron overload in Africans and African-Americans and a common mutation in the SCL40A1 (ferroportin 1) gene. *Blood Cells, Mol. Dis.* **31**, 299–304.

22. Beutler, E., Barton, J. C., Felitti, V. J., Gelbart, T., West, C., Lee, P. L. *et al.* (2003). Ferroportin 1 (SCL40A1) variant associated with iron overload in African-Americans. *Blood Cells, Mol Dis.* **31**, 305–309.

23. Cremonesi, L., Forni, G. L., Soriani, N., Lamagna, M., Fermo, I., Daraio, F. *et al.* (2005). Genetic and clinical heterogeneity of ferroportin disease. *Br. J. Haematol.* **131**, 663–670.

24. Robson, K. J. H., Merryweather-Clarke, A. T., Cadet, E., Viprakasit, V., Zaahl, M. G., Pointon, J. J. *et al.* (2004). Recent advances in understanding haemochromatosis: a transition state. *J. Med. Genet.* **41**, 721–730.

25. Sham, R. L., Phatak, P. D., West, C., Lee, P., Andrews, C. & Beutler, E. (2005). Autosomal dominant hereditary hemochromatosis associated with a novel ferroportin mutation and unique clinical features. *Blood Cells, Mol. Dis.* **34**, 157–161.

26. Liu, X. B., Yang, F. & Haile, D. J. (2005). Functional consequences of ferroportin 1 mutations. *Blood Cells, Mol Dis.* **35**, 33–46.

27. Schimanski, L. M., Drakesmith, H., Merryweather-Clarke, A. T., Viprakasit, V., Edwards, J. P., Sweetland, E. *et al.* (2005). *In vitro* functional analysis of human ferroportin (FPN) and hemochromatosis-associated FPN mutations. *Blood*, **105**, 4096–4102.

28. Drakesmith, H., Schimanski, L. M., Ormerod, E., Merryweather-Clarke, A. T., Viprakasit, V., Edwards, J. P. *et al.* (2005). Resistance to hepcidin is conferred by hemochromatosis-associated mutations of ferroportin. *Blood*, **106**, 1092–1097.

29. De Domenico, I., McVey Ward, D., Nemeth, E., Ganz, T., Corradini, E., Ferrara, F. *et al.* (2006). Molecular and clinical correlates in iron overload associated with mutations in ferroportin. *Haematologica*, **91**, 1092–1095.

30. De Domenico, I., Ward, D. M., Nemeth, E., Vaughn, M. B., Musci, G., Ganz, T. & Kaplan, J. (2005). The molecular basis of ferroportin-linked hemochromatosis. *Proc. Natl Acad. Sci. USA*, **102**, 8955–8960.

31. Drakesmith, H., Schimanski, L. M., Ormerod, E., Merryweather-Clarke, A. T., Viprakasit, V., Edwards, J. P. *et al.* (2005). Resistance to hepcidin is conferred by hemochromatosis-associated mutations of ferroportin. *Blood*, **106**, 1092–1097.

32. Krautwurst, D., Yau, K. W. & Reed, R. R. (1998). Identification of ligands for olfactory receptors by functional expression of a receptor library. *Cell*, **95**, 917–926.

33. Hu, Y. K. & Kaplan, J. H. (2000). Site-directed chemical labeling of extracellular loops in a membrane protein. The topology of the Na,K-ATPase alpha-subunit. *J. Biol. Chem.* **275**, 19185–19191.

34. Folta-Stogniew, E. (2006). Oligomeric states of proteins determined by size-exclusion chromatography coupled with light scattering, absorbance, and refractive index detectors. *Methods Mol. Biol.* **328**, 97–112.

35. Wen, J., Arakawa, T. & Philo, J. S. (1996). Size-exclusion chromatography with on-line light-scattering, absorbance, and refractive index detectors for studying proteins and their interactions. *Anal. Biochem.* **240**, 155–166.

36. Goncalves, A. S., Muzeau, F., Blaybel, R., Hetet, G., Driss, F., Delaby, C. *et al.* (2006). Wild-type and mutant ferroportins do not form oligomers in transfected cells. *Biochem. J.* **396**, 265–275.

37. De Domenico, I., Ward, D. M., Musci, G. & Kaplan, J. (2007). Evidence for the multimeric structure of ferroportin. *Blood*, **109**, 2205–2209.

38. Schimanski, L. M., Drakesmith, H., Talbott, C., Horne, K., James, J. R., Davis, S. J. *et al.* (2008). Ferroportin: lack of evidence for multimers. *Blood Cells, Mol. Dis.* **40**, 360–369.

39. Kawate, T. & Gouaux, E. (2006). Fluorescence-detection size-exclusion chromatography for precrystallization screening of integral membrane proteins. *Structure*, **14**, 673–681.

40. Nakano, A. (2002). Spinning-disk confocal microscopy—a cutting-edge tool for imaging of membrane traffic. *Cell Struct. Funct.* **27**, 349–355.

41. Pignatti, E., Mascheroni, L., Sabelli, M., Barelli, S., Biffo, S. & Pietrangelo, A. (2006). Ferroportin is a monomer *in vivo* in mice. *Blood Cells, Mol. Dis.* **36**, 26–32.

42. Sahin-Toth, M., Lawrence, M. C. & Kaback, H. R. (1994). Properties of permease dimer, a fusion protein containing two lactose permease molecules from *Escherichia coli. Proc. Natl Acad. Sci. USA*, **91**, 5421–5425.

43. Horiuchi, M., Nicke, A., Gomeza, J., Aschrafi, A., Schmalzing, G. & Betz, H. (2001). Surface-localized glycine transporters 1 and 2 function as monomeric proteins in *Xenopus* oocytes. *Proc. Natl Acad. Sci. USA*, **98**, 1448–1453.

44. De Domenico, I., Nemeth, E., Nelson, J. M., Phillips, J. D., Ajioka, R. S., Kay, M. S. *et al.* (2008). The hepcidin-binding site on ferroportin is evolutionarily conserved. *Cell Metab.* **8**, 146–156.

45. Rivera, S., Nemeth, E., Gabayan, V., Lopez, M. A., Farshidi, D. & Ganz, T. (2005). Synthetic hepcidin causes rapid dose-dependent hypoferremia and is concentrated in ferroportin-containing organs. *Blood*, **106**, 2196–2199.

46. Krogh, A., Larsson, B., von Heijne, G. & Sonnhammer, E. L. (2001). Predicting transmembrane protein topology with a hidden Markov model: application to complete genomes. *J. Mol. Biol.* **305**, 567–580.

47. Pietrangelo, A., Montosi, G., Totaro, A., Garuti, C., Conte, D., Cassanelli, S. *et al.* (1999). Hereditary hemochromatosis in adults without pathogenic mutations in the hemochromatosis gene. *N. Engl. J. Med.* **341**, 725–732.

48. Corradini, E., Montosi, G., Ferrara, F., Caleffi, A., Pignatti, E., Barelli, S. *et al.* (2005). Lack of enterocyte iron accumulation in the ferroportin disease. *Blood Cells, Mol. Dis.* **35**, 315–318.

49. Roetto, A., Merryweather-Clarke, A. T., Daraio, F., Livesey, K., Pointon, J. J., Barbabietola, G. *et al.* (2002). A valine deletion of ferroportin 1: a common mutation in hemochromatosis type 4. *Blood*, **100**, 733–734.

50. Njajou, O. T., de Jong, G., Berghuis, B., Vaessen, N., Snijders, P., Goossens, J. P. *et al.* (2002). Dominant hemochromatosis due to N144H mutation of SLC11A3: clinical and biological characteristics. *Blood Cells, Mol. Dis.* **29**, 439–443.

51. Strop, P. & Brunger, A. T. (2005). Refractive index-based determination of detergent concentration and its application to the study of membrane proteins. *Protein Sci.* **14**, 2207–2211.

52. Gasteiger, E., Gattiker, A., Hoogland, C., Ivanyi, I., Appel, R. D. & Bairoch, A. (2003). ExPASy: the proteomics server for in-depth protein knowledge and analysis. *Nucleic Acids Res.* **31**, 3784–3788.

53. van der Merwe, P. A., Brown, M. H., Davis, S. J. & Barclay, A. N. (1993). Affinity and kinetic analysis of the interaction of the cell adhesion molecules rat CD2 and CD48. *EMBO J.* **12**, 4945–4954.

Chapter 3:

Expression, Detergent Extraction, and Purification of Recombinant Human, Mouse, and Zebrafish Ferroportin from Bacteria and Baculovirus-Infected Insect Cells

In this chapter we report the over-expression, detergent extraction, purification, and preliminary analysis of recombinant ferroportin from various vertebrate species.

Introduction

This chapter focuses on the over-expression, detergent-extraction and purification of human, mouse, and zebrafish forms of ferroportin (Fpn) for use in various biophysical analyses and crystallization attempts. Prior to our studies, recombinant Fpn expression had been limited to small-scale eukaryotic systems. For example, the initial studies in which Fpn was identified and partially characterized involved small-scale recombinant expression Fpn utilizing such methods as microinjection in *Xenopus* oocytes (Donovan *et al.* 2000; McKie *et al.* 2000) or zebrafish embryos (Donovan *et al.* 2000), or by transient transfection in mammalian tissue culture lines, such as Madin-Darby canine kidney cells (MDCK) (McKie *et al.* 2000), CaCo-2 cells (McKie *et al.* 2000), or HEK293T cells (Abboud and Haile 2000). Fpn expression in these systems was evaluated by sensitive detection techniques such as Western blotting, direct fluorescence (in the case of Fpn-GFP), or immunofluorescence. Subsequent Fpn studies used these same small-scale eukaryotic expression methods (De Domenico *et al.* 2005, 2006, 2007a,b,c; Drakesmith *et al.* 2005; Goncalves *et al.* 2006; Nemeth *et al.* 2004; Schimanski *et al.* 2005; 2008), and no attempts at Fpn over-expression or purification beyond those reported in chapter 2 (Rice *et al.* 2009) have been reported to date.

Our Fpn over-expression strategy involved both prokaryotic and eukaryotic methods. Prokaryotic expression tests were performed in various strains of the bacterium *E. coli* and eukaryotic expression tests were performed using baculoviruses to infect High Five

and Sf9 insect cell lines. Initial efforts in both prokaryotic and eukaryotic systems yielded no Fpn expression (as assessed by Western blotting), however after extensive testing of various Fpn constructs under a large number of expression conditions we were able to successfully over-express human, mouse, and zebrafish Fpns at adequate levels for biophysical characterization and crystallization trials as will be described in this chapter.

Once an over-expression protocol was worked out, detergent-extraction protocols were developed for the solubilization of Fpn from prokaryotic and eukaryotic membranes. We found that Fpns expressed in insect cell plasma membranes were much more amenable to detergent extraction than Fpns expressed in the inner membrane of *E. coli*. The detergents that were capable of extracting Fpn were then used to develop purification protocols. The eukaryotic expression and purification was reported in Chapter 2 (Rice *et al.* 2009), but due to word limits in the published format, certain details were left out or not covered in full. These details will be discussed in more detail in this chapter. The first section of this chapter reports the expression, extraction, and purification for the expression of Fpn in bacteria, and the second portion is devoted to similar studies in insect cells.

Materials and Methods

Bacterial Expression Constructs

Human and mouse Fpn genes were gifts from Professor Alain Townsend (Oxford, UK) and zebrafish Fpn gene was a gift from Professor Nancy Andrews (Duke University). The human gene was contained within a mammalian expression construct, with the name hfpn1-V571A-myc-His6-pcDNA3.1. It contained an accidentally introduced V571A mutation. This mutation was reversed by site-directed mutagenesis, before sub-cloning of this gene continued. The mouse gene was contained within a mammalian expression construct, with the name mfpn1-myc-His6-pcDNA3.1. The zebrafish gene was contained within a mammalian expression construct with the name zfpn1-GFP-pEGFP-N1. The human and zebrafish genes naturally contained an NdeI restriction enzyme sequence within their ORFs, and these were removed by mutagenesis prior to further mutagenesis and/or sub-cloning into bacterial expression vectors. Our cloning strategy for bacterial expression constructs was to work with three separate forms of each Fpn: wild-type; A77D; and N144H. The A77D and N144H mutants have been identified as disease-causing Fpn mutations (Montosi *et al.* 2001; Njajou *et al.* 2001), however, how these mutations lead to disease was unknown. We surmised that these mutants were worth pursuing alongside the wild-type Fpn for initial expression studies, particularly if expression of the fully functional wild-type Fpn was toxic due to unregulated iron export from cells. Each Fpn form was then directionally subcloned into the NdeI and NotI sites of pET-23a (Novagen) for a C-terminal 6× His tag, pET-28b (Novagen) for an N-terminal

6× His tag, pMAL-p2E (New England Biolabs) for an N-terminal maltose binding

protein fusion, or alternately into pET-28b adding His and/or StrepTagII tags via PCR.

Gene expression in these vectors was driven by the T7 promoter in pET vectors and by

P_{tac} promoter in the pMAL vector, both of which were induced by isopropyl β-D-1-

thiogalactopyranoside (IPTG) addition. Sequencing the constructs revealed an unplanned

result for two forms of human Fpn in pET-28b (wild-type and N144H), in which the final

constructs had both N- and C-terminal His tags.   These constructs (pAER113a and

pAER115a) with affinity tags on both termini were included in the expression screening.

The bacterial expression constructs are summarized in table 3.1.

Table 3.1. Bacterial expression constructs

Plasmid Name	Gene or Insert Name	Parent Vector	N-terminal tag	C-terminal tag
pAER112	human Fpn (w.t.)	pET-23a	none	His6
pAER113a	human Fpn (w.t.)	pET-28b	His6	His6
pAER114	human Fpn N144H	pET-23a	none	His6
pAER115a	human Fpn N144H	pET-28b	His6	myc-His6
pAER116	human Fpn A77D	pET-23a	none	His6
pAER117	human Fpn A77D	pET-28b	His6	none
pAER118	mouse Fpn (w.t.)	pET-23a	none	His6
pAER119	mouse Fpn (w.t.)	pET-28b	His6	none
pAER120	mouse Fpn N144H	pET-23a	none	His6
pAER121	mouse Fpn N144H	pET-28b	His6	none
pAER122	mouse Fpn A77D	pET-23a	none	His6
pAER123	mouse Fpn A77D	pET-28b	His6	none
pAER124	zebrafish Fpn (w.t.)	pET-23a	none	His6
pAER125	zebrafish Fpn (w.t.)	pET-28b	His6	none
pAER126	zebrafish Fpn N144H	pET-23a	none	His6
pAER128	zebrafish Fpn A77D	pET-23a	none	His6
pAER136	mouse Fpn (w.t.)	pMAL-p2E	MBP	His6
pDZS110	human Fpn (w.t.)	pET-28b	His6	Strep
pET-HS-1c	human Fpn (w.t.)	pET-28b	His6-Strep	none
pET-HS-3a	human Fpn (w.t.)	pET-28b	His6-Strep	His6

Small-Scale Tests of Fpn Expression in E. coli

Expression constructs were tested for Fpn expression in over 900 expression conditions, exploring variables such as: *E. coli* strain; induction temperature; growth media formulation; induction length; concentration of inducer; and aeration levels. Media formulations are summarized in table 3.2 and expression tests are summarized in table 3.3. Overnight cultures in the media of choice were grown from glycerol stocks at 37 ºC shaking at 240 rpm. The following morning, 5 mL cultures in 50 mL plastic conical vials (Falcon) with their caps loosely taped in place to allow adequate aeration were inoculated with 100 μL of overnight culture and incubated at 37 ºC and 240 rpm. The optical density, as measured at 600 nm (OD_{600}), of the growth culture was monitored routinely. When cultures reached an OD_{600} between 0.5 and 1.0, cultures were moved to an incubator at a preset temperature agitating at 240 rpm, a 1 mL fraction was removed as the zero time point, and the remaining 4 mL were induced by addition of IPTG to a final concentration of 0.4 mM IPTG. Induced cultures were allowed to incubate for various times before 1 mL fractions were removed for analysis. Cells from fractions removed for analysis were spun down for 1 min at 13,000×g, after which the supernatant was aspirated and the cell pellet frozen at −20 ºC until Western blot analysis could be performed, as described below. Using this technique, a single 5 mL culture would be used to test up to 4 time points for a given condition. The expression tests summarized in table 3.3 that report >4 time points were performed in larger volumes but otherwise adhered to the protocol described here.

Table 3.2. Growth media formulations

	LB	2×YT	SOC	TB	TB1	TB2	TB3	TB4	TB5	TB6	TB7
bactotryptone (g/L)	10	16	20	12	12	12	12	12	12	12	12
yeast extract (g/L)	5	10	5	24	24	12	-	8	12	-	-
malt extract (g/L)	-	-	-	-	-	-	-	8	12	24	12
beef extract (g/L)	-	-	-	-	-	12	24	8	-	-	12
NaCl (g/L)	10	5	0.58	-	-	-	-	-	-	-	-
KCl (g/L)	-	-	0.18	-	-	-	-	-	-	-	-
$MgCl_2 \cdot 6H_2O$ (g/L)	-	-	2.03	-	-	-	-	-	-	-	-
$MgSO_4$ (g/L)	-	-	1.20	-	-	-	-	-	-	-	-
1M glucose (mL/L)	-	-	20	-	-	-	-	-	-	-	-
gycerol (mL/L)	-	-	-	4	8	8	8	8	8	8	8
KH_2PO_4 (g/L)	-	-	-	2.31	2.31	2.31	2.31	2.31	2.31	2.31	2.31
K_2HPO_4 (g/L)	-	-	-	12.54	12.54	12.54	12.54	12.54	12.54	12.54	12.54

Table 3.3. Bacterial expression test summary

Construct	*E. coli* Strain	Temp. (ºC)	Media	Media Additives	Induction Length (hr)	Expression Observed?
pAER112	BL21(DE3)	37	TB	-	1, 5	no
pAER114	BL21(DE3)	37	TB	-	1, 5	no
pAER116	BL21(DE3)	37	TB	-	1, 5	no
pAER118	BL21(DE3)	37	TB	-	1, 5	no
pAER120	BL21(DE3)	37	TB	-	1, 5	no
pAER122	BL21(DE3)	37	TB	-	1, 5	no
pAER124	BL21(DE3)	37	TB	-	1, 5	no
pAER113a	BL21(DE3)	37	TB	-	1, 5	yes
pAER115a	BL21(DE3)	37	TB	-	1, 5	yes
pAER117	BL21(DE3)	37	TB	-	1, 5	no
pAER119	BL21(DE3)	37	TB	-	1, 5	no
pAER121	BL21(DE3)	37	TB	-	1, 5	no
pAER123	BL21(DE3)	37	TB	-	1, 5	no
pAER125	BL21(DE3)	37	TB	-	1, 5	no
pAER112	BL21(DE3)	30	TB	-	3, 8	no
pAER114	BL21(DE3)	30	TB	-	3, 8	no
pAER116	BL21(DE3)	30	TB	-	3, 8	no
pAER118	BL21(DE3)	30	TB	-	3, 8	no
pAER120	BL21(DE3)	30	TB	-	3, 8	no
pAER122	BL21(DE3)	30	TB	-	3, 8	no
pAER124	BL21(DE3)	30	TB	-	3, 8	no
pAER113a	BL21(DE3)	30	TB	-	3, 8	no
pAER115a	BL21(DE3)	30	TB	-	3, 8	yes
pAER117	BL21(DE3)	30	TB	-	3, 8	no
pAER119	BL21(DE3)	30	TB	-	3, 8	no
pAER121	BL21(DE3)	30	TB	-	3, 8	no
pAER123	BL21(DE3)	30	TB	-	3, 8	no
pAER125	BL21(DE3)	30	TB	-	3, 8	no

Construct	*E. coli* Strain	Temp. (ºC)	Media	Media Additives	Induction Length (hr)	Expression Observed?
pAER112	BL21(DE3)	37	LB	-	1, 5	no
pAER114	BL21(DE3)	37	LB	-	1, 5	no
pAER116	BL21(DE3)	37	LB	-	1, 5	no
pAER118	BL21(DE3)	37	LB	-	1, 5	no
pAER120	BL21(DE3)	37	LB	-	1, 5	no
pAER122	BL21(DE3)	37	LB	-	1, 5	no
pAER124	BL21(DE3)	37	LB	-	1, 5	no
pAER113a	BL21(DE3)	37	LB	-	1, 5	no
pAER115a	BL21(DE3)	37	LB	-	1, 5	no
pAER117	BL21(DE3)	37	LB	-	1, 5	no
pAER119	BL21(DE3)	37	LB	-	1, 5	no
pAER121	BL21(DE3)	37	LB	-	1, 5	no
pAER123	BL21(DE3)	37	LB	-	1, 5	no
pAER125	BL21(DE3)	37	LB	-	1, 5	no
pAER112	BL21(DE3)	30	LB	-	3, 8	no
pAER114	BL21(DE3)	30	LB	-	3, 8	no
pAER116	BL21(DE3)	30	LB	-	3, 8	no
pAER118	BL21(DE3)	30	LB	-	3, 8	no
pAER120	BL21(DE3)	30	LB	-	3, 8	no
pAER122	BL21(DE3)	30	LB	-	3, 8	no
pAER124	BL21(DE3)	30	LB	-	3, 8	no
pAER113a	BL21(DE3)	30	LB	-	3, 8	no
pAER115a	BL21(DE3)	30	LB	-	3, 8	no
pAER117	BL21(DE3)	30	LB	-	3, 8	no
pAER119	BL21(DE3)	30	LB	-	3, 8	no
pAER121	BL21(DE3)	30	LB	-	3, 8	no
pAER123	BL21(DE3)	30	LB	-	3, 8	no
pAER125	BL21(DE3)	30	LB	-	3, 8	no
pAER112	BL21(DE3)	37	SOC	-	1, 5	no
pAER114	BL21(DE3)	37	SOC	-	1, 5	no
pAER116	BL21(DE3)	37	SOC	-	1, 5	no
pAER118	BL21(DE3)	37	SOC	-	1, 5	no
pAER120	BL21(DE3)	37	SOC	-	1, 5	no
pAER122	BL21(DE3)	37	SOC	-	1, 5	no
pAER124	BL21(DE3)	37	SOC	-	1, 5	no
pAER113a	BL21(DE3)	37	SOC	-	1, 5	no
pAER115a	BL21(DE3)	37	SOC	-	1, 5	no
pAER117	BL21(DE3)	37	SOC	-	1, 5	no
pAER119	BL21(DE3)	37	SOC	-	1, 5	no
pAER121	BL21(DE3)	37	SOC	-	1, 5	no
pAER123	BL21(DE3)	37	SOC	-	1, 5	no
pAER125	BL21(DE3)	37	SOC	-	1, 5	no
pAER112	BL21(DE3)	30	SOC	-	3, 8	no
pAER114	BL21(DE3)	30	SOC	-	3, 8	no
pAER116	BL21(DE3)	30	SOC	-	3, 8	no
pAER118	BL21(DE3)	30	SOC	-	3, 8	no

Construct	*E. coli* Strain	Temp. (ºC)	Media	Media Additives	Induction Length (hr)	Expression Observed?
pAER120	BL21(DE3)	30	SOC	-	3, 8	no
pAER122	BL21(DE3)	30	SOC	-	3, 8	no
pAER124	BL21(DE3)	30	SOC	-	3, 8	no
pAER113a	BL21(DE3)	30	SOC	-	3, 8	no
pAER115a	BL21(DE3)	30	SOC	-	3, 8	no
pAER117	BL21(DE3)	30	SOC	-	3, 8	no
pAER119	BL21(DE3)	30	SOC	-	3, 8	no
pAER121	BL21(DE3)	30	SOC	-	3, 8	no
pAER123	BL21(DE3)	30	SOC	-	3, 8	no
pAER125	BL21(DE3)	30	SOC	-	3, 8	no
pAER112	RosettaBlue(DE3)	37	TB	-	1, 5	no
pAER114	RosettaBlue(DE3)	37	TB	-	1, 5	no
pAER116	RosettaBlue(DE3)	37	TB	-	1, 5	no
pAER118	RosettaBlue(DE3)	37	TB	-	1, 5	no
pAER120	RosettaBlue(DE3)	37	TB	-	1, 5	no
pAER122	RosettaBlue(DE3)	37	TB	-	1, 5	no
pAER124	RosettaBlue(DE3)	37	TB	-	1, 5	no
pAER113a	RosettaBlue(DE3)	37	TB	-	1, 5	no
pAER115a	RosettaBlue(DE3)	37	TB	-	1, 5	no
pAER117	RosettaBlue(DE3)	37	TB	-	1, 5	no
pAER119	RosettaBlue(DE3)	37	TB	-	1, 5	no
pAER121	RosettaBlue(DE3)	37	TB	-	1, 5	no
pAER123	RosettaBlue(DE3)	37	TB	-	1, 5	no
pAER125	RosettaBlue(DE3)	37	TB	-	1, 5	no
pAER112	RosettaBlue(DE3)	23	TB	-	4, 8	no
pAER114	RosettaBlue(DE3)	23	TB	-	4, 8	no
pAER116	RosettaBlue(DE3)	23	TB	-	4, 8	no
pAER118	RosettaBlue(DE3)	23	TB	-	4, 8	no
pAER120	RosettaBlue(DE3)	23	TB	-	4, 8	no
pAER122	RosettaBlue(DE3)	23	TB	-	4, 8	no
pAER124	RosettaBlue(DE3)	23	TB	-	4, 8	no
pAER113a	RosettaBlue(DE3)	23	TB	-	4, 8	no
pAER115a	RosettaBlue(DE3)	23	TB	-	4, 8	no
pAER117	RosettaBlue(DE3)	23	TB	-	4, 8	no
pAER119	RosettaBlue(DE3)	23	TB	-	4, 8	no
pAER121	RosettaBlue(DE3)	23	TB	-	4, 8	no
pAER123	RosettaBlue(DE3)	23	TB	-	4, 8	no
pAER125	RosettaBlue(DE3)	23	TB	-	4, 8	no
pAER112	BL21(DE3)	37	2×YT	-	1, 5	no
pAER114	BL21(DE3)	37	2×YT	-	1, 5	no
pAER116	BL21(DE3)	37	2×YT	-	1, 5	no
pAER118	BL21(DE3)	37	2×YT	-	1, 5	no
pAER120	BL21(DE3)	37	2×YT	-	1, 5	no
pAER122	BL21(DE3)	37	2×YT	-	1, 5	no
pAER124	BL21(DE3)	37	2×YT	-	1, 5	no
pAER113a	BL21(DE3)	37	2×YT	-	1, 5	no

Construct	*E. coli* Strain	Temp. (ºC)	Media	Media Additives	Induction Length (hr)	Expression Observed?
pAER115a	BL21(DE3)	37	2×YT	-	1, 5	no
pAER117	BL21(DE3)	37	2×YT	-	1, 5	no
pAER119	BL21(DE3)	37	2×YT	-	1, 5	no
pAER121	BL21(DE3)	37	2×YT	-	1, 5	no
pAER123	BL21(DE3)	37	2×YT	-	1, 5	no
pAER125	BL21(DE3)	37	2×YT	-	1, 5	no
pAER112	BL21(DE3)	23	2×YT	-	4, 8	no
pAER114	BL21(DE3)	23	2×YT	-	4, 8	no
pAER116	BL21(DE3)	23	2×YT	-	4, 8	no
pAER118	BL21(DE3)	23	2×YT	-	4, 8	no
pAER120	BL21(DE3)	23	2×YT	-	4, 8	no
pAER122	BL21(DE3)	23	2×YT	-	4, 8	no
pAER124	BL21(DE3)	23	2×YT	-	4, 8	no
pAER113a	BL21(DE3)	23	2×YT	-	4, 8	no
pAER115a	BL21(DE3)	23	2×YT	-	4, 8	no
pAER117	BL21(DE3)	23	2×YT	-	4, 8	no
pAER119	BL21(DE3)	23	2×YT	-	4, 8	no
pAER121	BL21(DE3)	23	2×YT	-	4, 8	no
pAER123	BL21(DE3)	23	2×YT	-	4, 8	no
pAER125	BL21(DE3)	23	2×YT	-	4, 8	no
pAER112	RosettaBlue(DE3)	37	2×YT	-	1, 5	no
pAER114	RosettaBlue(DE3)	37	2×YT	-	1, 5	no
pAER116	RosettaBlue(DE3)	37	2×YT	-	1, 5	no
pAER118	RosettaBlue(DE3)	37	2×YT	-	1, 5	no
pAER120	RosettaBlue(DE3)	37	2×YT	-	1, 5	no
pAER122	RosettaBlue(DE3)	37	2×YT	-	1, 5	no
pAER124	RosettaBlue(DE3)	37	2×YT	-	1, 5	no
pAER113a	RosettaBlue(DE3)	37	2×YT	-	1, 5	no
pAER115a	RosettaBlue(DE3)	37	2×YT	-	1, 5	no
pAER117	RosettaBlue(DE3)	37	2×YT	-	1, 5	no
pAER119	RosettaBlue(DE3)	37	2×YT	-	1, 5	no
pAER121	RosettaBlue(DE3)	37	2×YT	-	1, 5	no
pAER123	RosettaBlue(DE3)	37	2×YT	-	1, 5	no
pAER125	RosettaBlue(DE3)	37	2×YT	-	1, 5	no
pAER112	RosettaBlue(DE3)	23	2×YT	-	10	no
pAER114	RosettaBlue(DE3)	23	2×YT	-	10	no
pAER116	RosettaBlue(DE3)	23	2×YT	-	10	no
pAER118	RosettaBlue(DE3)	23	2×YT	-	10	no
pAER120	RosettaBlue(DE3)	23	2×YT	-	10	no
pAER122	RosettaBlue(DE3)	23	2×YT	-	10	no
pAER124	RosettaBlue(DE3)	23	2×YT	-	10	no
pAER113a	RosettaBlue(DE3)	23	2×YT	-	10	no
pAER115a	RosettaBlue(DE3)	23	2×YT	-	10	no
pAER117	RosettaBlue(DE3)	23	2×YT	-	10	no
pAER119	RosettaBlue(DE3)	23	2×YT	-	10	no
pAER121	RosettaBlue(DE3)	23	2×YT	-	10	no

Construct	*E. coli* Strain	Temp. (ºC)	Media	Media Additives	Induction Length (hr)	Expression Observed?
pAER123	RosettaBlue(DE3)	23	2×YT	-	10	no
pAER125	RosettaBlue(DE3)	23	2×YT	-	10	no
pAER112	Rosetta(DE3)	37	TB	-	1, 5	no
pAER114	Rosetta(DE3)	37	TB	-	1, 5	no
pAER116	Rosetta(DE3)	37	TB	-	1, 5	no
pAER118	Rosetta(DE3)	37	TB	-	1, 5	no
pAER120	Rosetta(DE3)	37	TB	-	1, 5	no
pAER122	Rosetta(DE3)	37	TB	-	1, 5	no
pAER124	Rosetta(DE3)	37	TB	-	1, 5	no
pAER113a	Rosetta(DE3)	37	TB	-	1, 5	no
pAER115a	Rosetta(DE3)	37	TB	-	1, 5	no
pAER117	Rosetta(DE3)	37	TB	-	1, 5	no
pAER119	Rosetta(DE3)	37	TB	-	1, 5	no
pAER121	Rosetta(DE3)	37	TB	-	1, 5	no
pAER123	Rosetta(DE3)	37	TB	-	1, 5	no
pAER125	Rosetta(DE3)	37	TB	-	1, 5	no
pAER112	Rosetta(DE3)	30	TB	-	3, 8	no
pAER114	Rosetta(DE3)	30	TB	-	3, 8	no
pAER116	Rosetta(DE3)	30	TB	-	3, 8	no
pAER118	Rosetta(DE3)	30	TB	-	3, 8	no
pAER120	Rosetta(DE3)	30	TB	-	3, 8	no
pAER122	Rosetta(DE3)	30	TB	-	3, 8	no
pAER124	Rosetta(DE3)	30	TB	-	3, 8	no
pAER113a	Rosetta(DE3)	30	TB	-	3, 8	no
pAER115a	Rosetta(DE3)	30	TB	-	3, 8	no
pAER117	Rosetta(DE3)	30	TB	-	3, 8	no
pAER119	Rosetta(DE3)	30	TB	-	3, 8	no
pAER121	Rosetta(DE3)	30	TB	-	3, 8	no
pAER123	Rosetta(DE3)	30	TB	-	3, 8	no
pAER125	Rosetta(DE3)	30	TB	-	3, 8	no
pAER136	BL21(DE3)	37	TB	-	1, 5	no
pAER136	BL21(DE3)	30	TB	-	3, 8	no
pAER136	BL21(DE3)	37	2×YT	-	1, 5	no
pAER136	BL21(DE3)	30	2×YT	-	3, 8	no
pAER118	BL21(DE3)	37	TB1	-	0.5, 1, 2.5, 5	no
pAER119	BL21(DE3)	37	TB1	-	0.5, 1, 2.5, 5	no
pAER124	BL21(DE3)	37	TB1	-	0.5, 1, 2.5, 5	no
pAER125	BL21(DE3)	37	TB1	-	0.5, 1, 2.5, 5	no
pAER118	BL21(DE3)	37	TB2	-	0.5, 1, 2.5, 5	no
pAER119	BL21(DE3)	37	TB2	-	0.5, 1, 2.5, 5	no
pAER124	BL21(DE3)	37	TB2	-	0.5, 1, 2.5, 5	no
pAER125	BL21(DE3)	37	TB2	-	0.5, 1, 2.5, 5	no
pAER118	BL21(DE3)	30	TB1	-	0.75, 1.5, 4, 8	no
pAER119	BL21(DE3)	30	TB1	-	0.75, 1.5, 4, 8	no
pAER124	BL21(DE3)	30	TB1	-	0.75, 1.5, 4, 8	no
pAER125	BL21(DE3)	30	TB1	-	0.75, 1.5, 4, 8	no

Construct	*E. coli* Strain	Temp. (ºC)	Media	Media Additives	Induction Length (hr)	Expression Observed?
pAER118	BL21(DE3)	30	TB2	-	0.75, 1.5, 4, 8	no
pAER119	BL21(DE3)	30	TB2	-	0.75, 1.5, 4, 8	no
pAER124	BL21(DE3)	30	TB2	-	0.75, 1.5, 4, 8	no
pAER125	BL21(DE3)	30	TB2	-	0.75, 1.5, 4, 8	no
pAER118	BL21(DE3)	23	TB1	-	1, 3, 8, 16	no
pAER119	BL21(DE3)	23	TB1	-	1, 3, 8, 16	no
pAER124	BL21(DE3)	23	TB1	-	1, 3, 8, 16	no
pAER125	BL21(DE3)	23	TB1	-	1, 3, 8, 16	no
pAER118	BL21(DE3)	23	TB2	-	1, 3, 8, 16	no
pAER119	BL21(DE3)	23	TB2	-	1, 3, 8, 16	no
pAER124	BL21(DE3)	23	TB2	-	1, 3, 8, 16	no
pAER125	BL21(DE3)	23	TB2	-	1, 3, 8, 16	no
pAER113a	BL21(DE3)	37	TB1	-	0.5, 1, 2.5, 5	yes
pAER115a	BL21(DE3)	37	TB1	-	0.5, 1, 2.5, 5	yes
pAER125	BL21(DE3)	37	TB1	-	0.5, 1, 2.5, 5	no
pAER113a	BL21(DE3)	37	TB1	-	1, 3, 5, 7	no
pAER113a	BL21(DE3)	30	TB1	-	3, 5, 7, 9	no
pAER113a	BL21(DE3)	23	TB1	-	3, 5, 7, 9	no
pAER113a	BL21(DE3)	37	TB2	-	1, 3, 5, 7	no
pAER113a	BL21(DE3)	30	TB2	-	3, 5, 7, 9	no
pAER113a	BL21(DE3)	23	TB2	-	3, 5, 7, 9	no
pAER113a	BL21(DE3)	37	TB3	-	1, 3, 5, 7	yes
pAER113a	BL21(DE3)	30	TB3	-	3, 5, 7, 9	no
pAER113a	BL21(DE3)	23	TB3	-	3, 5, 7, 9	no
pAER113a	BL21(DE3)	37	TB4	-	1, 3, 5, 7	no
pAER113a	BL21(DE3)	30	TB4	-	3, 5, 7, 9	yes
pAER113a	BL21(DE3)	23	TB4	-	3, 5, 7, 9	no
pAER113a	BL21(DE3)	37	TB5	-	1, 3, 5, 7	yes
pAER113a	BL21(DE3)	30	TB5	-	3, 5, 7, 9	yes
pAER113a	BL21(DE3)	23	TB5	-	3, 5, 7, 9	yes
pAER113a	BL21(DE3)	37	TB6	-	1, 3, 5, 7	no
pAER113a	BL21(DE3)	30	TB6	-	3, 5, 7, 9	no
pAER113a	BL21(DE3)	23	TB6	-	3, 5, 7, 9	no
pAER113a	BL21(DE3)	37	TB7	-	1, 3, 5, 7	yes
pAER113a	BL21(DE3)	30	TB7	-	3, 5, 7, 9	yes
pAER113a	BL21(DE3)	23	TB7	-	3, 5, 7, 9	yes
pAER115a	BL21(DE3)	37	TB1	-	1, 3, 5, 7	yes
pAER115a	BL21(DE3)	30	TB1	-	3, 5, 7, 9	yes
pAER115a	BL21(DE3)	23	TB1	-	3, 5, 7, 9	no
pAER115a	BL21(DE3)	37	TB2	-	1, 3, 5, 7	yes
pAER115a	BL21(DE3)	30	TB2	-	3, 5, 7, 9	no
pAER115a	BL21(DE3)	23	TB2	-	3, 5, 7, 9	no
pAER115a	BL21(DE3)	37	TB3	-	1, 3, 5, 7	yes
pAER115a	BL21(DE3)	30	TB3	-	3, 5, 7, 9	no
pAER115a	BL21(DE3)	23	TB3	-	3, 5, 7, 9	no
pAER115a	BL21(DE3)	37	TB4	-	1, 3, 5, 7	yes

Construct	*E. coli* Strain	Temp. (ºC)	Media	Media Additives	Induction Length (hr)	Expression Observed?
pAER115a	BL21(DE3)	30	TB4	-	3, 5, 7, 9	yes
pAER115a	BL21(DE3)	23	TB4	-	3, 5, 7, 9	yes
pAER115a	BL21(DE3)	37	TB5	-	1, 3, 5, 7	yes
pAER115a	BL21(DE3)	30	TB5	-	3, 5, 7, 9	yes
pAER115a	BL21(DE3)	23	TB5	-	3, 5, 7, 9	yes
pAER115a	BL21(DE3)	37	TB6	-	1, 3, 5, 7	no
pAER115a	BL21(DE3)	30	TB6	-	3, 5, 7, 9	no
pAER115a	BL21(DE3)	23	TB6	-	3, 5, 7, 9	no
pAER115a	BL21(DE3)	37	TB7	-	1, 3, 5, 7	yes
pAER115a	BL21(DE3)	30	TB7	-	3, 5, 7, 9	yes
pAER115a	BL21(DE3)	23	TB7	-	3, 5, 7, 9	yes
pAER119	BL21(DE3)	37	TB3	-	0.5, 1, 2.5, 5	no
pAER119	BL21(DE3)	30	TB3	-	0.75, 1.5, 4, 8	no
pAER119	BL21(DE3)	23	TB3	-	1, 3, 8, 16	no
pAER119	BL21(DE3)	37	TB4	-	0.5, 1, 2.5, 5	no
pAER119	BL21(DE3)	30	TB4	-	0.75, 1.5, 4, 8	no
pAER119	BL21(DE3)	23	TB4	-	1, 3, 8, 16	no
pAER119	BL21(DE3)	37	TB5	-	0.5, 1, 2.5, 5	no
pAER119	BL21(DE3)	30	TB5	-	0.75, 1.5, 4, 8	no
pAER119	BL21(DE3)	23	TB5	-	1, 3, 8, 16	no
pAER119	BL21(DE3)	37	TB6	-	0.5, 1, 2.5, 5	no
pAER119	BL21(DE3)	30	TB6	-	0.75, 1.5, 4, 8	no
pAER119	BL21(DE3)	23	TB6	-	1, 3, 8, 16	no
pAER125	BL21(DE3)	37	TB3	-	0.5, 1, 2.5, 5	no
pAER125	BL21(DE3)	30	TB3	-	0.75, 1.5, 4, 8	no
pAER125	BL21(DE3)	23	TB3	-	1, 3, 8, 16	no
pAER125	BL21(DE3)	37	TB4	-	0.5, 1, 2.5, 5	no
pAER125	BL21(DE3)	30	TB4	-	0.75, 1.5, 4, 8	no
pAER125	BL21(DE3)	23	TB4	-	1, 3, 8, 16	no
pAER125	BL21(DE3)	37	TB5	-	0.5, 1, 2.5, 5	no
pAER125	BL21(DE3)	30	TB5	-	0.75, 1.5, 4, 8	no
pAER125	BL21(DE3)	23	TB5	-	1, 3, 8, 16	no
pAER125	BL21(DE3)	37	TB6	-	0.5, 1, 2.5, 5	no
pAER125	BL21(DE3)	30	TB6	-	0.75, 1.5, 4, 8	no
pAER125	BL21(DE3)	23	TB6	-	1, 3, 8, 16	no
pAER113a	BL21(DE3)	37	TB5	-	1, 2, 3, 4, 5, 6	yes
pAER113a	BL21(DE3)	37	TB5	1% glycine	1, 2, 3, 4, 5, 6	yes
pAER113a	BL21(DE3)	37	TB5	1.5% NaCl replacing K-salts	1, 2, 3, 4, 5, 6	yes
pAER113a	BL21(DE3)	37	TB5	50% less K-salts	1, 2, 3, 4, 5, 6	yes
pAER113a	BL21(DE3)	37	TB5	50% more K-salts	1, 2, 3, 4, 5, 6	yes
pAER113a	BL21(DE3)	37	TB5	1% lysine	1, 2, 3, 4, 5, 6	yes
pAER113a	C41(DE3)	37	TB5	-	2, 3, 4, 5, 6	no
pAER113a	C43(DE3)	37	TB5	-	2, 3, 4, 5, 6	no
pAER113a	BL21(DE3)	37	TB5	1% leucine	2, 3, 4, 5, 6	yes

Construct	*E. coli* Strain	Temp. (ºC)	Media	Media Additives	Induction Length (hr)	Expression Observed?
pAER113a	BL21(DE3)	37	TB5	1% tryptophan	2, 3, 4, 5, 6	yes
pAER113a	BL21(DE3)	37	TB5	1% histidine	2, 3, 4, 5, 6	yes
pAER113a	BL21(DE3)	37	TB5	1% methionine	2, 3, 4, 5, 6	yes
pAER113a	BL21(DE3)	30	TB5	1% lysine	1, 2, 3, 4, 5	yes
pAER113a	BL21(DE3)	30	TB5	1% lysine, 100 µM FeCl	1, 2, 3, 4, 5	yes
pAER113a	BL21(DE3)	30	TB5	1% lysine, 100 µM ZnCl$_2$	1, 2, 3, 4, 5	yes
pAER113a	BL21(DE3)	30	TB5	1% lysine, 50% more K-salts	1, 2, 3, 4, 5	yes
pDZS110	BL21(DE3)	37	LB	-	1, 3, 5, 7	no
pDZS110	BL21(DE3)	30	LB	-	2, 4, 6, 8	no
pDZS110	BL21(DE3)	37	TB	-	1, 3, 5, 7	no
pDZS110	BL21(DE3)	30	TB	-	2, 4, 6, 8	no
pDZS110	BL21(DE3)	37	TB5	-	1, 3, 5, 7	no
pDZS110	BL21(DE3)	30	TB5	-	2, 4, 6, 8	no
pDZS110	BL21(DE3)	37	TB5	1% lysine	1, 3, 5, 7	no
pDZS110	BL21(DE3)	30	TB5	1% lysine	2, 4, 6, 8	no
pDZS110	BL21(DE3)	37	TB5	1% lysine, 50% more K-salts	1, 3, 5, 7	no
pDZS110	BL21(DE3)	30	TB5	1% lysine, 50% more K-salts	2, 4, 6, 8	no
pET-HS-1c	BL21(DE3)	30	2×YT	-	1, 3, 5	no
pET-HS-1c	BL21(DE3)	30	TB	-	1, 3, 5	no
pET-HS-1c	BL21(DE3)	30	TB5	-	1, 3, 5	no
pET-HS-3a	BL21(DE3)	30	2×YT	-	1, 3, 5	no
pET-HS-3a	BL21(DE3)	30	TB	-	1, 3, 5	no
pET-HS-3a	BL21(DE3)	30	TB5	-	1, 3, 5	no

Freeze-Thaw Lysis Protocol

Bacterial pellets from small-scale expression tests were prepared for analysis by Western

blotting using freeze-thaw lysis in the presence of lysozyme and DNAse I. Lysis buffer

was made fresh just prior to use: 50 mM Tris pH 7.5; 150 mM NaCl, 5 mM MgCl$_2$; 1

EDTA-free protease inhibitor cocktail tablet (Roche) per 50 mL of buffer; 0.1 mg/mL

lysozyme (Sigma); and 0.1 mg/mL DNAse I (Sigma). Cell pellets were resuspended in

100 µL lysis buffer and allowed to incubate at room temperature for 15 min. Samples

were treated with 5 cycles of freeze-thaw, freezing in liquid N_2 and thawing at 37 ºC. The final thaw was postponed until ~1 hr prior to gel loading. It was observed that Fpn migrated with an anomalously high molecular weight if boiled in SDS loading dye prior to gel loading.   We observed that incubating samples in SDS loading dye at room temperature prevented this anomalous migration. Therefore, 50 µL of 4× reducing SDS-PAGE dye was added and samples were incubated at room temperature for 1 hr prior to loading.

Anti-His Western Blotting Protocol

SDS-PAGE was performed in SDS running buffer at 150 V until the dye front neared the bottom of the gel. The gel was removed from its casing and washed in Western transfer buffer: Laemmli buffer + 10% (v/v) MeOH for >5 min before being assembled into the filter sandwich and Western transfer apparatus. Transfer to nitrocellulose was carried out at 90 V for 40 min in a chilled Western transfer apparatus. The nitrocellulose was then removed from the apparatus and blocked in TBST (50 mM Tris pH 7.5, 150 mM NaCl, and 0.5% (v/v) Tween 20) + 3% (w/v) bovine serum albumin (BSA, Sigma) for >30 min at room temperature. Mouse anti-His primary antibody (GE Healthcare) was added to blocking solution at 1:10,000 and incubated at room temperature for 1 hr. Membranes were washed twice for 5 min in TBST. Membranes were incubated with goat anti-mouse alkaline phosphatase-conjugated secondary antibody (Rockland) in TBST + 1% (w/v) BSA at 1:10,000 at room temperature for 1 hr. Membranes were washed twice for 5 min with TBST. Membranes were briefly washed again with developing buffer (100 mM Tris

pH 9.5; 100 mM NaCl; 5 mM MgCl$_2$). Membranes were developed at room temperature

in 20 mL developing buffer by adding nitro blue tetrazolium chloride (NBT) (70 μL of

50 mg/mL NBT in 70% dimethylformamide) and 5-bromo-4-chloro-3-indolyl phosphate

(BCIP) (40 μL of 50 mg/mL BCIP in 100% dimethylformamide).

Detergent-Extraction Screening of Recombinant Fpn Expressed in E. coli

Wild-type human Fpn construct pAER113a was transformed into BL21(DE3) *E. coli* and

was used to inoculate a 50 mL 2×YT culture containing 100 μg/mL kanamycin. This

culture was incubated overnight at 37 ℃ while shaking at 240 rpm.   The following

morning, two beveled 2 L flasks, each containing 500 mL of TB5 media with 1% (w/v)

D-lysine and 100 μg/mL kanamycin and heated to 37 ℃, were inoculated with 10 mL of

overnight culture. Inoculated cultures were shaken at 240 rpm at 37 ℃ and OD$_{600}$ was

monitored routinely. When the OD$_{600}$ reached 0.8, the cultures were shifted to a shaking

incubator at 30 ℃ for 15 min before being induced with 0.4 mM IPTG for 3.5 hr. After

induction, cells were harvested by centrifugation, their supernatants were removed and

the cell pellets were split into 5 g portions and frozen at −20 ℃. Five grams of cell paste

were thawed and resuspended in 30 mL of buffer containing 50 mM Tris pH 7.5, 150 mM

NaCl, and 1 tablet of complete EDTA-free protease inhibitors (Roche). Cells were

disrupted by sonication on ice (settings: flat tip; 8 rounds of 30-second pulses; power 8;

25% duty cycle). Undisrupted cells were pelleted by centrifugation at 11,000×g at 4 ℃

and membranes were spun down from the supernatant at 125,000×g at 4 ℃.   This

supernatant was discarded and pelleted membranes were resuspended in 12 mL of buffer

containing 50 mM Tris pH 7.5, 150 mM NaCl, and half a tablet of complete EDTA-free protease inhibitors, using a Dounce homogenizer. Resuspended membranes were aliquotted into 180 μL fractions in 1.5 mL disposable centrifuge tubes. All detergents used in this analysis were prepared as 10% solutions in water (table 3.4). Twenty microliters of stock detergent solution was added to each aliquot of resuspended membranes, was mixed, and then was allowed to agitate gently at 4 ºC for 2 hr. After incubating the membranes in detergent, samples were ultracentrifuged at 140,000×g for 1 hr at 4 ºC. Thirty microliters of each supernatant were removed and mixed with 10 μL 4× SDS-PAGE loading dye and incubated at room temperature for 1 hr before being analyzed by Western blot as described above.

Table 3.4. Detergent screen for bacterial expression tests

Detergent Name	Chemical Name
CHAPS	3-[(3-Cholamidopropyl)-dimethylammonio]-1-propane sulfonate
Cholate	3α,7α,12α-Trihydroxy-5β-cholan-24-oic acid, monosodium salt
Deoxycholate	3α,12α-Dihydroxy-5β-cholan-24-oic acid, monosodium salt
Anzergent-3-12	n-Dodecyl-N,N-dimethyl-3-ammonio-1-propanesulfonate
Anzergent-3-14	n-Tetradecyl-N,N-dimethyl-3-ammonio-1-propanesulfonate
Cymal-3	3-Cyclohexyl-1-propyl−β−D-maltoside
Cymal-4	4-Cyclohexyl-1-butyl−β−D-maltoside
Cymal-5	5-Cyclohexyl-1-pentyl−β−D-maltoside
Cymal-6	6-Cyclohexyl-1-hexyl−β−D-maltoside
Fos-choline-9	n-Nonylphosphocholine
Fos-choline-10	n-Decylphosphocholine
Fos-choline-12	n-Dodecylphosphocholine
Fos-choline-14	n-Tetradecylphosphocholine
Dodecyldimethyl glycine	n-Dodecyl-N,N-dimethylglycine
Fos-choline-16	n-Hexadecylphosphocholine
Cyclofos-7	7-Cyclohexyl-1-heptylphosphocholine
Fos-choline-iso-11	2,8-Dimethyl-5-nonylphosphocholine
LDAO	n-Dodecyl-N,N-dimethylamine-N-oxide
Fos-MEA-8	Octylphospho-N-methylethanolamine
Fos-MEA-10	Decylphospho-N-methylethanolamine
Fos-MEA-12	Dodecylphospho-N-methylethanolamine

Detergent Name	Chemical Name
Fosfen-4	Tetraphenylphosphocholine
Fosfen-5	Pentaphenylphosphocholine
Fosfen-9	Nonylphenylphosphocholine
Octyl glucoside	n-Octyl−β−D-glucoside
Nonyl glucoside	n-Nonyl−β−D-glucoside
HEGA-9	Nonanoyl-N-hydroxyethylglucamide
HEGA-10	Decanoyl-N-hydroxyethylglucamide
MEGA-8	Octanoyl-N-methylglucamide
MEGA-9	Nonanoyl-N-methylglucamide
Nonyl maltoside	n-Nonyl−β−D-maltoside
Decyl maltoside	n-Decyl−β−D-maltoside
Undecyl maltoside	n-Undecyl−β−D-maltoside
Dodecyl maltoside	n-Dodecyl−β−D-maltoside
Tridecyl maltoside	n-Tridecyl−β−D-maltoside
Tween 20	Polyoxyethylene(20)sorbitan monolaurate
Brij-35	Polyethylene glycol (23) monododecyl ether
Brij-58	Polyethylene glycol (20) monohexadecyl ether
Tween 80	Polyoxyethylene(80)sorbitan monolaurate
$C_{10}E_6$	Polyoxyethylene(6)decyl ether
$C_{10}E_9$	Polyoxyethylene(9)decyl ether
$C_{12}E_8$	Polyoxyethylene(8)dodecyl ether
$C_{12}E_9$	Polyoxyethylene(9)dodecyl ether
$C_{12}E_{10}$	Polyoxyethylene(10)dodecyl ether
$C_{13}E_8$	Polyoxyethylene(8)tridecyl ether
Triton X-100	α-[4-(1,1,3,3-Tetramethylbutyl)phenyl]-ω-hydroxy-poly(oxy-1,2-ethanediyl)
Triton X-114	α-[(1,1,3,3-Tetramethylbutyl)phenyl]-ω-hydroxy-poly(oxy-1,2-ethanediyl)

Small-Scale Expression, Purification and SEC Detergent Screening of Fpn from E. coli

Wild-type human Fpn construct pAER113a transformed into BL21(DE3) was expressed in 500 mL volumes (as described above) and cell paste was divided into 1 g fractions for small-scale purification and size exclusion chromatography (SEC) detergent screening. All steps were performed on ice or at 4 ºC, unless otherwise indicated. One gram of cell paste was resuspended in 7.5 mL of buffer (50 mM Tris pH 7.5, 150 mM NaCl, and 1 EDTA-free Complete protease inhibitor tablet (Roche) per 50 mL). Resuspended cells were lysed by sonication on ice (flat tip, power level 8, 45 seconds total process time, 25% duty cycle). Cell debris was removed by centrifugation at 8,000×g. Membranes

were pelleted at 125,000×g for 1 hr. The membrane pellet was resuspended in 6 mL of the above buffer using a Dounce homogenizer. Homogenized membranes were transferred to a 15 mL plastic conical tube (Falcon). Fpn was solubilized by adding 1% (w/v) detergent and gently agitating ~12 hr at 4 ºC. After the detergent solubilization, 6 mL of salt-adjustment buffer (50 mM Tris pH 7.5, 425 mM NaCl, 100 mM imidazole pH 7.5, and 0.1 % (w/v) detergent) was added such that the final buffer concentration was 50 mM Tris pH 7.5, 500 mM NaCl, 50 mM imidazole pH 7.5, and 0.1% detergent. Pre-equilibrated Ni-NTA Superflow (Qiagen) resin (~0.25 mL) was added to the mixture and Fpn was loaded by gently rocking for 3 hr at 4 ºC. Ni-NTA resin slurry was poured over a disposable column and the flow through was collected by gravity flow.   Resin was washed with 10 mL Ni-NTA wash buffer (50 mM Tris pH 7.5, 500 mM NaCl, 50 mM imidazole pH 7.5, 2× the critical micelle concentration (CMC) for the detergent being tested, and 1 EDTA-free Complete protease inhibitor pellet per 500 mL). Fpn was eluted with 10 mL Ni-NTA elution buffer (50 mM Tris pH 7.5, 50 mM NaCl, 300 mM imidazole pH 7.5, detergent at 2× CMC, and 1 EDTA-free Complete protease inhibitor pellet per 500 mL). Eluate was concentrated using a 10,000 molecular weight cut-off 4 mL Amicon-Ultra spin concentrator (Millipore) to <100 µL volume. Concentrated eluate was centrifuged at 13,000×g for 10 min. A 50 µL portion was analyzed by SEC using a 1.4 mL Superdex 200 SEC column (GE Healthcare) driven by a SMART System FPLC (GE Healthcare) at 50 µL/min in SEC buffer (50 mM Tris pH 7.5, 150 mM NaCl, detergent at 2× CMC, and 1 EDTA-free Complete protease inhibitor pellet per 500 mL).

Fractions were collected and analyzed by SDS-PAGE anti-His Western blot as described above.

Large-Scale Expression and Purification of Fpn in E. coli

Sixty-liter expressions were carried out in a New Brunswick fermenter. BL21(DE3) *E. coli* containing the plasmid pAER113a was expressed in TB5 with 1% lysine and 100 μg∕mL kanamycin. The night before fermentation, a 25 mL overnight culture was inoculated from a single colony of a fresh transformation. In the morning, two 2 L flasks each containing 1 L of media were inoculated with 10 mL of the overnight culture and were grown at 37 ºC until the OD_{600} reached ~0.4, at which point it was used to inoculate 58 L of media warmed to 37 ºC in the fermenter. The fermenter was run at 300 rpm at 37 ºC until the $OD_{600} \approx 0.4$ and then the temperature was lowered to 30 ºC and was induced by adding 0.1 mM IPTG. Cells were harvested after 3 hr of induction.

Cells from approximately one-quarter to one-half of a fermenter run were used per purification. The following purification was for ~160 grams of wet cell paste (~half of that particular expression). Cells were resuspended by adding 600 mL resuspension buffer: 50 mM Tris pH 7.5; 150 mM NaCl; and 6 complete EDTA-free protease inhibitor tablets (Roche). Cells were split into 4 beakers (~175 mL each) and disrupted by sonication (on ice, flat tip, power level 10, 25% duty cycle, 2 min per beaker total process time). Large cellular debris was spun down at ~12,000×g for 15 min at 4 ºC. The membrane-containing supernatant was then ultracentrifuged at 125,000×g for 1 hr at 4 ºC

to pellet membranes. The supernatant was discarded and the membrane pellet was resuspended using a Dounce homogenizer in 100 mL resuspension buffer. Dry fos-choline-16 was added to resuspended membranes to a final concentration of 1.5% and solubilization was performed at 4 ºC overnight, with gentle stirring. After solubilization, unsolubilized material was pelleted by ultracentrifugation at 125,000×g for 1 hr at 4 ºC. The supernatant was carefully removed and its volume measured. Buffer components were carefully added to raise the NaCl concentration to 500 mM and to add imidazole pH 7.5 to a concentration of 50 mM. The final buffer concentration for the solubilized protein solution was 50 mM Tris pH 7.5, 500 mM NaCl, 50 mM imidazole pH 7.5, 1.5% fos-choline-16 and EDTA-free protease inhibitors. Two milliliters of pre-equilibrated Ni-NTA superose beads (Qiagen) were added to the solution and slowly stirred in batch at 4 ºC for several hours. Ni-NTA-protein slurry was loaded onto a glass column by peristaltic pump at 0.5 mL/min and 4 ºC, collecting the flow through. Once fully loaded in the glass column, the beads were washed with 50 mL wash buffer: 50 mM Tris pH 7.5; 500 mM NaCl; 50 mM imidazole pH 7.5; 0.01% fos-choline-16; 1/10 EDTA-free protease inhibitor tablet. Fpn was eluted from the Ni-NTA beads with 20 mL low imidazole elution buffer (50 mM Tris pH 7.5; 150 mM NaCl; 150 mM imidazole pH 7.5; 0.005% fos-choline-16; and 1/25 EDTA-free protease inhibitor tablet), and 20 mL high imidazole elution buffer (50 mM Tris pH 7.5; 150 mM NaCl; 500 mM imidazole pH 7.5; 0.005% fos-choline-16; and 1/25 EDTA-free protease inhibitor tablet).

Baculovirus Expression Constructs

Full-length human, mouse, and zebrafish Fpn genes were subcloned into pAcUW51 and pBacPAK8 baculovirus shuttle vectors (table 3.5). Both types of vectors utilized the polyhedron promoter to drive Fpn expression and included the consensus KOZAK sequence GCCGCCGCC. Fpn constructs subcloned into the pAcUW51 vector contained a C-terminal 6× His tag. Fpn constructs subcloned into pBacPAK8 contained an N-terminal Rho tag and C-terminal FLAG tag and/or a 10× His tag (table 3.5). The Rho tag is the first 20 amino acids of bovine rhodopsin, and has been shown to boost expression for some eukaryotic membrane proteins (Krautwurst *et al.* 1998). Baculoviruses were constructed and supplied by the Caltech Protein Expression Center. Baculoviruses constructed from the pBacPAK8 shuttle vectors were done so with ProGreen Baculovirus DNA (AB Vector), which included a soluble green fluorescent protein (GFP) driven by the p10 promoter. GFP expression was used to monitor and optimize infection for these baculoviruses.

Table 3.5. Baculovirus expression vectors

Plasmid Name	Gene or Insert Name	Parent Vector	N-terminal tag	C-terminal tag
pAER105	human Fpn (w.t.)	pAcUW51	none	His6
pAER106	human Fpn N144H	pAcUW51	none	His6
pAER107	human Fpn A77D	pAcUW51	none	His6
Rho-hFpn-His	human Fpn (w.t.)	pBacPAK8	Rho	His10
Rho-mFpn-His	mouse Fpn (w.t.)	pBacPAK8	Rho	His10
Rho-zFpn-His	zebrafish Fpn (w.t.)	pBacPAK8	Rho	His10
Rho-hFpn-His-FLAG	human Fpn (w.t.)	pBacPAK8	Rho	His10-FLAG
Rho-mFpn-His-FLAG	mouse Fpn (w.t.)	pBacPAK8	Rho	His10-FLAG
Rho-zFpn-His-FLAG	zebrafish Fpn (w.t.)	pBacPAK8	Rho	His10-FLAG

Small-Scale Tests of Fpn Expression in Baculovirus-Infected Insect Cells

High titer virus stocks were generated at the Caltech Protein Expression Center. Suspension-cultured High Five or Sf9 cells (Invitrogen) were grown in ESF 921 media (Expression Systems) with 1× penicillin/streptomycin (Gibco) and split daily in a shaking incubator at 27 ºC and shaking at 233 rpm. Two-liter beveled filter-capped Erlenmeyer flasks (Corning) containing 1 L media were seeded with insect cells to a starting density of $0.5 \cdot 10^6$ viable cells/mL and cultured until the density reached $\sim 3.5 \cdot 10^6$ viable cells/mL before enough virus to infect over 95% of cells was added. The infection was allowed to proceed for ~48 hr before cells were harvested by centrifugation. Cells from 1 mL of culture at the time of harvest were removed and frozen for later analysis by Western blot, probing against the Rho or His tags.

Sucrose Gradient Analysis of Fpn Expression in Insect Cell Membranes

Fpn constructs Rho-hFpn-His, Rho-mFpn-His, and Rho-zFpn-His were expressed in 1 L volumes of High Five insect cells as described above and split into thirds. The following protocol is adapted from Hu and Kaplan, 2000 (Hu and Kaplan 2000). Cells from one-third of a liter were resuspended in 50 mL ice-cold resuspension/lysis buffer (50 mM Tris pH 7.5, 150 mM NaCl, 2 EDTA-free Complete protease inhibitors (Roche), 1 mM EDTA pH 8.0). Cells were lysed by sonication (flat tip, power level 6, 3 min total process time, 25% duty cycle) and cellular debris was removed by centrifugation at 12,000×g for 20 min at 4 ºC. The supernatant was subject to ultracentrifugation at 125,000×g for 1 hr

at 4 ºC to spin down insect cell membranes. The ultracentrifugation supernatant was discarded and the pellet was resuspended with a Dounce homogenizer in 18 mL of membrane resuspension buffer (66.7 mM Tris pH 7.5, 200 mM NaCl, 1 EDTA-free Complete protease inhibitor tablet, 1.33 mM EDTA pH 8.0) and 11.5 grams of dry sucrose was added and agitated at 4 ºC until fully dissolved. The final volume of this membrane suspension was ~24 mL and the final buffer composition was 50 mM Tris pH 7.5, 150 mM NaCl, 1 mM EDTA, and 1.4 M sucrose. A step sucrose gradient was poured into thin-walled Ultra Clear ultracentrifuge tubes (Beckman) as follows: 3 mL 1.6 M sucrose; 12 mL 1.4 M sucrose-containing membranes; 12 mL 1.2 M sucrose; 6 mL 0.8 M sucrose; and 3 mL 0.4 M sucrose. Step gradients were subject to ultracentrifugation at 96,000×g for 2.5 hr at 4 ºC in a L8-80M Ultracentrifuge (Beckman) using a swinging bucket SW32 rotor (Beckman). Insect cell plasma membranes are known to migrate between the 0.8 and 1.2 M sucrose steps, whereas ER membranes are known to migrate between 1.2 and 1.4 M sucrose steps (Hu and Kaplan 2000). We found the junctions between these steps to have a buildup of off-white material, and they were harvested by puncturing the side of the thin-walled ultracentrifuge tube with a syringe. These layers were analyzed by Western blotting against the N- and C-terminal tags.

Detergent-Extraction Screening of Recombinant Fpn Expressed in Insect Cells

Plasma and ER membrane fractions from one-third liter of baculovirus-infected High Five cells were harvested from a step sucrose gradient as described above. Plasma and ER membrane fractions from Rho-mFpn-His constructs were each diluted to 20 mL with

dilution buffer (100 mM Tris pH 7.5, 300 mM NaCl, 2 mM EDTA, and 2 EDTA-free protease inhibitor tablets). These fractions were aliquoted into 400 µL fractions and 50 µL of 10% detergent stocks (table 3.4) were added to each. The detergent-membrane mixtures were allowed to incubate for 12 hr at 4 ºC with gentle agitation. After the detergent incubation, unsolubilized material was pelleted by ultracentrifugation at 140,000×g for 20 min at 4 ºC. The supernatant was removed and 15 µL was mixed with 5 µL reducing SDS-PAGE loading dye and incubated for 1 hr at room temperature before Western blot analysis.

Scaled-up Expression and Purification of Human, Mouse, and Zebrafish Fpn in Insect Cells

Expression and purification of human, mouse and zebrafish Fpns in baculovirus-infected insect cells was performed as described (Rice *et al.* 2009).

Results and Discussion

Recombinant Expression of Human, Mouse, and Zebrafish Fpn in E. coli

Small-scale human, mouse, and zebrafish Fpn expression tests were performed using 20 different expression constructs (table 3.1), in 5 different strains of *E. coli*, grown in over 10 types of expression media (table 3.2), under several different temperatures, induction conditions, and induction time points. Over 900 separate expression tests were performed (table 3.3) and Fpn expression was monitored by Western blotting against a His or

StrepTagII tag. Expression constructs each contained the full-length human, mouse, or zebrafish sequence in the presence of affinity tags on the N- and/or C-termini. We focused mainly on utilizing 6× His tags, but also screened constructs containing StrepTagII, myc epitope, or maltose binding protein fusions. We reasoned that if Fpn were expressed in *E. coli* and functional as an iron exporter, it might be toxic and thus difficult to express at high levels. In an attempt to prevent this toxicity, we also expressed two mutant forms of Fpn that had been shown to cause ferroportin disease in humans— A77D and N144H. At the time of cloning, these mutations had been freshly discovered, and we did not know if these mutants were unable to act as exporters, but went ahead and included them in our expression testing. Out of twenty Fpn expression constructs screened (table 3.1), we observed expression detectable by Western blot in only two— pAER113a and pAER115a (figure 3.1). The pAER113a construct encoded the wild-type human Fpn gene with N- and C-terminal His tags.   The pAER115a construct encoded the N144H human Fpn gene containing an N-terminal His tag and a C-terminal myc-His tag. Both pAER113a and pAER115a yielded expression of an Fpn band at ~60 kDa.   Both of these expression vectors were constructed from the pET-28b expression plasmid (Novagen) driven by the IPTG-inducible T7 promoter.   Interestingly, pAER113a and pAER115a were the only Fpn variants screened with both N- and C-terminal His tags. They were the product of a mis-annealed PCR and were only identified upon sequencing, but were added to the library of expression constructs because of their unique tagging configurations.   We did not re-clone mouse Fpn, zebrafish Fpn, nor other Fpn mutants with both N- and C-terminal His tags to further test bacterial expression of Fpn, however

we expect that these other Fpn forms are capable of being expressed in *E. coli* with His tagging on both termini.

While the details of the expression construct played an important part in bacterial expression of Fpn, we found that expression strain and media type were observed to be similarly critical parameters for obtaining detectable expression.   We found that BL21(DE3) *E. coli* was suitable for Fpn expression, but we did not observe expression in any other bacterial strain tested. Other strains tested include Rosetta(DE3) (Novagen) and RosettaBlue(DE3) (Novagen) strains, which express rare *E. coli* codon machinery and have been shown to help boost the expression of some eukaryotic proteins, and C41(DE3) and C43(DE3) strains, which have been shown to be capable of over-expressing eukaryotic membrane proteins (Arechaga *et al.* 2003). The culture media formulation also had an important effect on expression. We tested Fpn expression using 11 different media formulations (table 3.2). These media formulations were based on the common media formulations known as LB, SOC, 2×YT, and TB. The media formulations TB1-TB7 (also called GM1-GM7) were developed by Yan Poon (Poon 2008). They were derivatives of TB where some or all of the yeast extract was replaced with malt and/or beef extracts (table 3.2). Fpn expression was observed in some conditions with the TB, TB1, TB2, TB3, TB4, TB5, and TB7 media formulations, but not in the 2×TY, LB, SOC, or TB6 media formulations (table 3.3).

After screening and optimizing Fpn expression as described above, the best expression condition observed was using the pAER113a or pAER115a vector, BL21(DE3) strain, grown in TB5 media and induced at 30 ºC for 3 hr. We sought to further enhance expression by varying amino acid and salt additives in this formulation. We varied the salts in TB5 by increasing or reducing the amount of potassium phosphate salt solution or by replacing them with sodium chloride. Separate tests screened amino acid additives, where pure powdered L-glycine, L-lysine, L-tryptophan, L-leucine, L-histidine, or L-methionine were added to a level of 1% (w/v). Fpn expression was observed in all these tests, and the addition L-lysine lead to a small increase in expression (figure 3.2). Further tests were performed to test if the further addition of 100 μM $FeCl_2$ or $ZnCl_2$ would increase expression, however they did not.

The final optimized and scaled-up Fpn expression condition in *E. coli* was in BL21(DE3) cells transfected with pAER113a, grown in TB5 media with an additional 1% L-lysine, and induced by 0.1 mM IPTG for 3 hr at 30 ºC. Typical 55 L fermenter runs yielded ~320–350 grams of wet bacterial cell paste.

Boiling Fpn in Loading Dye Results in Aberrant SDS-PAGE Migration

Fpn expressed in *E. coli* was found to run at an anomalously high molecular weight if SDS-PAGE sample preparation protocol involved the usual 95–100 ºC incubation in SDS-containing loading dye. Under these conditions Fpn was observed to run at an apparent molecular weight of 150–250 kDa (figure 3.3). Fpn samples incubated at room

temperature for >20 min were shown to migrate with an apparent mass of 60 kDa, which was much closer to the predicted Fpn molecular weight of 65–70 kDa (depending on affinity tag configuration). Unless otherwise noted, Fpn samples analyzed by SDS-PAGE for subsequent Coomassie staining or Western blotting were all incubated at room temp for 20 min to 1 hr prior to loading.

Detergent-Extraction of Recombinant Fpn from E. coli Membranes

Human Fpn expressed in BL21(DE3) from the expression plasmid pAER113a was screened for its ability to be solubilized by 48 detergents as described above (table 3.4). Membranes solubilization was performed at 4 ºC for 2 hr, after which unsolubilized material was centrifuged and supernatants were analyzed by Western blot, probing with an anti-His antibody against the affinity tags on this Fpn construct. Comparing detergent extractions with non-detergent controls allowed for the clear identification of small amounts of solubilized Fpn in the presence of a subset of detergents screened. The detergents fos-choline-14, fos-choline-16, cyclofos-7, anzergent-3-12, anzergent-3-14, and to a lesser extent cymal-4, were capable of extracting Fpn from bacterial membranes to yield a band at ~60 kDa as detected by Western blot (figure 3.4). Interestingly, the Western blots of this analysis revealed that some detergents extracted Fpn in a form that was aggregated at >200 kDa as determined by SDS-PAGE, much like the bands observed when samples are boiled in SDS-PAGE loading dye. These high molecular weight Fpn aggregates were detected by Western blot upon solubilization with the detergents

anzergent-3-14, fos-choline-10, -12, -14, and -16, LDAO, dodecyldimethyl glycine, cyfos-7, and almost all polyoxyethylene detergents (table 3.6) (figure 3.4).

Table 3.6. Detergent extraction of Fpn expressed in *E. coli* and insect cells

Detergent Name	Bacterial Expression Extracted As:		Insect Cell Expression Extracted As:	
	60 kDa band	Aggregates	60 kDa band	Aggregates
CHAPS			+	
Cholate			+	
Deoxycholate			+	
Anzergent-3-12	+		+	+
Anzergent-3-14	+	+	+	+
Cymal-3			+	
Cymal-4			n.d.	n.d.
Cymal-5	+		+	
Cymal-6			+	
Fos-choline-9			n.d.	n.d.
Fos-choline-10		+	+	+
Fos-choline-12		+	+	+
Fos-choline-14	+	+	+	+
Dodecyldimethyl glycine		+	+	+
Fos-choline-16	+	+	+	
Cyclofos-7	+	+	n.d.	n.d.
Fos-choline-iso-11			n.d.	n.d.
LDAO		+	+	+
Fos-MEA-8			+	
Fos-MEA-10			+	
Fos-MEA-12			+	
Fosfen-4			+	
Fosfen-5				
Fosfen-9			n.d.	n.d.
Octyl glucoside				
Nonyl glucoside				
HEGA-9			+	+
HEGA-10				
MEGA-8				
MEGA-9			+	
Nonyl maltoside			+	
Decyl maltoside			+	
Undecyl maltoside			+	
Dodecyl maltoside			+	

Detergent Name	Bacterial Expression	Insect Cell Expression	
Tridecyl maltoside		+	
Tween 20	+	+	
Brij-35	+	+	
Brij-58	+	+	+
Tween 80			
$C_{10}E_6$	+	n.d.	n.d.
$C_{10}E_9$	+	+	+
$C_{12}E_8$	+	+	+
$C_{12}E_9$	+	+	+
$C_{12}E_{10}$	+	+	+
$C_{13}E_8$	+	+	+
Triton X-100	+	+	+
Triton X-114	+	n.d.	n.d.

Based on these results, a subset of the detergents screened was selected to move forward with small-scale preparations of Fpn. Samples were solubilized, purified by Ni-affinity chromatography, and analyzed by analytical size exclusion chromatography (SEC) using a 1.4 mL Superdex 200 column (GE Healthcare) performed using a Smart System FPLC (GE Healthcare), as described in the methods. The detergents chosen for the next phase of analysis included each detergent that was capable of extracting Fpn as an approximately 60 kDa band in the solubilization screen (fos-choline-14, fos-choline-16, cyclofos-7, anzergent-3-12, anzergent-3-14, and cymal-4), as well as a subset of the detergents that were shown to extract Fpn as a high molecular weight band (fos-choline-10, and fos-choline-12). Analytical SEC profiles revealed that fos-choline-14 and fos-choline-16 were capable of stabilizing solubilized Fpn as a predominantly single peak, suggesting a single species, though without accurate knowledge of the detergent micelle size, we were not capable of determining the oligomeric state of solubilized Fpn with these data (figure 3.5). The analytical SEC trace for the fos-choline-16

solubilization was the most symmetric, with the fos-choline-14 solubilization having a small high molecular weight shoulder in its trace. Extracting with fos-choline-12 revealed a complicated trace with much more material eluting at higher molecular weights, as well as in the void volume. We found that fos-choline-10 was poor at solubilizing Fpn from these membranes, with the little Fpn that was extracted being observed in the void volume. Cyclofos-7 was also a very poor Fpn extractor as assessed by this method. Anzergent-3-12 and anzergent-3-14 both yielded complicated SEC traces, indicative of heterogeneity in the aggregation state of these Fpn samples. We concluded that fos-choline-16 was the best detergent for the solubilization of Fpn from bacterial membranes into a homogenous population of solubilized protein-detergent complexes.

Purification of Recombinant Fpn from E. coli

Doubly His-tagged Fpn was expressed in BL21(DE3) *E. coli* as described above. Cells were harvested, lysed by sonication and whole-cell membranes were separated from soluble proteins and cellular debris by centrifugation. Purified membranes were incubated with fos-choline-16 detergent to extract Fpn and then unsolubilized membranes were removed by centrifugation. Fpn was then purified by Ni affinity chromatography and eluted with imidazole (figure 3.6). After Ni chromatography, Fpn purity was assessed by SDS-PAGE to be ~50%–60%. Fpn expression was verified by Western blotting against the His tag, as well as by proteolytic peptide sequencing by mass spec at the PPMAL facility in the Beckman Institute at Caltech. Yields were estimated at ~10–30 μg

purified Fpn per liter of bacterial culture. Further purification efforts using ion exchange chromatography or SEC were made as well, however due to the low initial yield, protein losses during these extra steps resulted in very little final protein.   While the bacterial expression of Fpn was possible, it was not suitable for its production in milligram quantities at high purity for biophysical analysis and crystallization attempts.

Recombinant Expression of Human, Mouse, and Zebrafish Fpn in Insect Cells

Small-scale tests screening the expression of human, mouse and zebrafish Fpn were carried out in shaking flasks of High Five cells grown in suspension. Baculoviruses used to infect these insect cells (table 3.5) encoded Fpn variants with or without an N-terminal Rho tag (Krautwurst *et al.* 1998). Each baculovirus tested utilized the polyhedron promoter to drive Fpn expression. We observed Fpn expression by Western blot for each baculovirus containing an N-terminal Rho tag, whereas no Fpn expression was observed for baculoviruses coding for Fpn lacking this tag. Western blotting was performed using probes against both the N-terminal Rho tag and C-terminal affinity tags, verifying full-length Fpn expression (figure 3.7).   Differences between the C-terminal affinity tags included in these constructs had minimal effect on expression levels.   Constructs with either a 10× His tag or a 10× His tag in tandem with a FLAG tag were expressed at similar levels.   Furthermore, the three Fpn homologues were found to express at comparable levels, as determined by Western blot.   Both High Five (derived from *Trichoplusia ni*) and Sf9 (derived from *Spodoptera frugiperda*) insect cell lines were

capable of expressing Fpn (figure 3.7), however all scaled-up expressions were performed in High Five cells (Rice *et al.* 2009).

While full-length Fpn expression was observed when baculovirus-infected insect cells were analyzed by Western blot, we sought to learn the subcellular location of this expressed Fpn. In particular, we wanted to determine if Fpn was fully processed and transported to the plasma membrane, or if it was building up within the cell at a processing organelle such as the endoplasmic reticulum. To assess the location of Fpn within these insect cells, we performed a coarse sucrose gradient fractionation. We observed that a large fraction of the expressed Fpn was fully processed and trafficked to the plasma membrane, with some significant fraction present in the ER (figure 3.8). These results indicated that insect cells were capable of expressing, processing and trafficking human, mouse, and zebrafish Fpn to the plasma membrane. Because we observed such a large fraction of Fpn in the plasma membrane, we suggest that the Fpn contained within subcellular compartments was proceeding along the biosynthetic pathway without significant bottlenecks.

Detergent Extraction of Recombinant Fpn from Insect Cell Membranes

In contrast to bacterially expressed Fpn, which was only capable of being extracted by a few detergents, insect cell–expressed Fpn was broadly extractable by many detergents screened (table 3.6) (figure 3.9). Some detergents, such as cymals, maltosides, fos-choline-16, fos-MEAs, and MEGA-9, extracted Fpn as a band migrating with an apparent

mass of ~60 kDa with little to no aggregate observed by Western blot. Other detergents, such as the lower chain length fos-cholines, polyoxyethylenes, anzergents and LDAO, were capable of extracting Fpn as an ~60 kDa band, but also extracted a significant portion of Fpn as aggregates (table 3.6). These high molecular weight aggregates were not observed in samples treated without detergent, and perhaps suggests that some detergents extract Fpn in a partially unstable form tending toward aggregation.

Purification of Recombinant Fpn from Insect Cells

The expression, detergent extraction, and purification of human Fpn to levels suitable for biophysical characterization has been described (Rice *et al.* 2009). Mouse and zebrafish Fpns were purified using identical methods, with similar results (figures 3.10 and 3.11). Numerous crystallization attempts (>5,000) were carried out with purified human, mouse and zebrafish Fpn (see appendix), however no Fpn crystals were observed.
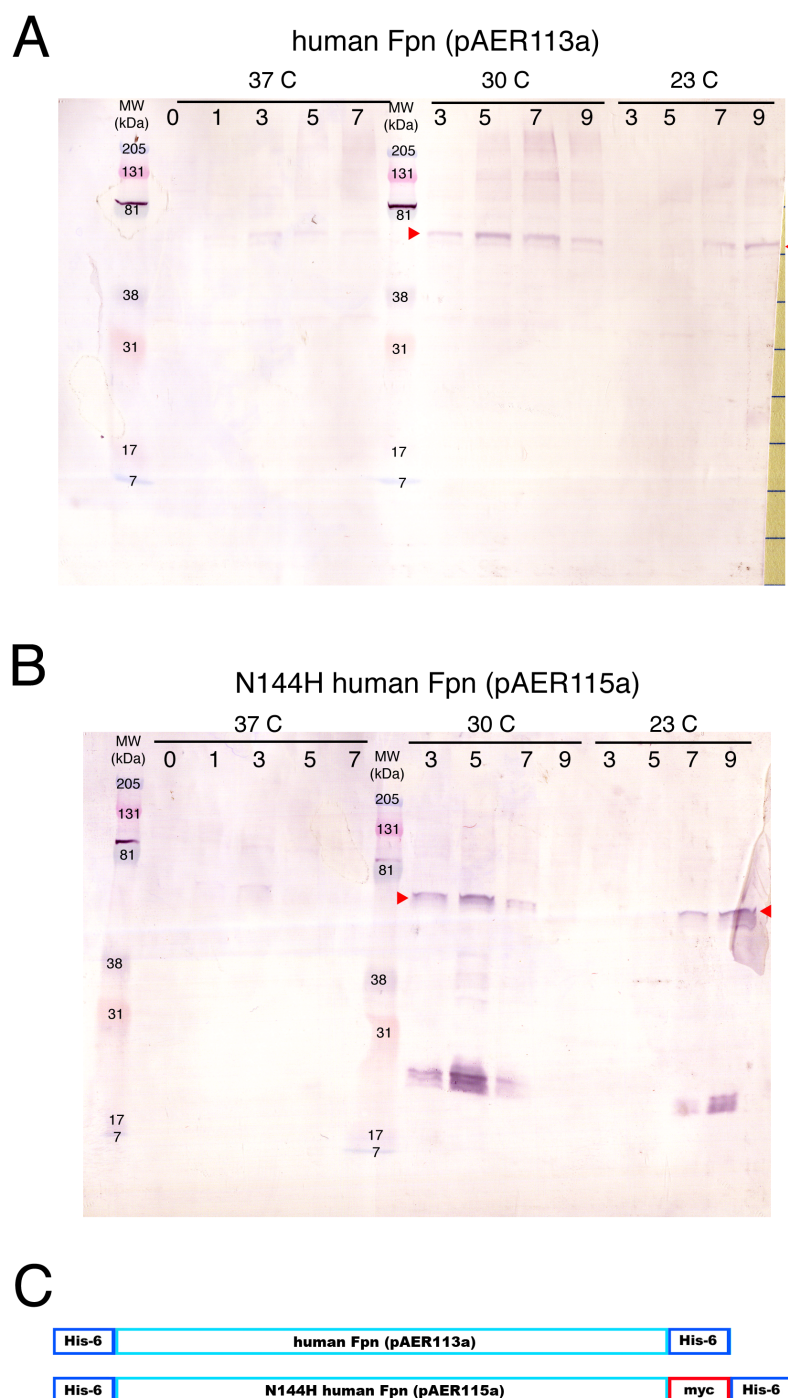
Figure 3.1. Western blot of small-scale bacterial expression of wild-type (panel A) and N144H (panel B) Fpns. As described in the methods, BL21(DE3) *E. coli* were transformed with either pAER113a or pAER115a, cultured in TB5 media at 37 °C, shifted to the final temperature, induced with IPTG, and harvested after the time shown, in hours. Panel C shows a schematic depicting the tagging orientation of the constructs used. The ~60 kDa Fpn bands are indicated (red arrows).
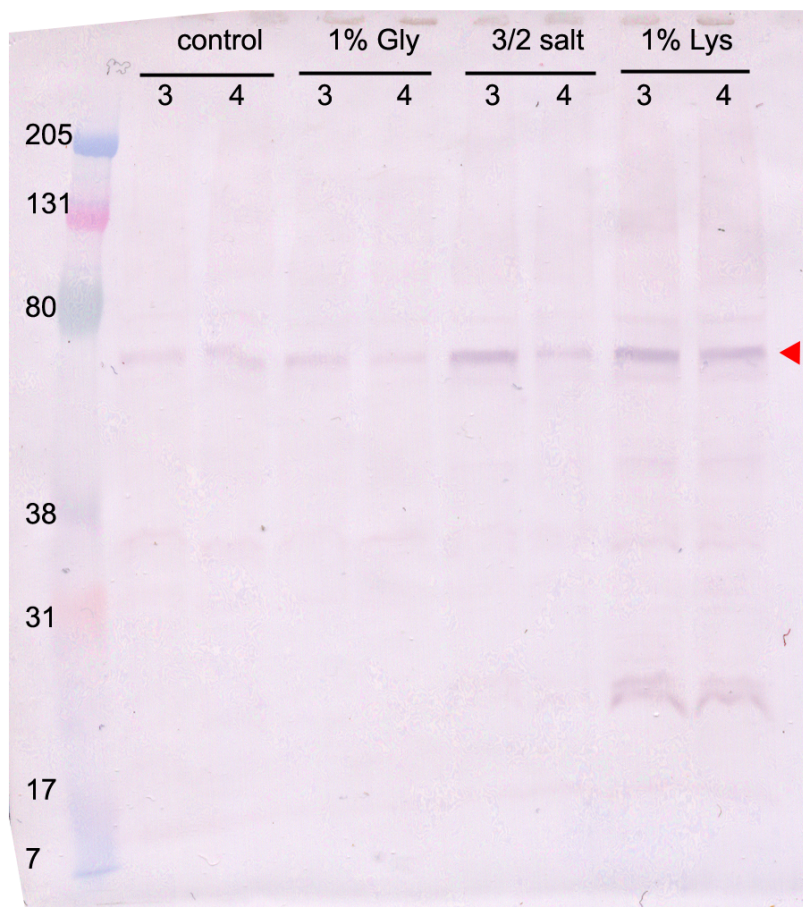
Figure 3.2. Western blot of test for the affect of growth media additives to bacterial cultures. BL21(DE3) *E. coli* was transformed with wild-type Fpn (pAER113a) and was cultured in TB5 media with 1% L-glycine, 1% L-lysine or 50% extra salt as additives, as indicated in the methods. Induction length is indicated in hours, for each lane. "Control" is expression in TB5 media alone. The ~60 kDa Fpn bands are indicated (red arrow).
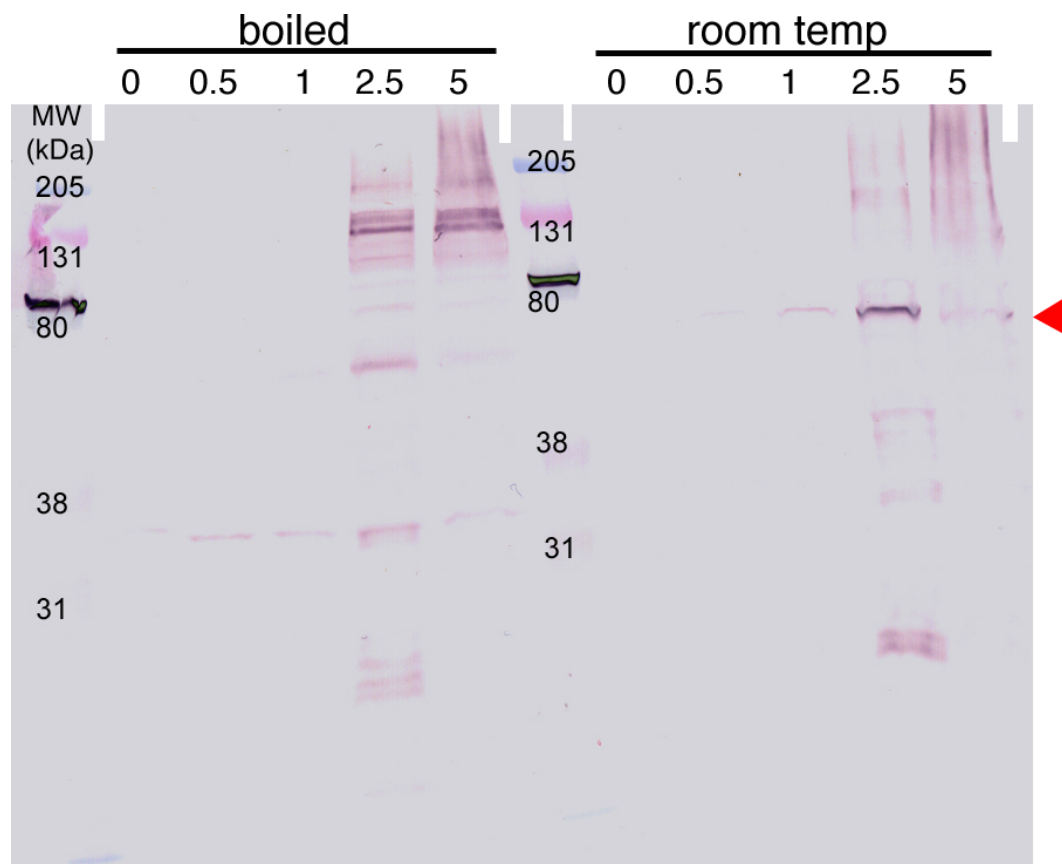
Figure 3.3. Boiling samples in loading dye leads to aberrant SDS-PAGE migration. A Western blot is shown for an expression time course of N144H Fpn (pAER115a) in BL21(DE3) *E coli*. Samples loaded in the "boiled" or "room temp" lanes were taken from the same time course, with the only difference being their treatment immediately prior to gel loading. Samples were either boiled in loading dye for 1 min or incubated at room temperature for 1 hr prior to SDS-PAGE. Induction length is indicated in hours, for each lane. The ~60 kDa Fpn band is noted by a red arrow.
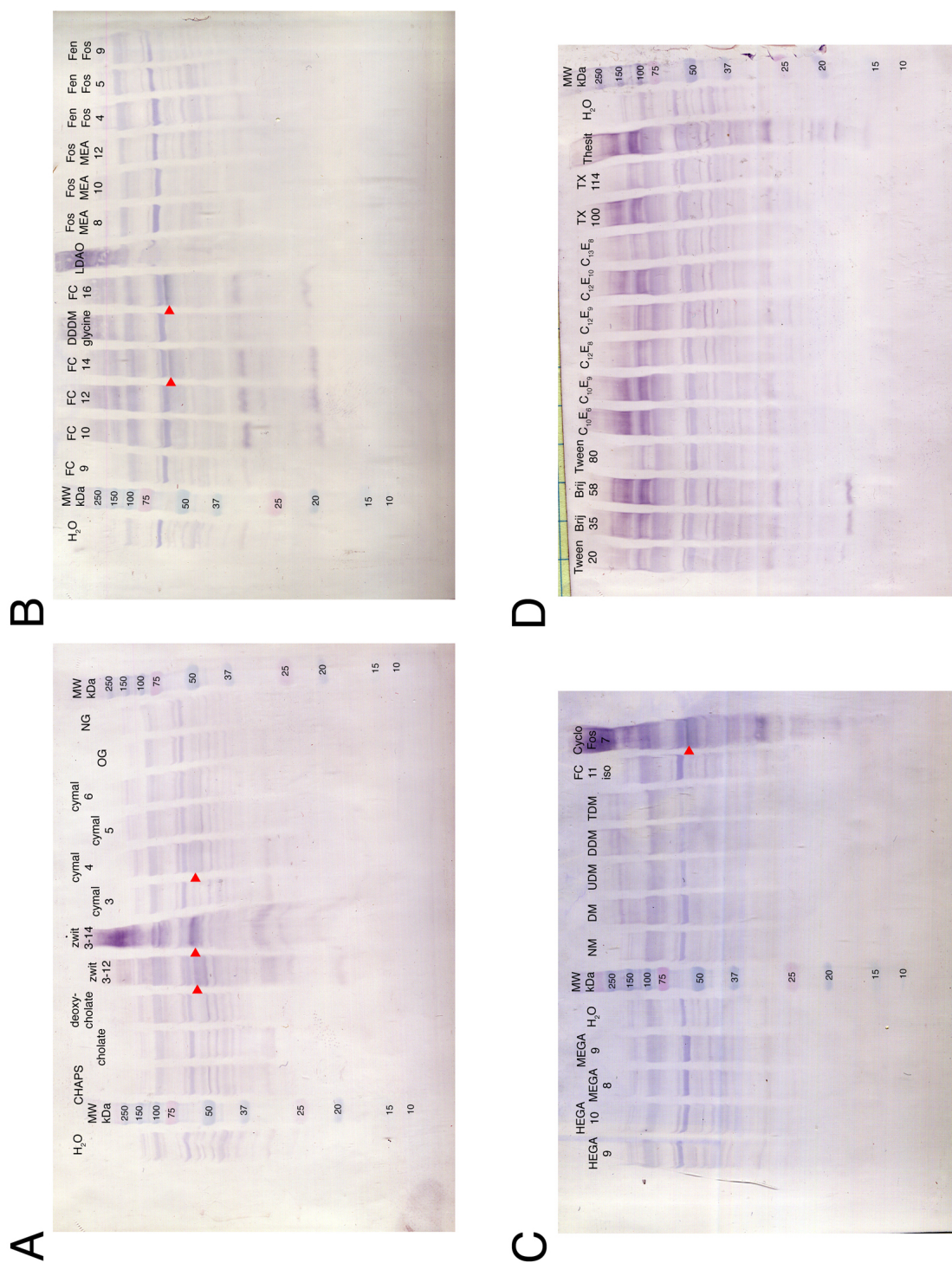
Figure 3.4. Detergent solubilization screen of Fpn expressed in BL21(DE3) *E.coli.* Samples were incubated in water or 1% detergent and Western blots against the His tag were performed. Fpn bands at ~60 kDa are noted by red arrows. See table 3.6 for a full summary of these data.
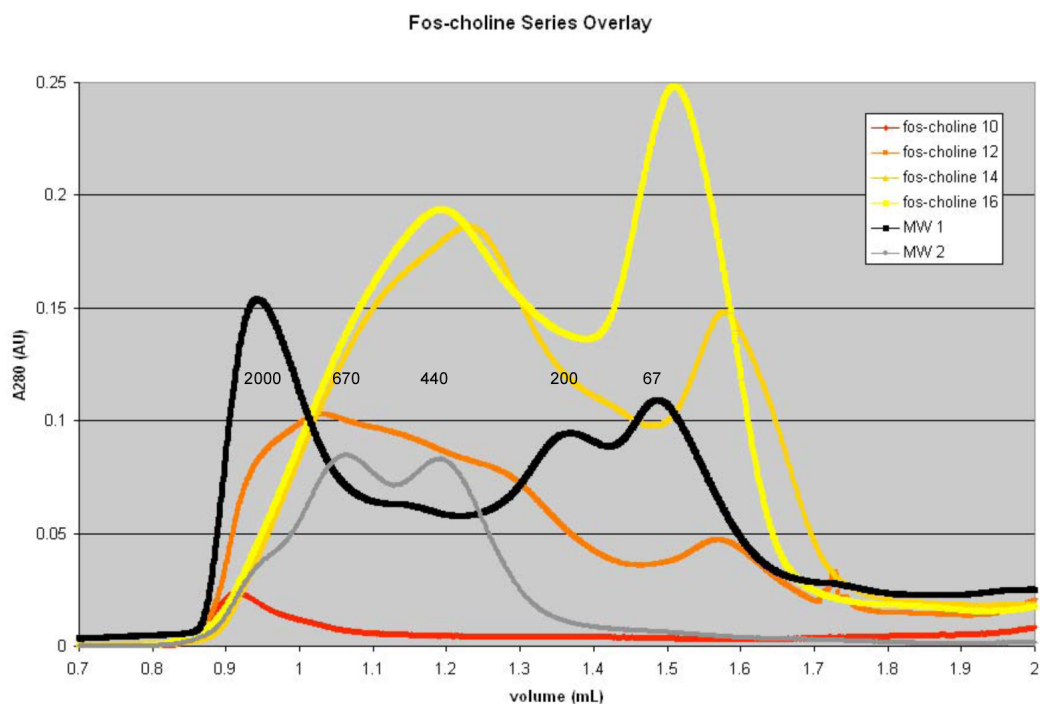
Figure 3.5. Quality analysis by SEC for fos-choline extraction of Fpn from *E. coli* membranes. Fos-choline 10, 12, 14, and 16 were used to extract Fpn from BL21(DE3) *E. coli*. Extracts were purified by Ni affinity chromatography, concentrated, and analyzed by SEC using a SMART system FPLC. Traces for molecular weight standards are shown in gray or black for reference (MW1 and MW2), and the molecular weight, in kDa, corresponding to each peak is labeled.
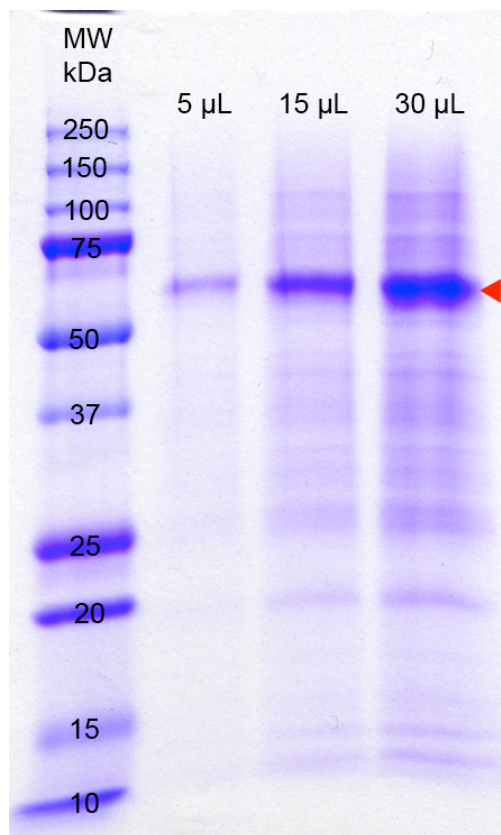
Figure 3.6. Ni-NTA purification of N144H human Fpn (pAER115a) expressed in BL21(DE3) *E. coli*. Purified Fpn was eluted with imidazole (see Methods) and 5, 15, or 30 µL were loaded on a 12% polyacrilamide gel and analyzed by SDS-PAGE. Coomasie staining revealed a Fpn band at ~60 kDa (red arrow). Molecular weight standards are shown at left and labeled in kDa.
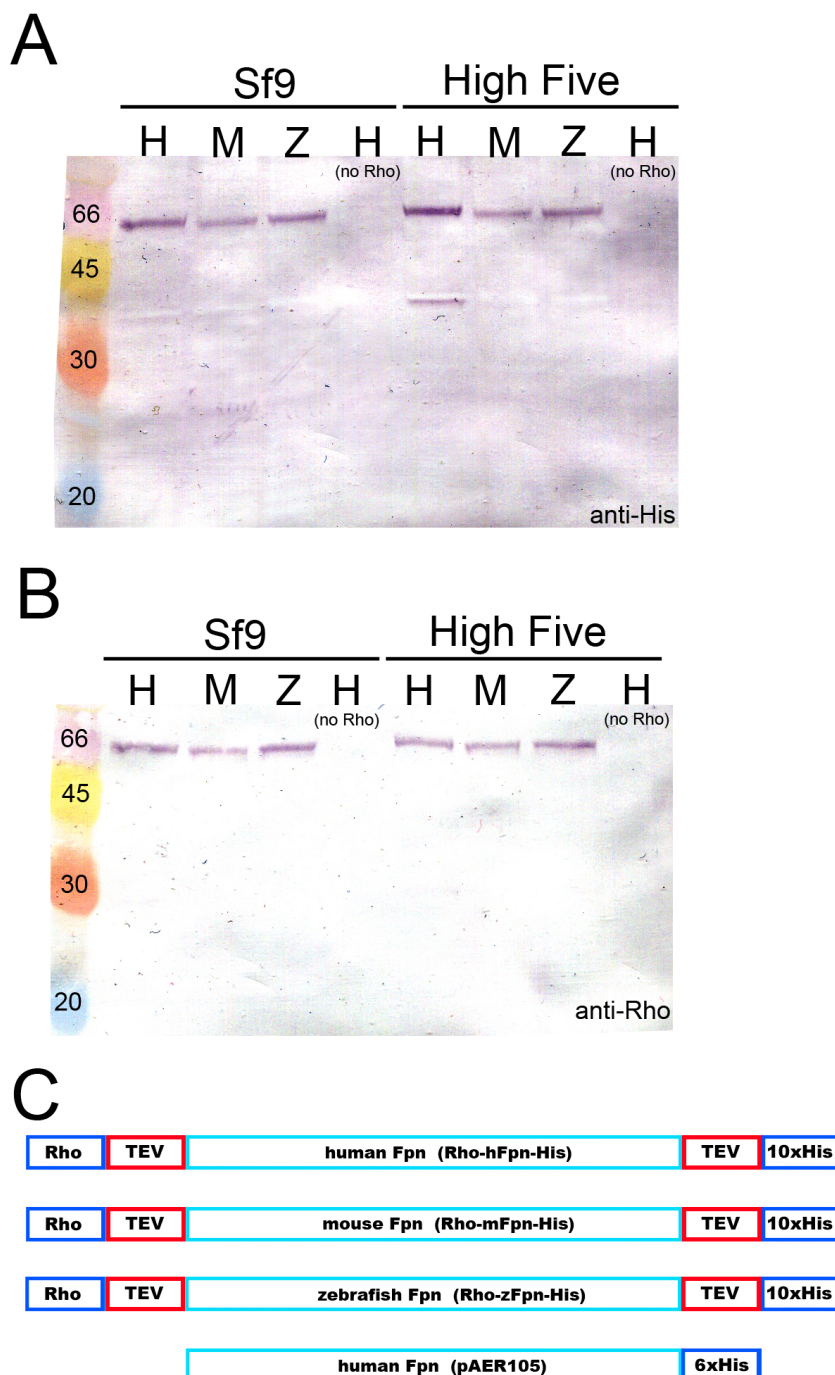
Figure 3.7. Expression of Fpn in baculovirus-infected insect cells. Baculoviruses encoding full-length human, mouse, or zebrafish Fpn with an N-terminal Rho tag and a C-terminal His tag (H, M, and Z, respectively) or only a C-terminal His tag (H (no rho)), were used to infect Sf9 and High Five insect cells. Cells were harvested 48 hr post-infection and Westerns against the His (panel A) or Rho (panel B) tags were performed. Molecular weight markers are labeled on the left in kDa. Panel C shows a schematic depicting the tagging orientation of the constructs used.
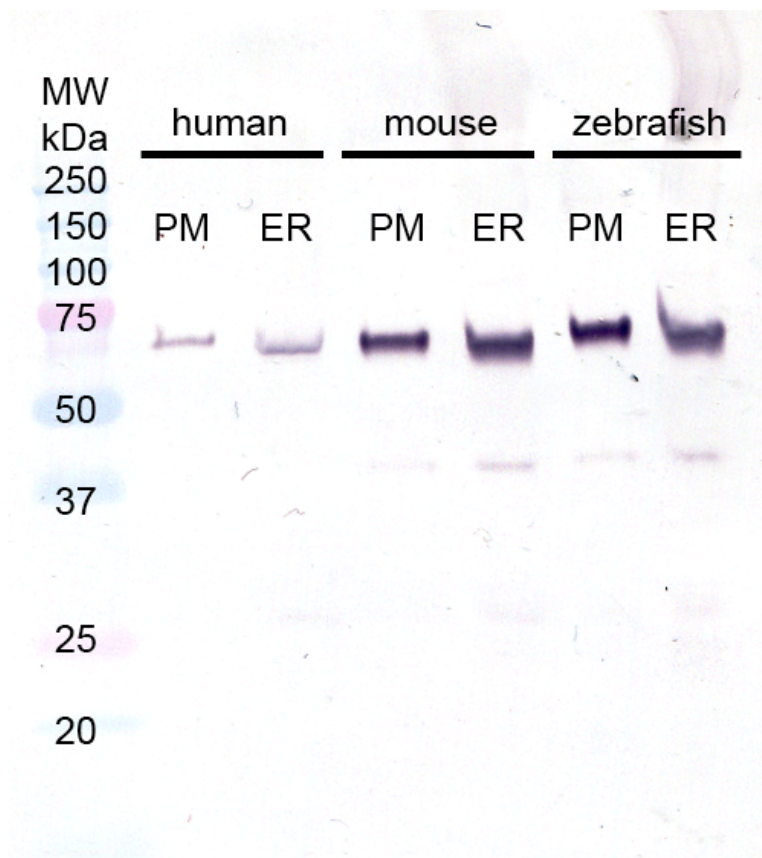
Figure 3.8. Sucrose gradient of membranes from Fpn-expressing baculovirus-infected insect cells. A Western blot against the Rho tag of human, mouse, and zebrafish Fpn reveals that Fpn was found in both plasma membrane (PM) and endoplasmic reticulum (ER) fractions. Molecular weight standards are shown in kDa.
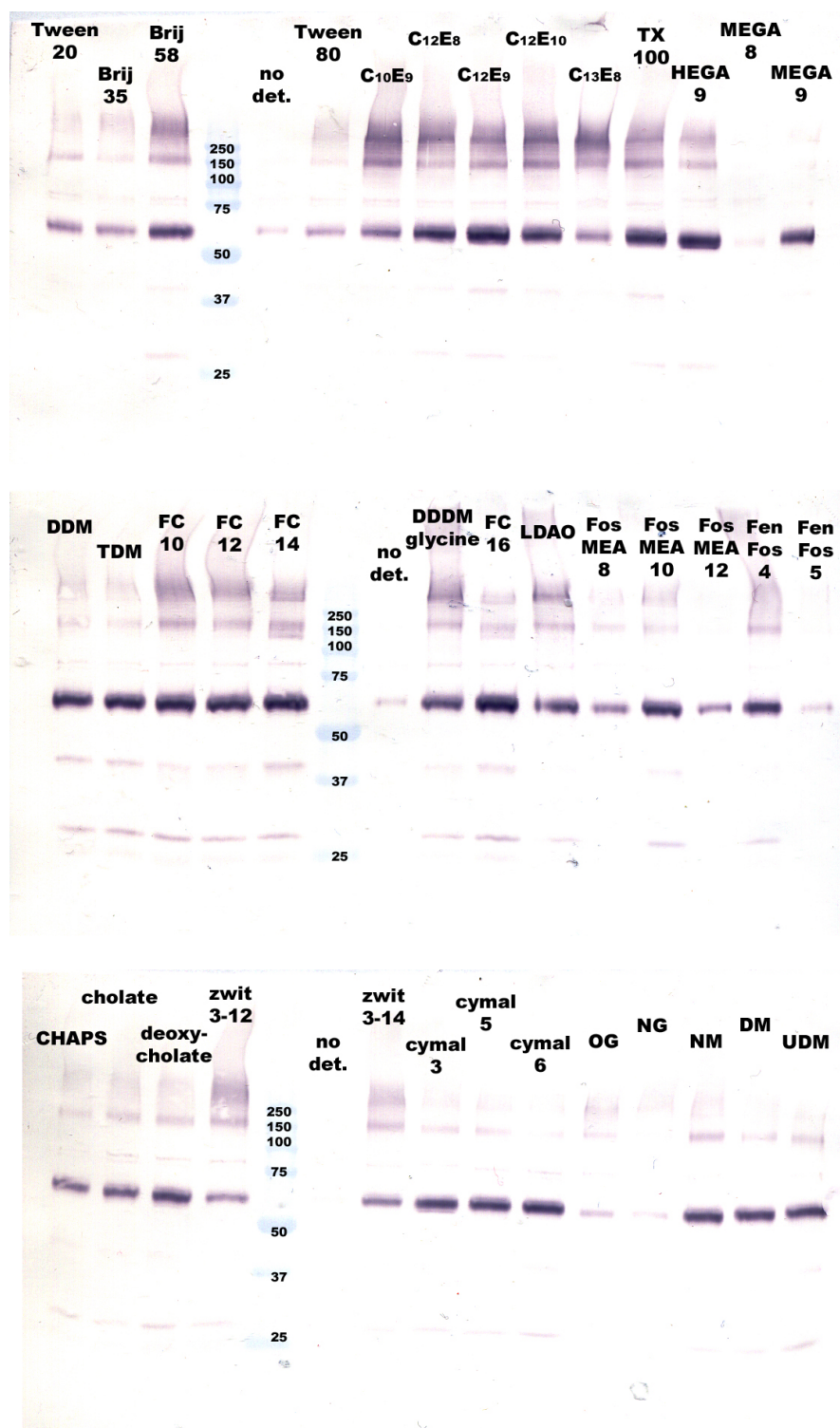
Figure 3.9. Detergent solubilization screen of Fpn expressed in insect cells. Solubilization was performed in water ("no det.") or 1% detergent (see methods) and Western blots against the Rho tag were performed. Fpn bands at ~60 kDa were observed for solubilization for many detergents tested. See table 3.6 for a full summary of these data.
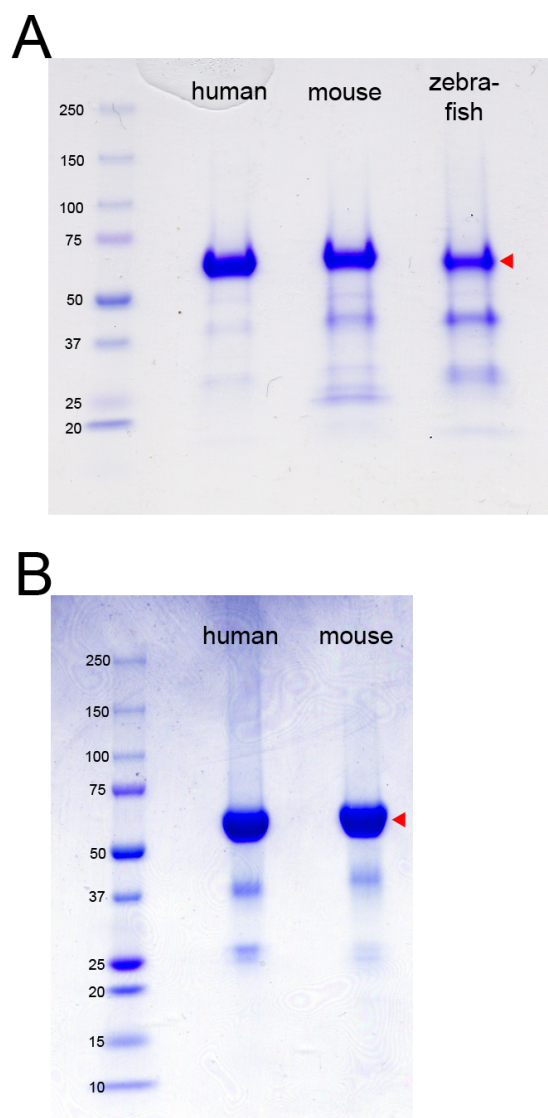
Figure 3.10. Coomassie-stained SDS-PAGE analysis of purified Fpn expressed in baculovirus-infected High Five cells. Full-length human, mouse and zebrafish Fpn with an N-terminal Rho tag, and a C-terminal tandem 10×His-FLAG tag were expressed in insect cells. Panel A shows human, mouse, and zebrafish Fpns after TALON and FLAG column purification. Panel B shows human and mouse Fpns after an additional SEC separation. Molecular weight standards are shown at left and labeled in kDa.
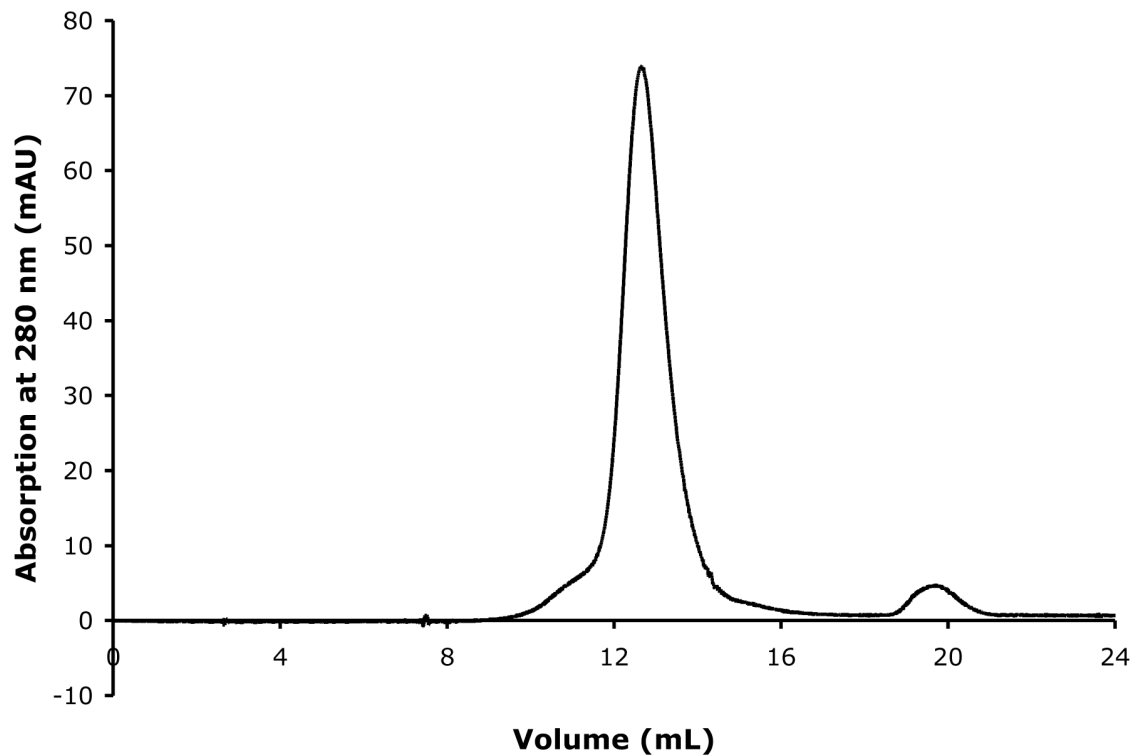
Figure 3.11. SEC analysis of mouse Fpn after purification over TALON and FLAG columns. The mouse Fpn elution profile is a symmetrical peak with a small high molecular weight shoulder.

References

Abboud, S., and Haile, D. J. (2000). A novel mammalian iron-regulated protein involved in intracellular iron metabolism. *J Biol Chem* **275**, 19906–19912.

Arechaga, I., Miroux, B., Runswick, M. J., and Walker, J. E. (2003). Over-expression of *Escherichia coli* F1F(o)-ATPase subunit a is inhibited by instability of the uncB gene transcript. *FEBS Lett* **547**, 97–100.

De Domenico, I., McVey Ward, D., Nemeth, E., Ganz, T., Corradini, E., Ferrara, F., Musci, G., Pietrangelo, A., and Kaplan, J. (2006). Molecular and clinical correlates in iron overload associated with mutations in ferroportin. *Haematologica* **91**, 1092–1095.

De Domenico, I., Vaughn, M. B., Yoon, D., Kushner, J. P., Ward, D. M., and Kaplan, J. (2007a). Zebrafish as a model for defining the functional impact of mammalian ferroportin mutations. *Blood* **110**, 3780–3783.

De Domenico, I., Ward, D. M., Langelier, C., Vaughn, M. B., Nemeth, E., Sundquist, W. I., Ganz, T., Musci, G., and Kaplan, J. (2007b). The molecular mechanism of hepcidin-mediated ferroportin down-regulation. *Mol Biol Cell* **18**, 2569–2578.

De Domenico, I., Ward, D. M., Musci, G., and Kaplan, J. (2007c). Evidence for the multimeric structure of ferroportin. *Blood* **109**, 2205–2209.

De Domenico, I., Ward, D. M., Nemeth, E., Vaughn, M. B., Musci, G., Ganz, T., and Kaplan, J. (2005). The molecular basis of ferroportin-linked hemochromatosis. *Proc Natl Acad Sci USA* **102**, 8955–8960.

Donovan, A., Brownlie, A., Zhou, Y., Shepard, J., Pratt, S. J., Moynihan, J., Paw, B. H., Drejer, A., Barut, B., Zapata, A.*, et al.* (2000). Positional cloning of zebrafish ferroportin1 identifies a conserved vertebrate iron exporter. *Nature* **403**, 776–781.

Drakesmith, H., Schimanski, L. M., Ormerod, E., Merryweather-Clarke, A. T., Viprakasit, V., Edwards, J. P., Sweetland, E., Bastin, J. M., Cowley, D., Chinthammitr, Y.*, et al.* (2005). Resistance to hepcidin is conferred by hemochromatosis-associated mutations of ferroportin. *Blood* **106**, 1092–1097.

Goncalves, A. S., Muzeau, F., Blaybel, R., Hetet, G., Driss, F., Delaby, C., Canonne-Hergaux, F., and Beaumont, C. (2006). Wild-type and mutant ferroportins do not form oligomers in transfected cells. *Biochem J* **396**, 265–275.

Hu, Y. K., and Kaplan, J. H. (2000). Site-directed chemical labeling of extracellular loops in a membrane protein. The topology of the Na,K-ATPase alpha-subunit. *J Biol Chem* **275**, 19185–19191.

Krautwurst, D., Yau, K. W., and Reed, R. R. (1998). Identification of ligands for olfactory receptors by functional expression of a receptor library. *Cell* **95**, 917–926.

McKie, A. T., Marciani, P., Rolfs, A., Brennan, K., Wehr, K., Barrow, D., Miret, S., Bomford, A., Peters, T. J., Farzaneh, F*., et al.* (2000). A novel duodenal iron-regulated transporter, IREG1, implicated in the basolateral transfer of iron to the circulation. *Molecular Cell* **5**, 299–309.

Montosi, G., Donovan, A., Totaro, A., Garuti, C., Pignatti, E., Cassanelli, S., Trenor, C. C., Gasparini, P., Andrews, N. C., and Pietrangelo, A. (2001). Autosomal-dominant hemochromatosis is associated with a mutation in the ferroportin (SLC11A3) gene. *J Clin Invest* **108**, 619–623.

Nemeth, E., Tuttle, M. S., Powelson, J., Vaughn, M. B., Donovan, A., Ward, D. M., Ganz, T., and Kaplan, J. (2004). Hepcidin regulates cellular iron efflux by binding to ferroportin and inducing its internalization. *Science* **306**, 2090–2093.

Njajou, O. T., Vaessen, N., Joosse, M., Berghuis, B., van Dongen, J. W. F., Breuning, M. H., Snijders, P., Rutten, W. P. F., Sandkuijl, L. A., Oostra, B.A*., et al.* (2001). A mutation in SLC11A3 is associated with autosomal dominant hemochromatosis. *Nature Genetics* **28**, 213–214.

Poon, Y. S. (2008). The characterization and structure of mechanosensitive channels of small conductance. Ph.D. dissertation, California Institute of Technology, 2008, 1–133.

Rice, A. E., Mendez, M. J., Hokanson, C. A., Rees, D. C., and Björkman, P. J. (2009). Investigation of the biophysical and cell biological properties of ferroportin, a multipass integral membrane protein iron exporter. *J Mol Biol* **386**, 717–732.

Schimanski, L. M., Drakesmith, H., Merryweather-Clarke, A. T., Viprakasit, V., Edwards, J. P., Sweetland, E., Bastin, J. M., Cowley, D., Chinthammitr, Y., Robson, K. J*., et al.* (2005). In vitro functional analysis of human ferroportin (FPN) and hemochromatosis-associated FPN mutations. *Blood* **105**, 4096–4102.

Schimanski, L. M., Drakesmith, H., Talbott, C., Horne, K., James, J. R., Davis, S. J., Sweetland, E., Bastin, J., Cowley, D., and Townsend, A. R. (2008). Ferroportin: lack of evidence for multimers. *Blood Cells Mol Dis* **40**, 360–369.

Chapter 4:

Lack of Evidence for Interactions between Ferroportin and the Hereditary Hemochromatosis Protein, HFE

In this chapter we report various assays aimed at detecting a physical and/or functional interaction between Fpn and HFE.

Introduction

Since the initial identification and cloning of the HFE gene, its precise role in iron homeostasis has been a mystery (Feder *et al.* 1996). Clearly HFE plays a critical role in regulating iron stores, as recessive mutations within this gene were shown to account for the majority of worldwide hereditary hemochromatosis (HH) (Feder *et al.* 1996). It was also shown that HFE interacted with transferrin receptor (TfR), that this binding reduced TfR's affinity for transferrin (Tf), and that the disease-causing HFE mutations interfere with this interaction (Feder *et al.* 1998). The discovery of the HFE-TfR interaction gave clear evidence that HFE could play a role in regulating cellular iron levels by modulating the TfR-Tf iron uptake pathway, but it was still unclear how mutations in HFE might lead to the severe iron overload observed in HH patients. In 2000, three groups independently identified the only known vertebrate ionic iron exporter, ferroportin (Fpn) (Abboud and Haile 2000; Donovan *et al.* 2000; McKie *et al.* 2000). It was shown that both HFE (Parkkila *et al.* 1997) and Fpn (Donovan *et al.* 2000) are expressed on the basolateral membrane of duodenal enterocytes, the main site of systemic iron uptake. It was also noted that HFE expression in the duodenum was highest in the duodenal crypt cells (Parkkila *et al.* 1997), whereas Fpn expression was highest at the villus tips, though still present in the crypts at lower levels (Donovan *et al.* 2000). It had been hypothesized that body iron stores were sensed in the duodenal crypt cells (Roy and Enns 2000), and this lead Townsend and Drakesmith to introduce the hypothesis that HFE could act as an iron sensor by negatively regulating the functions of both TfR and Fpn in duodenal crypt cells

(Townsend and Drakesmith 2002). A schematic for this hypothesis is depicted in figure 4.1. In brief, the hypothesis predicted that HFE was capable of reducing iron uptake by binding to and inhibiting the iron export function of Fpn. It suggested that HFE could bind to either TfR or Fpn and these three proteins (along with serum Tf) were in a dynamic equilibrium on the basolateral serum-facing membrane (figure 4.1A). If iron stores in an individual were low (and thus Tf iron saturation was low) then Tf would be unable to bind tightly to TfR at the cell surface, and thus HFE would be sequestered by TfR. This would prevent HFE from binding to and inhibiting Fpn and would allow iron uptake to proceed as normal (figure 4.1B). On the other hand, if iron stores were high (and thus Tf iron-saturation was high) Tf would bind tightly to TfR, competing away any HFE. HFE would then be allowed to bind Fpn and iron uptake would be prevented (figure 4.1C). This hypothesis was further strengthened by a study in macrophage-like cells reporting that soluble HFE added to iron-loaded cells was capable of inhibiting iron export (Drakesmith *et al.* 2002). Following from this, I pursued a line of investigation aimed at identifying a physical or functional interaction between Fpn and HFE. While I was ultimately unsuccessful, the experiments described here may prove useful for future scientists interested in pursuing a similar line of research.

Materials and Methods

Analytical Size-Exclusion Chromatography

Analytical size-exclusion chromatography (SEC) was performed using a SMART system

FPLC (GE Healthcare) with a 1.4 mL Superdex 200 column (GE Healthcare) with a flow

rate of 50 µL/min equilibrated in 50 mM Tris pH 7.5, 150 mM NaCl, 0.05% fos-

choline-16, and EDTA-free protease inhibitors (Roche). His-tagged human Fpn was

expressed in one liter of pAER113a-transformed BL21(DE3) *E. coli* grown in TB5 media

(see chapter 3).   Fpn was solubilized in fos-choline-16, purified by Ni-NTA

chromatography as described in chapter 3, concentrated to ~120 µL, centrifuged at

16,000×g for 10 min, and then split into two 60 µL fractions. Soluble HFE was purified

from Chinese hamster ovary (CHO) cell supernatants as described (Lebrón *et al.* 1998).

One Fpn-containing fraction was mixed with soluble HFE at a concentration of 18 µM.

No additions were made to the other Fpn fraction and it acted as the Fpn-only control. A

similar control for HFE alone was prepared by diluting it as above into 60 µL running

buffer.   All samples were incubated at 4 ºC for 3 hr prior to size-exclusion

chromatography. SEC was performed by injecting 50 µL of each sample over the column

in sequence. Traces were compared to molecular weight standards of known mass run in

similar conditions: Blue Dextran (2000 kDa), thyroglobulin (670 kDa), ferritin

(440 kDa), catalase (200 kDa), and albumin (67 kDa) (all standards from GE Healthcare's

SEC MW standard kit).

Testing for binding between Fpn and HFE by surface plasmon resonance

Experiments evaluating the interaction between human Rho-Fpn-His and soluble human HFE were performed at 10 ºC using a Biacore 2000 Instrument (GE Healthcare). Interactions between immobilized Fpn on a sensor chip and soluble HFE injected over the sensor surface were monitored in real time as response units (RU). Biosensor chips were prepared as described in chapter 2 (Rice *et al.* 2009). Briefly, two flow cells of a CM5 biosensor chip were prepared by covalently coupling ~2000 RU of B630N mouse monoclonal anti-Rho antibody. Rho-Fpn-His expressed in baculovirus-infected insect cells was purified by Ni-NTA metal affinity chromatography followed by size-exclusion chromatography in 50 mM Tris pH 7.5, 150 mM NaCl, 0.2% (w/v) DM and injected over the anti-Rho surface, capturing ~500 RU to the antibody surface of one flow cell, leaving the other flow cell as antibody-only reference. After capturing Fpn, the sensor surface was monitored for 3 hr in the same buffer at a flow rate of 5 µL/min, at which time Fpn was slowly shedding from the surface at a constant rate of ~0.3 RU/min. A serial dilution series of HFE was prepared (15.1 µM, 7.55 µM, and 3.775 µM) by diluting concentrated HFE in the above buffer. Samples containing 0, 3.775, 7.55, and 15.1 µM HFE were injected simultaneously over control and experimental surfaces at 5 µL/min for 90 s and then allowed to dissociate for an additional 90 s. Sensorgrams were analyzed in Scrubber (BioLogic Software Pty. Ld.).

Transferrin Iron-Loading

Aqueous solutions of ferric iron chloride ($FeCl_3$, 25 mM) and nitrilotriacetic acid (NTA, 50 mM) were freshly prepared and filtered at 0.22 μm. Dry human holo-transferrin (Tf, Sigma) was dissolved in 1.5 mL 100 mM ammonium bicarbonate and filtered at 0.22 μm. Tf concentration was approximated spectrophotometrically to be 150 μM using an extinction coefficient of 5000 $cm^{-1} M^{-1}$ for absorbance at 454 nm. Buffer was prepared by mixing 100 mM ammonium bicarbonate, adjusting its pH to 7.5, and filtering at 0.22 μm. Two milliliters of 1:2 $FeCl_3$·NTA were prepared by mixing 1 mL $FeCl_3$ with 1 mL NTA solutions. The $FeCl_3$·NTA levels of the Tf solution were raised to 300 μM by adding 36.9 μL 12.5 mM $FeCl_3$·NTA to the 1.5 mL Tf solution. Tf was incubated in the presence of $FeCl_3$·NTA for 2 hr before excess $FeCl_3$·NTA was removed by overnight serial dialysis in 100 mM ammonium bicarbonate, pH 7.5. After dialysis, the concentration of iron-loaded Tf was again measured and the degree of iron incorporation was estimated to be complete by the ratio of spectrophotometric absorbances at 465 and 280 nm equaling approximately 0.050 ($A_{465}/A_{280} = 0.052$) (He and Mason 2002).

Investigating a Possible Effect by HFE on the Hepcidin-Induced Internalization of Fpn

HeLa cells were grown in Dulbelcco's modified Eagle's medium containing 4.5 g/L of D-glucose, 4 mM L-glutamine, 110 mg/L of sodium pyruvate (Gibco), with 1× penicillin/ streptomycin (Gibco), and 10% (v/v) fetal bovine serum (Atlanta Biologicals). All transfections were performed using lipofectamine 2000 (Invitrogen) as per the manufacturer's instruction. HeLa cells were seeded onto poly-L-lysine-treated glass

coverslips in 6-well format ($0.5 \cdot 10^6$ cells/well), transfected with human Fpn-GFP the following day, and then ~20 hr post-transfection were used to test the effects of soluble human HFE on the hepcidin-induced internalization of Fpn. All internalizations were performed in growth media supplemented with cycloheximide, hepcidin-25 (Bachem), and/or soluble human HFE purified from CHO supernatants as described (Lebrón et al. 1998). Internalizations were performed after a 2 hr 75 µg/mL cycloheximide pretreatment, followed by 4 hr of 0 or 2 µM hepcidin-25 (Bachem) internalization, as described (Rice *et al.* 2009). As measured relative to the start of the hepcidin-25 incubation, HFE incubation time was initiated at t equals −2, −0.5, and 0 hr. HFE was added at a concentration of 300 nM. At the 4 hr time point after hepcidin-25 addition, the internalization was stopped by quickly washing three times with PBS followed by 20 min of fixing in 4% PFA at room temperature. After fixing, the cover slips were mounted in DAPI-containing Prolong Gold anti-fade mounting media (Invitrogen), sealed with nail polish, and then imaged by confocal fluorescence microscopy. Imaging was performed on an UltraVIEW ERS Rapid Confocal Imager (Perkin-Elmer) using a 100× objective lens (αPlan-APOCHROMAT 1.46 Oil DIC, Zeiss). Full confocal stacks were imaged for GFP fluorescence at 0.25 µm spacing in z and representative slices are shown.

Internalization reactions were repeated, as above, with an increased HFE concentration (690 nM) and an excess of iron-loaded Tf (400 nM) to saturate transferrin receptor (TfR) and out-compete its HFE-binding capabilities. Tf was added 30 min prior to hepcidin-25 addition. HFE was added 15 min prior to hepcidin-25 addition. This set of experiments

varied hepcidin-25 concentration, testing 0 or 2 μM hepcidin-25 concentrations. Incubations were stopped, fixed, mounted, and imaged as described above.

Results and Discussion

Analytical Size-Exclusion Chromatography

The potential binding between wild-type human Fpn expressed and purified from *E. coli* and soluble human HFE expressed in CHO cells was assessed by analytical SEC (figure 4.2). As described in chapter 3, Fpn extracted in fos-choline-16 elutes as a broad peak centered at approximately 1.2 mL (see chapter 3, figure 3.5). We found that soluble HFE eluted as a symmetrical peak centered at approximately 1.6 mL (figure 4.2). Fpn and HFE were pre-mixed at a high HFE concentration (18.2 μM). After pre-incubation the mixture was analyzed by analytical SEC, however no evidence of a Fpn-HFE complex was detected (see figure 4.2, blue curve).

These results are not conclusive. If fos-choline-16 interfered with an Fpn-HFE interaction, we would expect to not detect it under these conditions. Also, Fpn contains potential glycosylation sites (Devalia *et al.* 2002) and these carbohydrate moieties would be absent in bacterially expressed Fpn. If glycosylation of Fpn was necessary for an interaction with HFE, we would not expect to observe binding in this assay. Finally, a weak interaction might not be detectable by a technique like analytical SEC, which allows time for dissociation before detection.

Testing for an Interaction between Fpn and HFE by Surface Plasmon Resonance

The potential binding between wild-type human Fpn expressed and purified from baculovirus-infected insect cells and soluble human HFE was assessed by surface plasmon resonance (figure 4.3). Rho-tagged Fpn was coupled to an anti-Rho antibody surface, soluble HFE was injected at various concentrations (0–15.1 µM HFE), and the response was continuously monitored in an effort to detect binding. Despite high levels of HFE injected over the Fpn surface, no binding was observed (figure 4.3).

As with the analytical SEC experiments above, these results are not fully conclusive. Unlike analytical SEC, surface plasmon resonance is capable of detecting weak interactions with quick dissociation rates, however detergent or improper glycosylation could still be potentially interfering with a Fpn-HFE interaction.

Investigating a Possible Effect by HFE on Hepcidin-Induced Internalization of Fpn

We were unable to detect an interaction between Fpn and HFE with biophysical methods using detergent solubilized Fpn, and thus we moved on to cell-based assays. In these experiments we attempted to detect a functional interaction between Fpn and HFE. After developing a hepcidin-induced Fpn-GFP internalization assay in HeLa cells (Rice *et al.* 2009), we asked if this internalization was disrupted in the presence of soluble HFE. We used 300 nM HFE, a concentration shown to have an inhibitory effect on iron export in macrophage-like cells (Drakesmith *et al.* 2002). In this experiment we asked whether

soluble HFE would prevent the internalization of Fpn-GFP by hepcidin-25; however we saw no internalization defect (figure 4.4). This internalization assay was performed in the presence of Tf-containing fetal calf serum, however to ensure that our HFE was not being sequestered by endogenous TfR on the surface of these cells, we performed another experiment with elevated HFE concentration (690 nM) and an additional 400 nM iron-loaded human Tf added on top of the bovine Tf that is naturally present in the serum (figure 4.5). Under these conditions, hepcidin-induced internalization of Fpn was not prevented.
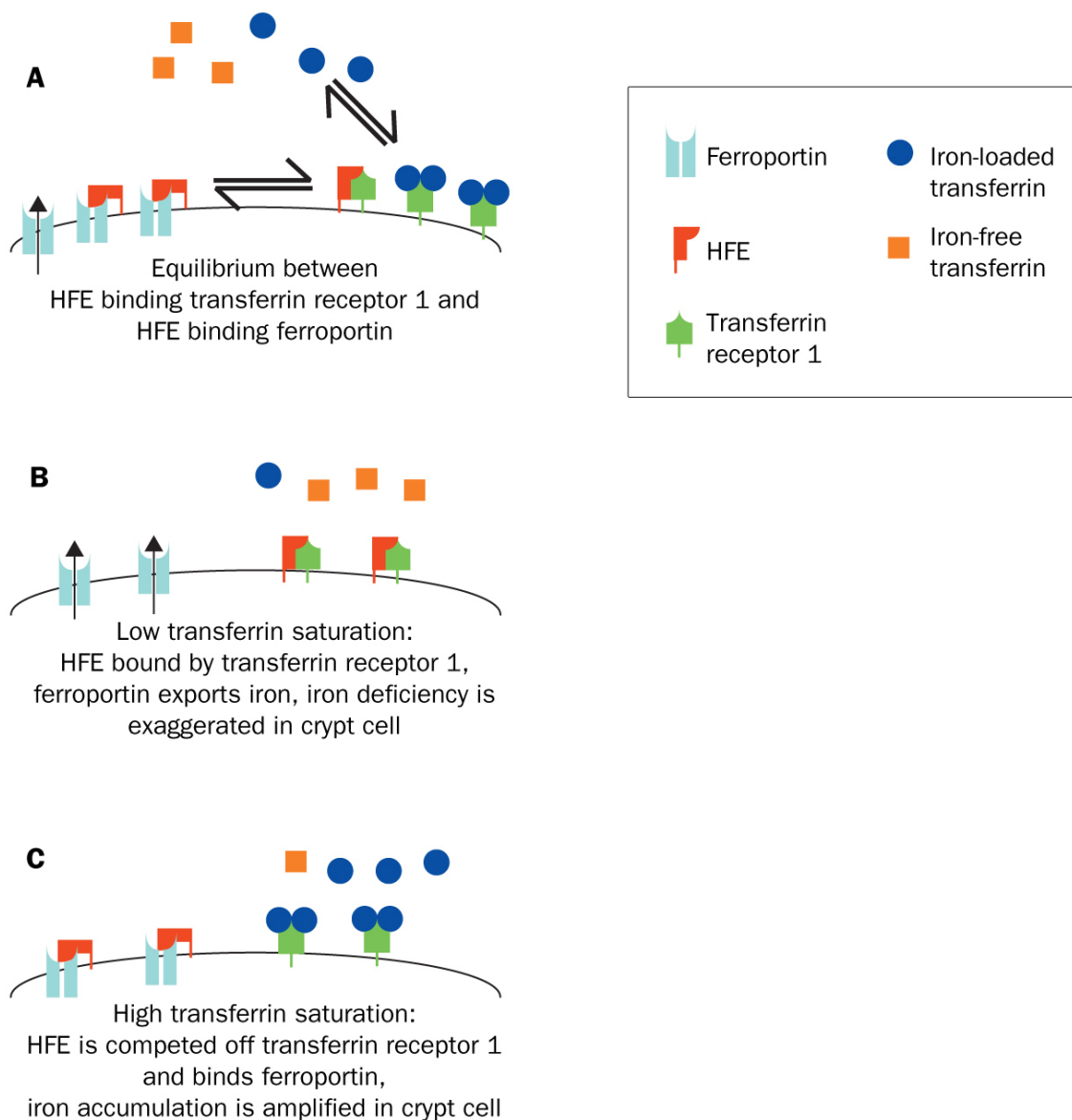
Figure 4.1. Townsend-Drakesmith HFE hypothesis. A regulatory role for HFE is proposed whereby a dynamic equilibrium exists between HFE, Fpn, TfR, and iron-loaded Tf on the basolateral membrane of duodenal crypt cells. Panel A depicts this hypothetical equilibrium. When Tf saturation is low (panel B), HFE binds TfR and iron is exported. When Tf saturation is high (panel C), HFE is unable to bind TfR and instead binds Fpn, inhibiting iron export. Figure adapted from Townsend and Drakesmith 2002.
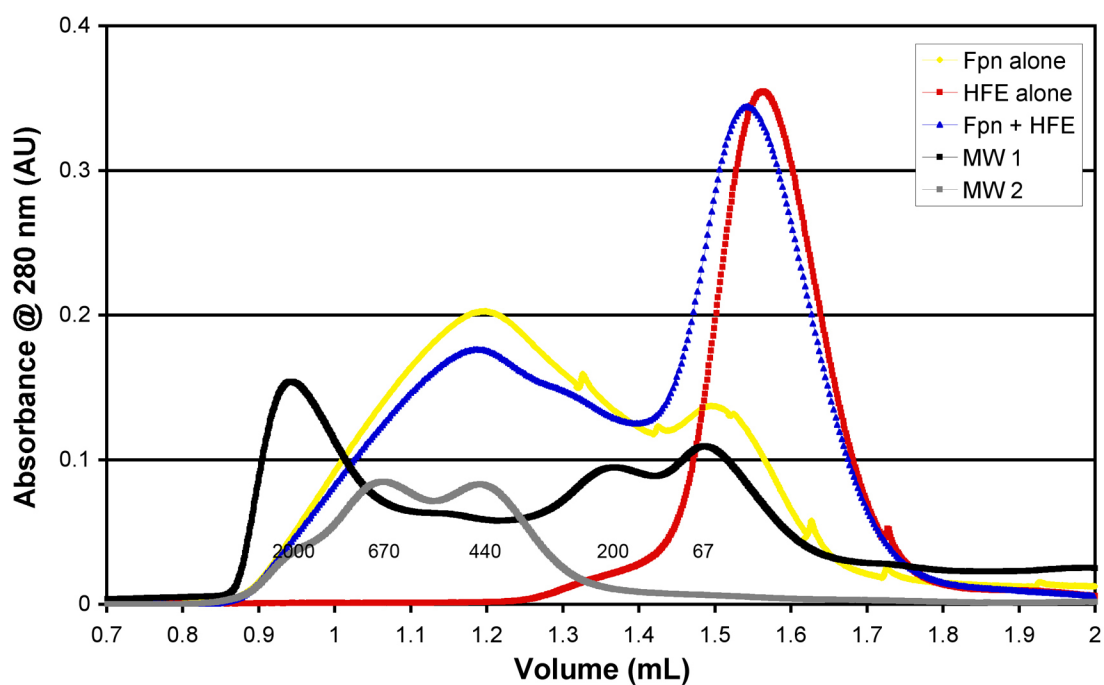
Figure 4.2. Potential interactions between bacterially expressed Fpn and soluble HFE was screened by analytical size-exclusion chromatography as described in the methods. Traces for molecular weight standards are shown (MW 1 in black and MW 2 in grey) and are labeled in kDa.
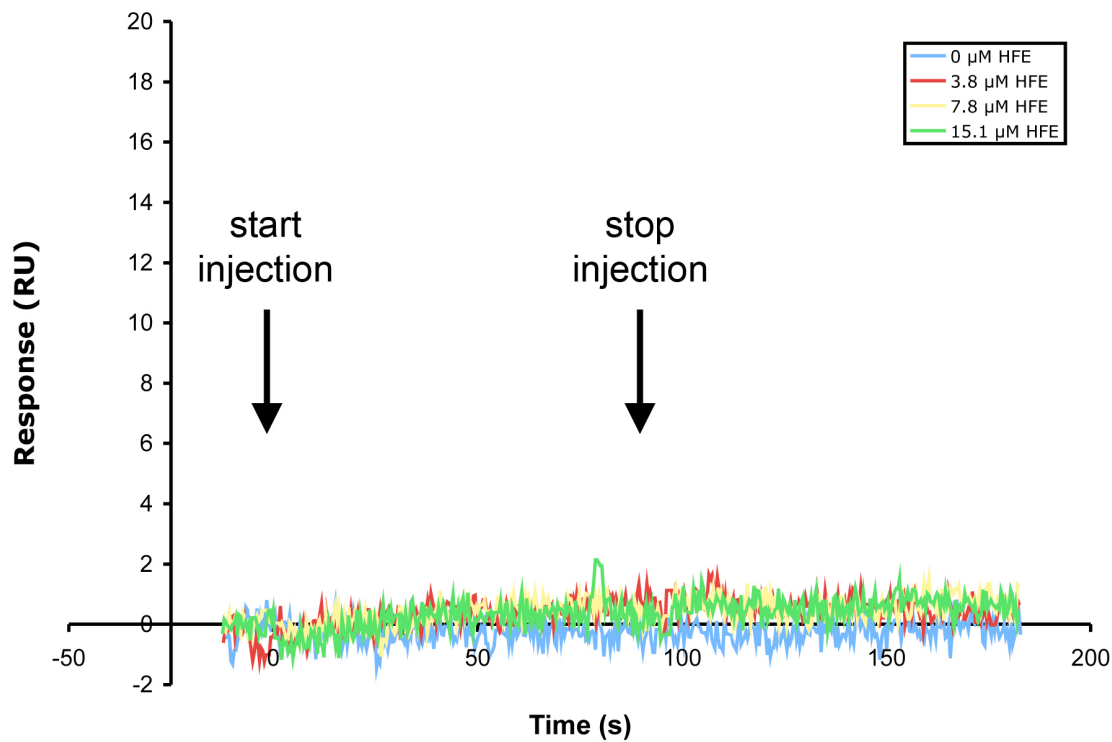
Figure 4.3. Potential interactions between Fpn expressed in baculovirus-infected insect cells and soluble HFE were screened by surface plasmon resonance. A dilution series of soluble human HFE (0, 3.8, 7.8, and 15.1 µM) was injected over a biosensor surface containing ~500 RU human Rho-Fpn-His. Reference-subtracted response curves are shown.
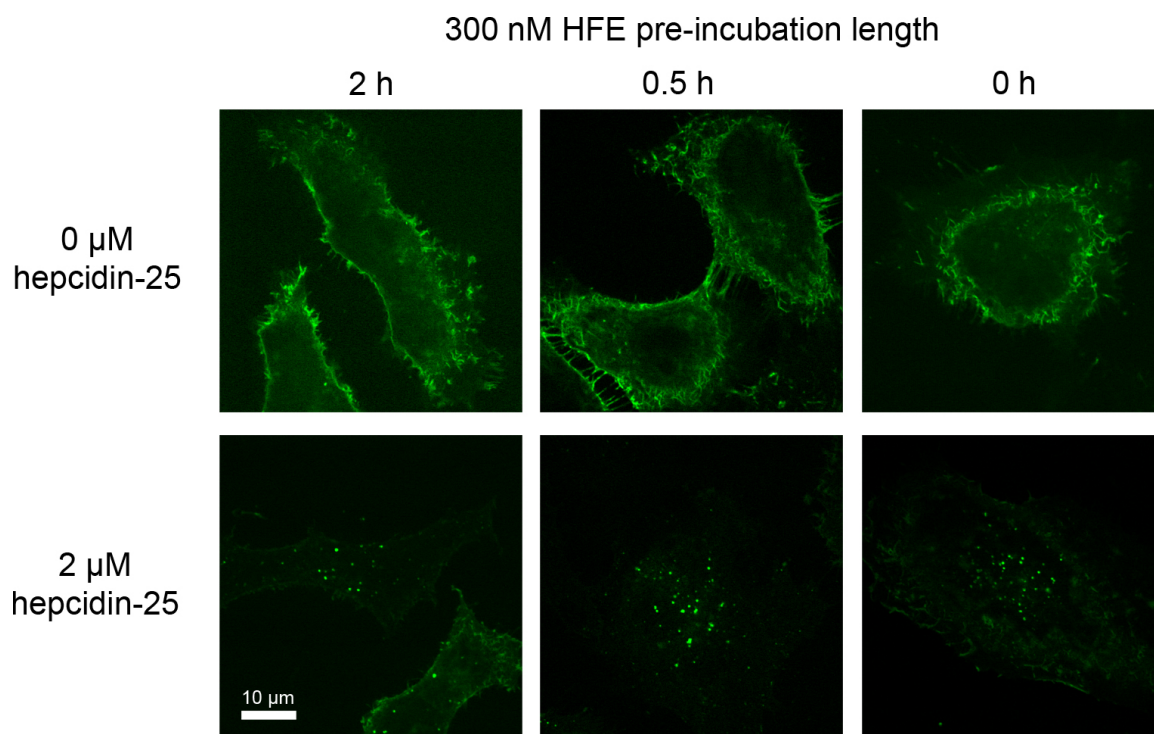
300 nM HFE pre-incubation length

Figure 4.4. Fpn-GFP was transiently transfected into HeLa cells, as described in the methods. Hepcidin-induced internalization of Fpn-GFP was performed in the presence of 300 nM HFE and analyzed by confocal microscopy. HFE was added either 2 hr prior to, 30 min prior to, or together with hepcidin-25 addition.
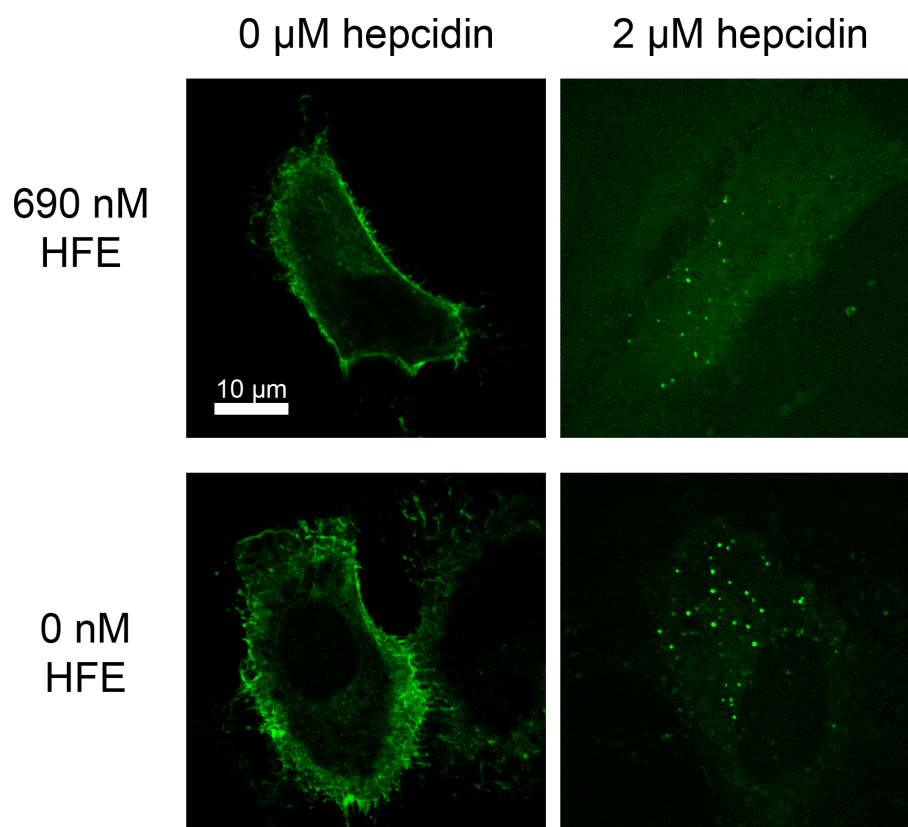
0 µM hepcidin   2 µM hepcidin

690 nM
HFE

10 µm

0 nM
HFE

Figure 4.5. Fpn-GFP was transiently transfected into HeLa cells, as described in the methods. Under conditions of Tf saturation (400 nM iron-loaded Tf) hepcidin-induced internalization of Fpn-GFP was performed in the presence or absence of 690 nM HFE and analyzed by confocal microscopy.

References

Abboud, S., and Haile, D. J. (2000). A novel mammalian iron-regulated protein involved in intracellular iron metabolism. *J Biol Chem* **275**, 19906–19912.

Devalia, V., Carter, K., Walker, A. P., Perkins, S. J., Worwood, M., May, A., and Dooley, J. S. (2002). Autosomal dominant reticuloendothelial iron overload associated with a 3-base pair deletion in the ferroportin 1 gene (SLC11A3). *Blood* **100**, 695–697.

Donovan, A., Brownlie, A., Zhou, Y., Shepard, J., Pratt, S. J., Moynihan, J., Paw, B. H., Drejer, A., Barut, B., Zapata, A.*, et al.* (2000). Positional cloning of zebrafish ferroportin1 identifies a conserved vertebrate iron exporter. *Nature* **403**, 776–781.

Drakesmith, H., Sweetland, E., Schimanski, L., Edwards, J., Cowley, D., Ashraf, M., Bastin, J., and Townsend, A. R. (2002). The hemochromatosis protein HFE inhibits iron export from macrophages. *Proc Natl Acad Sci USA* **99**, 15602–15607.

Feder, J. N., Gnirke, A., Thomas, W., Tsuchihashi, Z., Ruddy, D. A., Basava, A., Dormishian, F., Domingo, R., Jr., Ellis, M. C., Fullan, A.*, et al.* (1996). A novel MHC class I-like gene is mutated in patients with hereditary haemochromatosis. *Nat Genet* **13**, 399–408.

Feder, J. N., Penny, D. M., Irrinki, A., Lee, V. K., Lebron, J. A., Watson, N., Tsuchihashi, Z., Sigal, E., Björkman, P. J., and Schatzman, R. C. (1998). The hemochromatosis gene product complexes with the transferrin receptor and lowers its affinity for ligand binding. *Proc Natl Acad Sci USA* **95**, 1472–1477.

He, Q.-Y., Mason, A. B. (2002). Molecular aspects of release of iron from transferrin. In *Molecular and Cellular Iron Transport*, D. M. Templeton, editor (New York, Basel: Marcel Dekker), pp. 95–124.

Lebrón, J. A., Bennett, M. J., Vaughn, D. E., Chirino, A. J., Snow, P. M., Mintier, G. A., Feder, J. N., and Björkman, P. J. (1998). Crystal structure of the hemochromatosis protein HFE and characterization of its interaction with transferrin receptor. *Cell* **93**, 111–123.

McKie, A. T., Marciani, P., Rolfs, A., Brennan, K., Wehr, K., Barrow, D., Miret, S., Bomford, A., Peters, T. J., Farzaneh, F*., et al.* (2000). A Novel Duodenal Iron-Regulated Transporter, IREG1, Implicated in the Basolateral Transfer of Iron to the Circulation. *Molecular Cell* **5**, 299–309.

Parkkila, S., Waheed, A., Britton, R. S., Bacon, B. R., Zhou, X. Y., Tomatsu, S., Fleming, R. E., and Sly, W. S. (1997). Association of the transferrin receptor in human placenta with HFE, the protein defective in hereditary hemochromatosis. *Proc Natl Acad Sci USA* **94**, 13198–13202.

Rice, A. E., Mendez, M. J., Hokanson, C. A., Rees, D. C., and Björkman, P. J. (2009). Investigation of the biophysical and cell biological properties of ferroportin, a multipass integral membrane protein iron exporter. *J Mol Biol* **386**, 717–732.

Roy, C. N., and Enns, C. A. (2000). Iron homeostasis: new tales from the crypt. *Blood* **96**, 4020–4027.

Townsend, A., and Drakesmith, H. (2002). Role of HFE in iron metabolism, hereditary haemochromatosis, anaemia of chronic disease, and secondary iron overload. *Lancet* **359**, 786–790.

Appendix:

Crystallization Attempts of Ferroportin and the

Ferroportin:Hepcidin-25 Complex

Construct	Detergent	Purification	Conc. (mg/mL)	Temp. (ºC)	Screen	Method
Rho-hFpn-His	DDM	TALON	11	20	Index	vapor diffusion
Rho-hFpn-His	DDM	TALON	11	20	Wizard I&II	vapor diffusion
Rho-hFpn-His	DDM	TALON	11	20	Crystal Screen I&II	vapor diffusion
Rho-hFpn-His	DDM	TALON	11	20	Cation Screen	vapor diffusion
Rho-zFpn-His	DDM	TALON	4	20	Index	vapor diffusion
Rho-zFpn-His	DDM	TALON	4	20	Wizard I&II	vapor diffusion
Rho-zFpn-His	DDM	TALON	4	20	Crystal Screen I&II	vapor diffusion
Rho-zFpn-His	DDM	TALON	4	20	Cation Screen	vapor diffusion
Rho-zFpn-His	DDM	TALON	4	20	Cryo I&II	vapor diffusion
Rho-zFpn-His	DDM	TALON	8	20	PEG I	vapor diffusion
Rho-zFpn-His	DDM	TALON	8	20	PEG II	vapor diffusion
Rho-zFpn-His	DDM	TALON	8	20	Index	vapor diffusion
Rho-zFpn-His	DDM	TALON	8	20	Crystal Screen I&II	vapor diffusion
Rho-zFpn-His	DDM	TALON	8	20	Salt Rx	vapor diffusion
Rho-zFpn-His	DDM	TALON	8	20	pH Clear	vapor diffusion
Rho-zFpn-His	DDM	TALON	10	20	Crystal Screen I&II	vapor diffusion
Rho-zFpn-His	DDM	TALON	10	20	Memfac	vapor diffusion
Rho-zFpn-His	DDM	TALON	10	20	PEG Ion	vapor diffusion
Rho-zFpn-His	DDM	TALON	10	20	Wizard I&II	vapor diffusion
Rho-zFpn-His	DDM	TALON	10	20	Index	vapor diffusion
Rho-zFpn-His + 0.16 mM hepcidin-25	DDM	TALON	10	20	Crystal Screen I&II	vapor diffusion
Rho-zFpn-His + 0.16 mM hepcidin-25	DDM	TALON	10	20	Memfac	vapor diffusion
Rho-zFpn-His + 0.16 mM hepcidin-25	DDM	TALON	10	20	PEG Ion	vapor diffusion
Rho-zFpn-His + 0.16 mM hepcidin-25	DDM	TALON	10	20	Wizard I&II	vapor diffusion
Rho-zFpn-His + 0.16 mM hepcidin-25	DDM	TALON	10	20	Index	vapor diffusion
Rho-hFpn-His-FLAG	DDM	TALON-FLAG	9	20	Wizard I&II	fluidigm
Rho-hFpn-His-FLAG	DDM	TALON-FLAG	9	20	Index	fluidigm
Rho-hFpn-His-FLAG	DDM	TALON-FLAG	9	20	Memfac	fluidigm
Rho-hFpn-His-FLAG	DDM	TALON-FLAG	9	20	Nextal PEG	fluidigm
Rho-hFpn-His-FLAG + 0.14 mM hepcidin-25	DDM	TALON-FLAG	9	20	Wizard I&II	fluidigm
Rho-hFpn-His-FLAG + 0.14 mM hepcidin-25	DDM	TALON-FLAG	9	20	Index	fluidigm
Rho-hFpn-His-FLAG + 0.14 mM hepcidin-25	DDM	TALON-FLAG	9	20	Memfac	fluidigm
Rho-hFpn-His-FLAG + 0.14 mM hepcidin-25	DDM	TALON-FLAG	9	20	Nextal PEG	fluidigm
Rho-mFpn-His-FLAG	DDM	TALON-FLAG	7.5	20	Wizard I&II	fluidigm
Rho-mFpn-His-FLAG	DDM	TALON-FLAG	7.5	20	Index	fluidigm
Rho-mFpn-His-FLAG	DDM	TALON-FLAG	7.5	20	Memfac	fluidigm
Rho-mFpn-His-FLAG	DDM	TALON-FLAG	7.5	20	Nextal PEG	fluidigm
Rho-zFpn-His-FLAG	DDM	TALON-FLAG	5.2	20	Wizard I&II	fluidigm
Rho-zFpn-His-FLAG	DDM	TALON-FLAG	5.2	20	Index	fluidigm
Rho-zFpn-His-FLAG	DDM	TALON-FLAG	5.2	20	Memfac	fluidigm
Rho-zFpn-His-FLAG	DDM	TALON-FLAG	5.2	20	Nextal PEG	fluidigm
Rho-hFpn-His-FLAG	CHAPS	TALON-FLAG	4	20	Wizard I&II	fluidigm
Rho-hFpn-His-FLAG + 0.06 mM hepcidin-25	CHAPS	TALON-FLAG	4	20	Wizard I&II	fluidigm
Rho-hFpn-His-FLAG	CHAPS	TALON-FLAG	4	20	Index	fluidigm
Rho-hFpn-His-FLAG + 0.06 mM hepcidin-25	CHAPS	TALON-FLAG	4	20	Index	fluidigm
Rho-hFpn-His-FLAG	CHAPS	TALON-FLAG	4	20	Crystal Screen I&II	fluidigm

Construct	Detergent	Purification	Conc. (mg/mL)	Temp. (ºC)	Screen	Method
Rho-hFpn-His-FLAG + 0.06 mM hepcidin-25	CHAPS	TALON-FLAG	4	20	Crystal Screen I&II	fluidigm
Rho-hFpn-His-FLAG	cymal-6	TALON-FLAG	4	20	Wizard I&II	fluidigm
Rho-hFpn-His-FLAG + 0.06 mM hepcidin-25	cymal-6	TALON-FLAG	4	20	Wizard I&II	fluidigm
Rho-hFpn-His-FLAG	cymal-6	TALON-FLAG	4	20	Index	fluidigm
Rho-hFpn-His-FLAG + 0.06 mM hepcidin-25	cymal-6	TALON-FLAG	4	20	Index	fluidigm
Rho-hFpn-His-FLAG	cymal-6	TALON-FLAG	4	20	Crystal Screen I&II	fluidigm
Rho-hFpn-His-FLAG + 0.06 mM hepcidin-25	cymal-6	TALON-FLAG	4	20	Crystal Screen I&II	fluidigm
Rho-hFpn-His-FLAG	DDM	TALON-FLAG-SEC	9	20	MacKinnon #1	vapor diffusion
Rho-hFpn-His-FLAG	DDM	TALON-FLAG-SEC	9	20	MacKinnon #2	vapor diffusion
Rho-mFpn-His-FLAG	DDM	TALON-FLAG-SEC	8	20	MacKinnon #3	vapor diffusion